UNIVERSIDAD MICHOACANA DE SAN NICOLAS DE HIDALGO

INSTITUTO DE INVESTIGACIÓN EN METALURGIA Y MATERIALES

Synthesis and anticorrosion characterization of marine geopolymer concrete

Tesis para obtener el Doctorado en Ciencias en Metalurgia y Ciencias de los Materiales

PRESENTA:
M.C. Xing Li

ASESOR:
Dr. Feng Rao Wu

COASESOR:
Dr. Shaoxian Song Hu

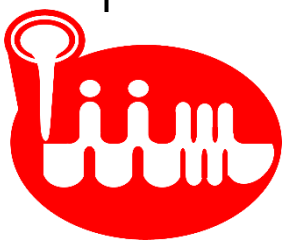

Morelia, Michoacán, México, Septiembre 2020

Acknowledgement

First, I want to express my thanks to the Consejo Nacional de Ciencia y Tecnolog á (CONACyT) of Mexico under the grant No. 270186 and the National Natural Science Foundation of China (NSFC) under the project No. 51474167 for their support to this project. I would also like to thank the CONACyT for a scholarship under the grant No. 831134 during my Ph.D. studying. I appreciate Universidad Michoacana de San Nicol ás de Hidalgo (UMSNH) and the Instituto de Investigacion en Metalurgia y Materials (IIMM) which provide an enjoyable working environment.

Next, I would like to express my sincere gratitude to Prof. Feng Rao Wu. As my supervisor, Prof. Feng helped me enhance my English writing, guided my research work, gave me valuable courses, cared for my life and encouraged me to overcome the difficulties. After that, I want to give my great gratitude to my co-supervisor, Prof. Shaoxian Song Hu. His fund of knowledge and serious attitude in work were worthy of my learning. And he also gaved me great help in my experiment and research.

And I would like to express my sincere gratitude to Prof. Mario Alberto Corona Arroyo, Prof. Noemi Ortiz Lara and Prof. Ena Athenea Aguilar Reyes for their invaluable advice in my work. I also want to thank Prof. Victor Hugo Lopez Morelos, Prof. Arnoldo Bedolla Jacuinde and Prof. Francisco Vapeani Guerra Lopez. Thanks for their help and support in my graduation procedure during the COVID-19 pandemic.

During my Ph.D study, I received so much important help from my classmate Dr. Qian Wan, Dr. Zhili Li, M.C. Xiang Tian, Ing. Alma Ileana Gallegos Estrada and Ing. Maria Guadalupe Mateos Lopez. I would like to express sincere thanks and best regards to them.

Furthermore, I present a special thanks to my families for their support. During my Ph.D study, I encountered so many difficulties and problems, but my families encouraged and helped me wherever and whenever I needed. I deeply want to express my sincere gratitude to my husband Hongzheng Zhu for his permanent support and encouragement incenting me to strive towards my goal.

Content

Index of Figures

Index of Tables

Abstract

Concrete exposed to seawater is easily corroded by seawater, for example, heat-cool and dry-wet cycle, SO_4^{2-} and Mg^{2+} corrosion and Cl^- penetration. Geopolymers are considered as a good application of concrete. In this work, different geopolymers were synthesized to evaluate their resistance to sea water corrosion. To applicate geopolymers in marine engineering, the silica sand and steel fiber (8.5 mm in length and 0.2 mm in diameter) were first prepared in geothermal clay to synthesize geopolymer concrete. After that, metakaolin based geopolymer and geothermal clay based geopolymer were cured in the sea water, dry-wet cycle, heat-cool cycle. Then alkali-activated binders based on metakaolin, fly ash and slag without curing were exposed directly in air, Na_2SO_4 and $MgSO_4$ solutions. In the end, reinforced alkali activated metakaolin-tailing concrete were exposed in sea water though electrochemical accelerated corrosion to observe the corrosion of steel bars by chloride ions.

In a transitional experiment for synthesizing geopolymer concrete, about 10% to 60% silica sand replaced geothermal clay to synthesize mortars first and then a comparison was made with and without steel fiber. Their mechanical behavior and microstructures were studied. For studying the resistance to different seawater corrosion factors, different geopolymers were prepared and cured in different sea water corrosion conditions. Then the products were characterized by scanning electron microscopy (SEM), x-ray diffraction (XRD), fourier transform infrared spectroscopy (FTIR) to evaluated morphology and microstructures, and mechanical tester for compressive strength. Besides, ^{29}Si nuclear magnetic resonance (NMR) spectra were used to study the microstructure of products, the short-range ordering and the molecular structure. Gaussian peak deconvolution was employed to separate and quantify the $Q^n(mAl)$ species ($0 \leq m \leq n \leq 4$, m, n = integer) in geopolymer gel.

With the addition of silica sand and steel fiber, geothermal clay-based geopolymer shows good compressive strength and flexural strength. For the metakaolin-based geopolymers and geothermal clay-based geopolymer exposed in air, seawater, dry-wet and heat-cool cycles of seawater for 90 days, it was found that seawater environment inhibited the geopolymerization reactions, and a low amount of tetrahedral silicon of $Q^4(4Al)$, $Q^4(3Al)$ and $Q^4(2Al)$ were formed. In alkali-activated binders based on metakaolin, fly ash and slag cured in Na_2SO_4 solution, a higher percentage of zeolite was formed. While in $MgSO_4$, a precipitate layer (e.g., brucite and gypsum), forming on the binder surface plays an important role in protecting the formation of gel, promoting the compressive strength improvement of alkali-activated slag, and compensating the decrease in compressive strength of alkali-activated metakaolin. A high corrosion is observed in alkali-activated metakaolin-tailing mortars because chloride intrudes along the cracks formed by gypsum and ettringite.

Keywords: Geopolymer; Alkali-activated binder; Sea water corrosion; Microstructure; NMR spectra

Resumen

El concreto expuesto al agua de mar es fácilmente corroído por el agua de mar, por ejemplo, el ciclo de calor-frío y seco-húmedo, la corrosión de SO_4^{2-} y Mg^{2+} y la penetración de Cl^-. Los geopolímeros se consideran una buena aplicación del hormigón. En este trabajo, se sintetizaron diferentes geopolímeros para evaluar su resistencia a la corrosión del agua de mar. Para aplicar geopolímeros en ingeniería marina, arena de sílice y fibra de acero (8.5 mm de longitud y 0.2 mm de diámetro) se prepararon primero en arcilla geotérmica para sintetizar hormigón geopolímero. Después, el geopolímero a base de metacaolín y geopolímero a base de arcilla geotérmica se curaron en agua de mar, ciclos de seco-húmedo y calor-frío. Luego, los aglutinados activados con álcali basados en metacaolín, cenizas volantes y escoria sin curar se expusieron directamente al aire, soluciones de Na_2SO_4 y $MgSO_4$. Al final, el concreto reforzado metacaolín-jales activado con álcali el hormigón se expuso en agua de mar a través de la corrosión acelerada electroquímica para observar la corrosión de las barras de acero por los iones de cloruro.

En un experimento de transición para sintetizar concreto activado con álcali, aproximadamente 10% a 60% de arena sílice reemplazó la arcilla geotérmica para sintetizar morteros primero y luego se realizó una comparación con y sin fibra de acero. Se estudiaron su comportamiento mecánico y microestructuras. Para estudiar la resistencia a diferentes factores de corrosión del agua de mar, se prepararon y curaron diferentes geopolímeros en diferentes condiciones de corrosión del agua de mar. Después, los concretos fueron caracterizados por microscopía electrónica de barrido (SEM), difracción de rayos X (XRD), espectroscopía infrarroja por transformada de Fourier (FTIR) para evaluar su morfología y microestructuras, y prueba mecánica de resistencia a la compresión. Además, espectros de resonancia magnética nuclear (RMN) ^{29}Si se utilizaron para estudiar la microestructura de los productos, el ordenamineto de corto alcance y la estructura molecular. Los picos gaussianos de deconvolución se emplearon para separar y cuantificar las especies $Q^n(mAl)$ ($0 \leq m \leq n \leq 4$, m, n = entero) en el gel de geopolímero.

Con la adición de arena sílice y fibras de acero, el concreto activado con álcalis basado en arcilla geotérmica mostró una buena resistencia a la compresión y resistencia a la flexión. Para los geopolímeros a base de metacaolín y el geopolímero a base de arcilla geotérmica expuestos al aire, agua de mar, ciclos seco-húmedo y calor-frío en agua de mar por 90 días, se encontró que el ambiente del agua de mar inhibe las reacciones de geopolimerización y se formó una baja cantidad de silicio tetraédrico de $Q^4(4Al)$, $Q^4(3Al)$ y $Q^4(2Al)$. En los aglutinados activados con álcalis basados en metacaolín, cenizas volantes curados en soluciones de Na_2SO_4, se formó un mayor porcentaje de zeolita. Mientras que en soluciones de $MgSO_4$, se formó una capa de precipitado (por ejemplo de brucita y yeso), la formación sobre la superficie de los aglutinados activados juega un papel importante en la protección de la formación de gel, promoviendo la mejora de la resistencia a la compresión de la escoria activada con álcali y compensando la disminución de la resistencia a la compresión del metacaolín activado con álcali. Una alta corrosión fue observada en los morteros de metacaolin-jales activados con álcali porque los cloruros se introducen a lo largo de las grietas formadas por el yeso y la ettringita.

Palabras clave: Geopolímero; Aglutinante activado con álcali; Corrosión del agua de mar; Microestructura; Espectros de RMN

1. Introduction

Geopolymers have attracted extensive attention due to their superior properties in replacement of ordinary Portland cement (OPC) concrete, but of low CO_2 emission in the synthesis (Provis, 2013). Geopolymers are prepared with aluminosilicates and alkaline activators. They are considered to possess high mechanical strength (Luukkonen et al. 2018), good durability (Pacheco-Torgal et al. 2012), mesoporous structure (Glad and Kriven 2013), and ion-exchange capacity (Bortnovsky et al. 2008; Skorina 2014).

The OPC concrete has been widely used in harbor terminals, sea walls, artificial offshore islands, etc. However the corrosion usually occurs due to the exposure in sea water. Corrosive ions such as SO_4^{2-} and Mg^{2+} can react with the hydration products, namely calcium silicate hydrate (C-S-H) and calcium hydroxide $Ca(OH)_2$, forming ettringite, brucite, magnesium silicate hydrate, etc. (Li et al., 2017). The precipitation and crystallization of these salts in pores of the OPC concrete, which are accelerated by the dry-wet and heat-cool cycles, leads to cracks and corrosion (Zhang et al., 2011; Arbi et al., 2016). In addition, the chloride ions do not react with the hydration products. They enter concrete to damage rebar passivation film and initiate pitting corrosion of the reinforcement when their concentration at the reinforcement reaches a critical level (Osio-Norgaard et al., 2018). The repair of the corroded concrete is costly, troublesome, or even impossible. Accordingly, the introduction of new materials to improve the anticorrosion property of marine concrete structures has become the focus of the civil engineering and material science (Val and Stewart, 2003; Binici et al., 2008).

Compared to the OPC concrete, the geopolymers show low corrosion in the sea water. In the same sea water environment, the geopolymers present lower compressive strength loss and less structural degradation (Astutiningsih et al., 2010), because the geopolymers possess compact ceramic-like gel in their microstructure which reduces penetration of sea water and corrosion ions. In addition, the hydration products of the binder show low reaction to the corrosion ions. However, explanations of the anticorrosion properties were based on ambiguous and indirect evidences. For example, low permeability was used to verify their ability from chloride intrusion (Chindaprasirt et al., 2014). There is lack of study on the evolution of tetrahedral silica and aluminum structures in geopolymer especially containing calcium under marine environment.

In the current thesis work, the effects of silica sand and steel fiber in the geopolymer concrete were discussed as the transitional work. Then, we synthesized alkali-activated materials with no calcium, low calcium and high calcium to form N-A-S-H, C-A-S-H and C-S-H gels. After they were exposed in sea water, sodium sulfate and magnesium sulfate solution, their resistance to dry-wet and heat-cool cycle, sulfate, and magnesium was evaluated and the evolution of N-A-S-H, C-A-S-H and C-S-H gels were studied. In the end, the resistance of alkali-activated metakaolin/tailing to chloride penetration was evaluated by electrochemistry techniques.

1.1 Objectives

1.1.1 General Objective

Different geopolymers with waste silicate source (e.g., geothermal clay, iron ore tailing) were synthesize. Their corrosion mechanism in sea water environment and the evolution of microstructure were studied. The clues for geopolymer replacing marine concrete were provided.

1.1.2 Specific Objectives

1) To add effective additives in geopolymer concretes for studying their mechanical properties.

2) To synthesize geopolymer by using metakaolin and industrial by-products such as geothermal clay, fly ash and iron ore tailing.

3) To investigate the anticorrosion mechanism of geopolymers through studying their microstructures and mechanical character.

4) To compare the anticorrosion performance of different geopolymer.

5) To observe the corrosion behaviors of alkali activated materials with different calcium content in sulfate solution.

6) To investigate the effect of calcium content on the chloride penetration of reinforced alkali activated concrete in sea water.

1.2 Justification

Some studies show that the silica sand can be used to improve the compressive strength of OPC and reduce the dry shrinkage. And the addition of steel fiber can be used to improve the flexural strength. These advantages of aggregate materials are considered to promote the application of geopolymers in marine concrete. Thus the roles of silica sand and steel fiber in the microstructural and mechanical properties of geopolymer was studied.

Dry-wet cycles and heat-cold cycles threaten coastal and offshore structural concrete exposed to seawater. They accelerate the precipitation and crystallization of corrosive salts in the pores of concrete, leading to the formation of cracks and breaks. The compact tetrahedral silica and aluminum structure of geopolymer reduces the destruction of dry-wet cycle and heat-cool cycles. Thus the present work studied on the evolution of tetrahedral silica and aluminum structures in geopolymer under marine environment with dry-wet and heat-cool cycles.

The microstructures, mechanical properties and chemical properties are affected by the compositions of geopolymers, and they are related to the corrosion resistance. Geothermal clay is rich in cristobalite (SiO_2) compared to the metakaolin. Thus through comparison of the geothermal clay-based geopolymer and metakaolin-based geopolymer, the effect of cristobalite on the corrosion resistance of geopolymer in artificial sea water was studied.

Calcium silicate hydrate (C-S-H) and calcium hydroxide $Ca(OH)_2$ in OPC cement exposed to sea water are easily attacked by the SO_4^{2-} and Mg^{2+} ions. The corrosive products such as ettringite, brucite and magnesium silicate hydrate can cause expansion and cracking. Alkali-activated binders show good compactness and low reactivity, which are attributed to the different microstructure in N-A-S-H and C-A-S-H gels. It is significant to study the evolution in microstructure of alkali-activated binders without curing when exposing in sulfate solutions, especially the evolution of different gels (e.g., N-A-S-H and C-A-S-H).

Different gel structures are formed when increasing calcium content in alkali-activated material, leading to the unpredictable chloride diffusion resistance of the alkali-activated materials. The present work prepares metakaolin/iron ore tailing-based mortars with different contents of iron

ore tailing (calcium). It attempts to clarify the effect of gel structure on chloride diffusion in alkali-activated materials. It is expected that the calcium presented in the gel will be against to the resistance of chloride diffusion.

1.3 Hypothesis

In this work, we hypothesize that the geopolymer with highly interconnect three-dimensional structure is more compact than OPC binder. The compact structure leads to high compressive strength and low permeability, which helps geopolymer possess superior anticorrosion properties in marine environment.

1.4 Research outline

Research line of the work is presented schematically in Figure 1.1. The Chapter 1 is the introduction. In Chapter 2, the literature about the property of alkali-activated binders and anticorrosion of them in sea water were reviewed. Chapter 3 was the experimental of the thesis work. Chapter 4.1 was the transitional work, the effects of silica sand and steel fiber aggregates on the microstructure and mechanical strength of the geothermal-metakaolin-based geopolymer were studied. It provided fundamentals for the synthesis of marine geopolymer concrete. In Chapter 4.2, metakaolin-based geopolymers were synthesized to study their deterioration in marine environment. It was found that seawater environment inhibited the geopolymerization reactions. This work not only showed the good seawater corrosion resistance of geopolymer, but also gave a clue on using industrial waste (e.g., geothermal clay) in the synthesis of geopolymers. In Chapter 4.3, the effects of the cristobalite on the mechanical behavior and microstructure of geopolymers were characterized. This work showed that the composition of geopolymers affected their resistance to seawater corrosion. In Chapter 4.4, alkali-activated binders based on metakaolin, fly ash and slag without curing were exposed directly in air, Na_2SO_4 and $MgSO_4$ solutions for studying the evolution in mechanical property and microstructure. This work showed that it was feasible to directly prepare alkali-activated concrete in aggressive sulfate attack environment. In Chapter 4.5, the electrochemical method was used to evaluate the chloride resistance of reinforced alkali-activated metakaolin/iron ore tailing in sea water. It provided clues on the effect of different calcium content on the chloride resistance of reinforcement alkali-activated materials.

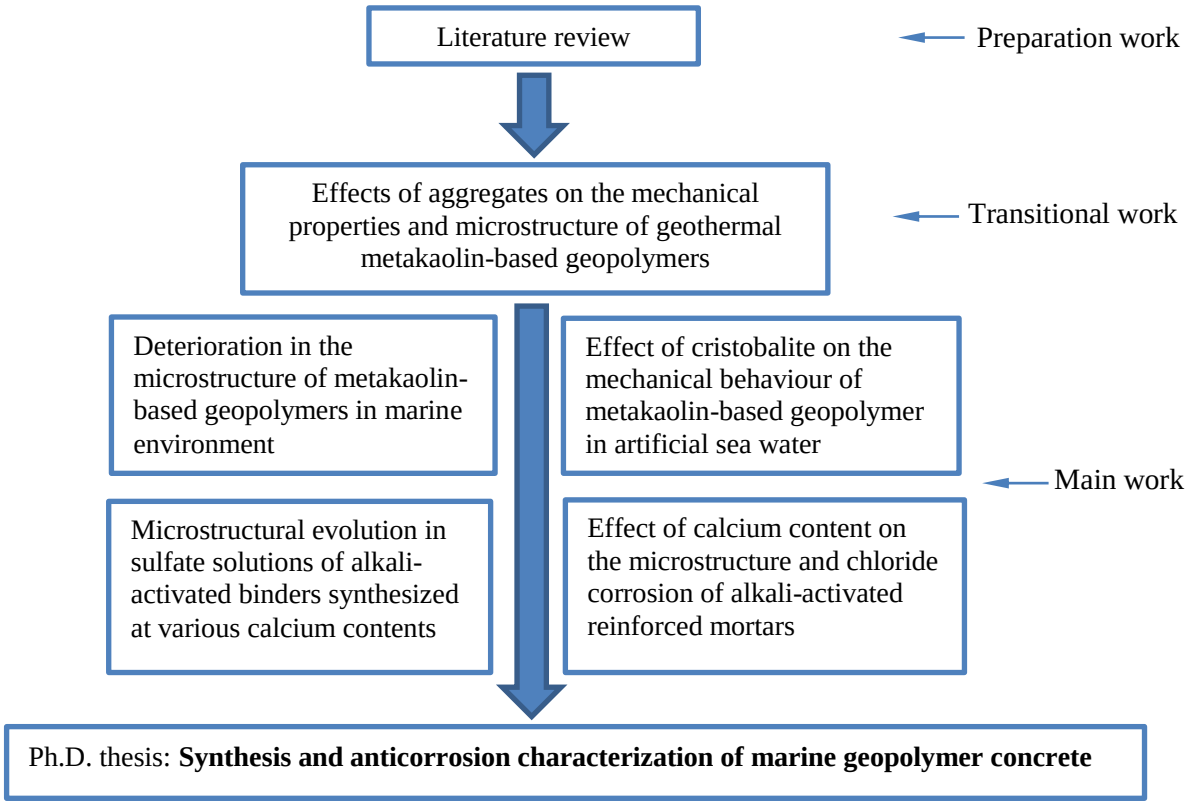

Figure 1.1. Schematic presentation of the research line

2. Literature Review

2.1. Geopolymers and alkali-activated materials

Geopolymers are aluminosilicate materials with three-dimensional (3D) amorphous micro-structures. They are formed by geopolymerization processes in which the oxides of silicon and aluminum minerals or aluminosilicate minerals are activated by alkalis to form 3D polymeric chains (Provis and van Deventer, 2009). Geopolymers are considered to be the third generation of cement after lime and ordinary Portland cement. The earliest inorganic polymer cementitious materials can be traced back to 1939 when Feret used slag in cement. And Purdon (1940) first conducted extensive laboratory research on free cement composed of slag and sodium hydroxide or slag, alkali and alkaline salt. After 1957, a systematic study by Glukhovsky and Davidovits, The alkali-activated material system has made great progress. Although Glukhovsky and Krivenko used alkali activated metallurgical slag in construction in 1950s (Glukhovsky 1994), and even some ancient structures, like the Pyramids in Egypt, are believed to be products of geopolymerization (Barsoum et al. 2006), the terms ‘‘geopolymer’’ and ‘‘geopolymerization’’ were first coined by Davidovits in 1972 (Davidovits 1999) and in the 1980s (Davidovits 1982), respectively.

Alkali-activated materials (AAMs) are also aluminosilicate minerals attacked by the alkalis and then to regroup and harden (Provis and van Deventer, 2013). The different from geopolymer is the concept of AAMs is broader. AAMs are traditionally classified into two groups (Gao et al., 2017). One type of low calcium content leads to the formation of N-A-S-H [(Na, K)$_2$O-Al$_2$O$_3$-SiO$_2$-H$_2$O] gel, which is named geopolymer (Davidovits, 1984; Provis and van Deventer, 2009). The other type of high calcium content that is mainly composed of calcium silicate hydrate (C-S-H) gel and/or C-A-S-H [(Na, K)$_2$O-CaO-Al$_2$O$_3$-SiO$_2$-H$_2$O] gel (Krivenko, 2017). In addition, calcium in AAMs also leads to the formation of other phases at given conditions, which are hydrotalcite [Mg$_6$Al$_2$CO$_3$(OH)$_{16}$·4H$_2$O] (Fernandez-Jimenez and Palomo, 2003; Ben Haha et al., 2011), Calcium sulphoaluminate monohydrate (AFm) (Ca$_4$Al$_2$SO$_{10}$·12H$_2$O) (Bonk et al., 2003; Schilling et al., 1994), zeolites of gismondine (Ca$_4$Al$_8$Si$_8$O$_{32}$·16H$_2$O) and garronite (NaCa$_3$Al$_6$Si$_{10}$O$_{32}$·13H$_2$O) (Zhang et al., 2008; Bernal et al., 2010), etc.

2.1.1. Raw materials

The performance of geopolymers can be optimized by selecting raw materials and activators, and mixing and processing different raw materials to adapt to specific environments. Most investigations directly correlated the geopolymer performance with the precursor materials such as the type of aluminosilicates and the type and concentration of alkali activators (Khale and Chaudhary 2007).

The reactivity of aluminosilicate sources depend on their chemical composition, mineral composition, morphology, fineness and glass phase content. Therefore, the stable raw materials must have the following properties: 1) highly amorphous structure and sufficient reactivity; 2) low water demand; 3) easy to release aluminum. As reported in the literature, the raw aluminosilicate materials can be broadly divided into two groups: 1) calcined materials such as fly ash, metakaolinite, slag, construction residues and pozzolanic wastes; 2) noncalcined materials such as kaolinite, feldspar, clays, and mineral processing tailings. Geopolymerization of calcined raw materials generally has faster dissolution and gelation rate that results in geopolymers, which show higher early compressive strength than non-calcined materials. This phenomenon was attributed to the fact that calcination improves the reactivity of the raw

materials by changing the crystalline structure into an amorphous structure that is easier to leach. However, geopolymers synthesized from non-calcined raw materials display a higher increase in the compressive strength in the later stage of the geopolymerization reaction. And geopolymers synthesized from a mixture of calcined and non-calcined materials benefit from the interaction between the raw materials that could activate each other and enhance the extent of the reaction to generate a high compressive strength products (Xu and van Deventer, 2002).

So far, various aluminosilicate materials such as kaolinite, feldspar, industrial solid residues such as fly ash, metallurgical slag, and mine waste residue have been used as solid raw materials for synthesis. Diaz-Loya et al. (2011) studied the mechanical properties of 25 fly ash-based geopolymers from different sources. They reported that the mechanical behavior of these geopolymer cements were similar to that of ordinary Portland cement (OPC) concrete. Xu and van Deventer (2000) used 16 natural minerals, which were classified into four crystal structure groups (ortho-, di-and ring- silicates, chain silicates, sheet silicates, and framework silicates) and six mineral groups (garnet, mica, feldspar, clay, sodalite, and zeolite), to synthesize geopolymers. They found that natural aluminosilicate minerals could be a source material for geopolymers, and the aluminosilicate frameworks show a higher extent of dissolution in alkaline solution, thus a higher compressive strength was obtained after geopolymerization, than the chain, sheet and ring structure aluminosilicates.

In addition, the type of activator also affects the performance of inorganic polymers. Glukhovsky et al., (1980) divided alkali stimulators into six categories based on their chemical composition, where M is an alkali ion: 1) alkali, MOH; 2) Weak acid salt, M_2CO_3, M_2SO_3, M_3PO_4 and MF; 3) Silicate $M_2O{\cdot}nSiO_3$; 4) Aluminate, $M_2O{\cdot}nAl_2O_3$; 5) Aluminum silicate, $M_2O{\cdot}A1_2O_3{\cdot}(2\text{-}6)\ SiO_2$; 6) Strong acid salt, M_2SO_4. Although different designs were reported, it can be concluded that alkali activators usually consists a very high alkali concentration and an optimal silicate additive (Phair et al., 2004; Cheng and Chiu, 2003; Silva et al., 2007). In most studies, the high alkali concentrations were expressed as weight ratios with respect to the raw materials, for example, metakaolinite and fly ash, or as stoichiometric concentration in the precursor solutions. For instance, Wang et al. (2005) reported that the flexural strength, compressive strength and apparent density of metakaolinite geopolymer increased with increasing NaOH concentration from 4 mol/L to 14 mol/L. They attributed this increase to the enhanced dissolution of the metakaolinite particulates at high-alkali concentrations. The effect of pH of the precursor slurry on the mechanical properties of synthesized geopolymers has also been reported. Phair and van Deventer (2001) synthesized fly ash based geopolymers and stated that the compressive strength at pH 14 was 50 times higher than that at pH 12. They observed that the geopolymer precursors remained viscous and behaved like cement at lower pH, and attained a more fluid gel composition at higher pH, which was less viscous and more workable. They found that more small silicate oligomers and monomers were formed at higher slurry pH (Phair et al. 2000). In general, researchers agreed that a higher alkali concentration prompted the geopolymerization reactions, and thus resulted in better mechanical properties of the geopolymers. However, Fernández-Jiménez and Palomo (2005a) reported from an alkali activation of a fly ash geopolymer that increasing Na_2O from 14.1 wt% to 14.9 wt% led to a reduction of the mechanical properties, although the reason was not clear. The effect of alkali concentration on the geopolymer's mechanical properties and the leaching or catalytic mechanism is still an interesting area that can be studied further. However, this effect should be studied together with the cation and anion type of the alkalis and the addition of silicate. For instance, carbonate ion

can form sodium bicarbonate that decreases the degree of geopolymerization when carbonate alkalis are utilized (Fernández-Jiménez and Palomo 2005b).

2.1.2. Effect of calcium content

Presence of calcium affects the formation of the gels in alkali-activated binders. Metakaolin and fly ash are the main low-calcium aluminosilicates for the formation of N-A-S-H. The formation is summarized as follows (Palomo et al., 2005; Fernández-Jiménez and Palomo, 2005; Duxson et al., 2007; Shi et al., 2011). The aluminosilicate is first dissolved into silica and alumina monomers in the alkaline solution. Then these monomers interact to form multimer, in which the Si^{4+} and Al^{3+} cations are connected by the oxygen bonds to form a three-dimensional (3D) skeleton. The negative charge in the skeleton is neutralized by the cations of alkaline (typically Na^+ or K^+). As reported in the literature, the alkaline activator sodium silicate (Na_2SiO_3), soluble and easily taken up into the N-A-S-H gel, is likewise considered as an origin of silicon for forming the N-A-S-H gel (Duxson et al., 2007; Criado et al., 2007). Through characterization of the ^{29}Si nuclear magnetic resonance (NMR) spectra, the N-A-S-H gel shows that all the silicon sites are in tetrahedral coordination. And the gel has a predominance cross-link density of $Q^4(nAl)$ sites ($0 \leq n \leq 4$) (Rahier et al., 1996; Barbosa et al., 2000). In addition, the N-A-S-H gel presents a very compact and uniform microstructure through scanning electron microscope (SEM). The C-A-S-H gel forms in alkali-activated calcium-rich precursors such as blast furnace slag, iron ore tailing, and other Ca-rich industrial by-products. Similar to the C-S-H gel obtained during Portland cement hydration, C-A-S-H takes up Al in its structure (Wang et al., 1995). Most researches about C-A-S-H gel in the alkali-activated slag indicate that the structure and composition depend on the used activator. The C-A-S-H in the NaOH activated slag shows a higher Ca/Si ratio and a more ordered structure than the C-A-S-H type gel formed in Na_2SiO_3 activated slag binders (Escalante-Garcia et al., 2003; Fernández-Jiménez et al., 2003a). Puertas et al. (2011) identified that C-A-S-H type gels in Na_2SiO_3 activated slag binders were likely to have a structure comparable to tobermorite-like phases. Based on ^{29}Si and ^{27}Al MAS NMR studies, Schilling et al. (1994) proposed that Al was taken up in the C-S-H gels generated in alkali-activated slag pastes, in which aluminum tetrahedral replaced silicon tetrahedral in bridging positions to give rise to Q^1, Q^2 and $Q^2(1Al)$ units.

Compared with the C-S-H gel in ordinary Portland cement (OPC) concrete, the N-A-S-H gel contains a three-dimensional structure in which the dissolved SiO_4 and AlO_4 tetrahedron randomly distributes, and the C-A-S-H gel consists of cross-linked and non-cross linked structures resembling tobermorite (Myers et al. 2013, 2014). The AAMs are usually formed of compact and homogeneous microstructure with N-A-S-H and C-A-S-H gels.

2.1.3. Other Factors

Beside the raw starting materials and alkali activators, many other factors also play an important role in the synthesis of AAMs. For instance, mechanical activation has been tested as an effective means to improve the reactivity of fly ash (Kumar et al. 2007). Temuujin et al. (2009) reported that grinding fly ash in a vibration mill with a milling media to powder ratio of 10:1 led to an 80% increase in compressive strength of the produced geopolymers when compared with geopolymers synthesized from raw material. Another study stated that (1) vibratory mill shows superiority over other mills on inducing reactivity, and (2) the fly ash reactivity varies non-linearly with median particle size in mechanical activation (Kumar and Kumar 2011). The curing time and

curing temperature are different, resulting in different compressive strengths of the geopolymers even with similar raw materials and activator. Muñiz-Villarreal et al. (2011) reported that the optimum curing temperature was 60 °C for a metakaolin geopolymer after investigating temperatures of 30, 40, 50, 60, 75 and 90 °C. Furthermore, the water content in the geopolymerization process varied widely, and the ratio of water to silicate in raw materials (H_2O/SiO_2) or the ratio of water to alkali activators (H_2O/M_2O) were tested as geopolymer synthesizing parameters.

AAMs are accepted as a new material to replace OPC. The urge to reduce emissions of carbon dioxide (1 tonne of OPC generates almost 1 tonne of CO_2) and the fact that OPC structures which have been built a few decades ago, are already facing disintegration problems points out the handicaps of OPC binders. In fact, the number of premature cases of OPC structures disintegration is overwhelming. Mehta (2005) mentioned a case of pile foundations disintegrated just after 12 years and also the case of a tunnel in Dubai, which was concluded in 1975 and needed to be completely repaired in 1986. Gjorv (1994) mentioned a study about Norway OPC bridges which indicates that 25% of those built after 1970 presented corrosion problems. Compared to OPC binders, the AAMs possess good characteristics as following: 1) low energy consumption and pollution. The raw materials of AAMs are mainly industrial waste, which is cheap and abundant. In addition, the preparation process is simple and the production energy consumption is extremely low; 2) fast setting and good mechanical properties. AAMs lose their fluidity within 2h ~ 4h and harden quickly. Generally, the strength of AAMs can reach 30 MPa after cured 7 days. 3) good durability and corrosion resistance. The AAMs have a compact structure and a good pore structure. There is no transition zone of $Ca(OH)_2$ and coarse crystals such as ettringite, so it has strong corrosion resistance and good durability; 4) low heat and high temperature resistance. AAMs are prepared at lower temperatures. Compared with ordinary Portland cement, they have less excess energy and show a lower heat of hydration.

2.2. Silica sand and steel fiber reinforced geopolymer

In OPC concrete, aggregate materials of silica sand and steel fiber are commonly used in practices, and the incorporation behavior is fully reported (Moosberg-Bustnes et al., 2004). However, the incorporation of aggregate materials in geopolymers is hypothesized to behave differently because of the alkaline activation process. For example, quartz sand was added in metakaolin-based geopolymer. Combination on quartz particle surface was found to form and associate them into geopolymer gel, so that the compressive strengths of geopolymers with only silicate and with silicate plus quartz sand were 31.2 and 52.2 MPa, respectively (Wan et al., 2017b). In another study, the drying shrinkage of metakaolin-based geopolymer was found to reduce from 8% to 1% with the addition of silica sand (38 vol%) (Kuenzel et al., 2013). In a synthesis of alkali-activated slag concrete, the addition of steel fiber (1.5 vol%) was found to improve 40% of its flexural strength (Bernal et al., 2010).

2.3. Corrosion status of marine concrete

Compared to other building materials, OPC concrete have low price and stable performance (Pang and Li, 2016; Thanapol et al., 2016). In recent years, early-stage marine structures have gradually aged and failed, causing huge economic losses and serious safety risks. The reasons for the instability of marine structures include heat-cool and dry-wet cycle, ion corrosion, steel bars

corrosion and so on (Mehta, 1990). These physical and chemical attacks lead to cracks and breakage (Mather, 1964).

Heat-cool cycle is recognized as a common factor of the crack and peeling of concrete, because the freeze of water in the concrete capillary will cause an increase in the volume (Arbi et al., 2016). Ions in the surface pores of the concrete migrate to the interior mainly through the diffusion in dry and wet cycles. Water inside the pores will evaporate in different degrees under the dry state. When the ions in the concrete pores achieve saturated concentration, the ions will crystallize and the increased stress causes the crack at the concrete (Wu et al., 2016). The dry-wet and freeze-thaw cycles will promote various chemo-physical erosions.

Gypsum and ettringite can be produced through the reaction between the invasive SO_4^{2-} from the external environment and interior hydrate of the concrete (Monteiro and Kurtis, 2003). This behavior directly causes expansion, crack and peeling of the concrete structure. Brucite is precipitated at pH of pore solution in concrete between 12.5-13.5, due to the reaction between the Mg^{2+} and calcium hydroxide. A stable brucite skin having a thickness of 30 μm was observed on a concrete surface after 4 days of soaking in sea water (Buenfeld and Newman, 1986). The Mg^{2+} in sea water erodes the C-S-H through ions exchange with Ca^{2+} which causes the deterioration.

A dense and protective passivation film is formed on the surface of the reinforcement under the alkaline pore solution in OPC, which isolates the steel bar with oxygen and moisture. The chloride in the marine migrates to the surface of the rebar through the pores and causes a pitting damage that forms a corrosion micro-battery (Shang et al., 2016). The corrosion products [$Fe(OH)_3$] of the micro-battery holds a volume as large as 4-6 times to the reactants, thereby the concrete is cracked and spalled.

2.4. Anticorrosion of alkali activated materials in sea water

In recent years, some researchers explored alkali-activated materials to serve as high anticorrosion concrete for marine structures (Jaya et al., 2017; Bayuaji et al., 2016; Seon-Ju et al., 2011; Astutiningsih et al., 2010). After exposed in simulated seawater for 12 months, the alkali-activated blast furnace slag gave good performance, with an increase in compressive strength and no corrosion of embedded steel. (Kukko et al., 1982). Zhang et al. (2010a; 2010b; 2012) used alkali-activated fiber-reinforced metakaolin/blast furnace slag as a coating for marine concrete structures, which showed a good resistance and durability under the marine environment. Compared with OPC concrete, the alkali-activated materials usually formed a compact, 3D and homogeneous microstructure with N-A-S-H and C-A-S-H gels.

2.4.1. Deterioration of geopolymer in sea water

The compact tetrahedral silica and aluminum structure of geopolymers may give concrete a protection from intrusion of corrosive ions in marine environment (Albitar et al., 2017). For example, it is reported that chloride diffusion coefficient in fly ash-based geopolymers was half of that in OPC concrete (Kwan et al., 2018). Skvara et al. (2005) immersed a fly ash-based geopolymer into 44 g/L Na_2SO_4 or 5 g/L $MgSO_4$ solutions for 720 days, and found that the mass and dimension of the geopolymers kept constant. A fly ash-based geopolymer concrete was prepared, cured in air for 28 days and then exposed in tidal zone of marine environment for 3 years, of which the compressive strength increased slightly, low chloride intrusion and steel corrosion were observed (Chindaprasirt et al., 2014). These studies provide clues for the

anticorrosion of geopolymers from intrusive ions in marine environment. But the mechanism of sea water attack on the geopolymer is not yet fully understood, primarily due to the wide range of compositions of geopolymers. Different compositions of geopolymers lead to diverse microstructures, mechanical properties and chemical properties, which are related to corrosion resistance (Duxson et al., 2007). For example, Astutiningsih et al. (2010) synthesized a metakaolin-based geopolymer concrete and a fly ash-based geopolymer concrete, and then exposed them to the sea water for 90 days. The compressive strength of the metakaolin-based geopolymer remained almost constant and the compressive strength of the fly ash-based geopolymer showed a decrease before 56 days and then remained stable. Likewise, Rashad et al. (2018) synthesized alkali-activated metakaolin using 40% quartz powder to replace metakaolin by weight. The samples with 40% quartz powder exposed to sea water for 12 months showed a 40% strength loss while the metakaolin-only samples showed a 50% strength loss. These researchers suggest that a geopolymer will gain different anticorrosion characteristics with changing compositions. Therefore, it is important to know how these compositions affect the anticorrosion characteristics of a geopolymer. Current studies on geopolymers in sea water are mainly focused on their mechanical properties and durability (Zhang et al., 2010a; Seon-Ju et al., 2011; Bayuaji et al., 2016; Jaya et al., 2017). However, few studies have focused on how the mineral compositions of the raw materials affect the mechanical properties or how a geopolymer gel evolves in sea water environments.

2.4.2. Deterioration of alkali-activated materials in sulfate solution

Many studies reported that alkali-activated binders showed high durability against sulfate attack, which was attributed to the different microstructure in N-A-S-H and C-A-S-H gels (Komljenovic et al., 2013). For example, when undergoing 32 heating-cooling cycles in 5% magnesium sulfate ($MgSO_4$) solution, compressive strength of an alkali-activated fly ash binder lost 12.7%, while that of an OPC concrete lost 17.8% (Long et al., 2017). In another comparison, after 21 days of immersion in sulfate solution, an alkali-activated fly ash mortar showed no change in appearance while the OPC mortar exhibited superficial fractures caused by the gypsum and ettringite formation (Mobili et al., 2016). However, the reported alkali-activated concretes were synthesized and cured sufficiently before immersion in sulfate solutions, while some applications require exposure of the binders in sulfate solutions during the synthesizing process, e.g., the marine concrete and underground pipes (Zhang et al., 2012; Montes and Allouche, 2012). Limited studies were contributed to the evolution in microstructure of alkali-activated binders without curing when exposing in sulfate solutions (Zhang et al., 2018; Rajamane et al., 2012). For example, Salami et al. (2017) reported that the compressive strength of an alkali-activated palm oil fuel ash based-binder decreased from 24.2 to 16.2 MPa in sulfate solutions, and the dilution of alkalis was attributed as the main reason. For another alkali-activated fly ash-based binder without curing, the geopolymer gel was destroyed and the Si was leached out when exposing in Na_2SO_4 solution (Bascarevic et al., 2015).

2.4.3. Chloride permeability of alkali-activated binder

The structure of AAMs determines penetration of chloride ions, so as the chloride-induced corrosion which usually takes place in particular environments like marine condition and when using deicing salts. Although it is supposed that the compact and low porosity structure of AAMs inhibits the diffusion of chloride ions (Kupwade-Patil and Allouche, 2013; Ganesan et al., 2015), some researchers have reported a low chloride diffusion resistance of several AAMs. For

example, Noushini et al. (2020) found well-interconnected pore structures and/or high amounts of capillary pores in a fly ash-based geopolymer concrete, so that it had the low chloride diffusion resistance and chloride binding capacity. In a study of fly ash based geopolymer exposed in saline environment for 6 years, it was found that the N-A-S-H gel and unreacted fly ash particles led to low chloride diffusion resistance (Pasupathy et al., 2017).

However, other researchers gave conflicting results on chloride diffusion resistance of AAMs when blended gel structures are present. For instance, Tennakoon et al. (2017) synthesized alkali-activated mortar with 50% low calcium fly ash and 50% high calcium slag and compared their chloride diffusion rate with OPC concrete. They reported that the alkali-activated fly ash/slag possessed higher resistance to chloride diffusion, because the slag promoted the formation of the C-A-S-H in N-A-S-H gel and the blended gel had more impenetrable structure compared with the C-S-H gel. In another preparation of alkali-activated slag/metakaolin mortars, it is found that the metakaolin forms stable space-filling the N-A-S-H in C-A-S-H gel to reduce chloride permeability. Nevertheless even when blended gel structures are present, inconsistent results are reported. Hu et al. (2019) used low fly ash partially replaced slag in the preparation of alkali activated slag/fly ash mortars. They report that the involvement of low calcium fly ash leads to high porosity N-A-S-H gel formation in the C-A-S-H gel, resulting to the increase of total porosity, so as the low chloride diffusion resistance.

3. Experimental

3.1 Materials

Table 3.1 shows the properties of raw materials, which was measured by Laser particle size analyzer (Bettersize 2000) and X-ray fluorescence (XRF, PANalytical Axios). Geothermal clay rock was collected from the Los Azufres geothermal field, Michoacan, Mexico at the depth of 250 m where the temperature exceeds 150 ℃. The rock was crushed and grinded into powder. And then it obtained reactive through limited calcination (200°C for 6 h). Metakaolin was obtained by the calcination of kaolin (Hubei province, China) at 800 °C for 6 h. Fly ash was collected from the Tianjiaan power plant, China. Slag and iron ore tailing were collected from the Zincamex metallurgy plant, Mexico. Almost no calcium was presented in geothermal clay and metakaolin. The content of CaO was medium in fly ash and high in slag and iron ore tailing, respectively. In addition, the content of Fe_2O_3 was about 25.6% and 16.7% in slag and iron ore tailing, respectively.

Table 3.1. Material properties of the raw materials.

Materials	Particle sizes (μm)			Main chemical composition (wt%)							Si/Al
	distribution	d_{50}	d_{80}	SiO_2	Al_2O_3	CaO	SO_3	K_2O	Fe_2O_3	P_2O_5	
Geothermal clay	1.66~42.72	13	27.4	67.2	15.5	0.04	7.25	7.15	1.18	1.16	3.7:1
Metakaolin	1.74~39.45	13.2	26.9	59.5	35.1	N.A.	0.15	2.56	0.97	0.05	1:1
Fly ash	9.57~72.29	30.2	65.4	49.9	28.3	8.51	2.0	1.4	5.5	1.2	1.5:1
Slag	17.52~83.17	42.1	78.3	18.5	5.5	27.6	5.1	0.6	25.6	1.7	2.9:1
Iron ore tailing	15.38~104.57	43.5	97.3	44.1	14.0	15.4	N.A.	2.8	16.7	1.4	3.2:1

Figure 3.1 shows the XRD patterns of the raw materials in the study. After calcination, kaolin was dehydroxylated to form highly active metakaolin. Geothermal clay was rich in cristobalite and kaolin, which was good material to synthesize geopolymer. Only quartz was presented in fly ash and a hump centered at approximately 27-29° 2θ. It was suggested the fly ash was highly reactive. Many crystals were presented in slag and iron ore tailing. Compared to other raw materials, they showed low reactivity.

Sodium silicate (Na_2SiO_3) and sodium hydroxide (NaOH) (ACS reagent grade) grade were purchased from Sigma-Aldrich and used as alkaline activator in the syntheses. Steel fiber was purchased from Shangta plant in Shanghai, China, which was 8.5 mm in length, 0.2 mm in diameter, and 7.9 g cm^{-3} in density. Silica sand was purchased from Zwick Roell Group, Mexico, which was in the size range of 0.3-0.6 mm and of 2.7 g cm^{-3} in density. The carbon steel bars of 6 mm in diameter, 150mm in length, and 7.82 g/cm^3 in density were used as reinforcements. The sea water was prepared with 29.25 g/L NaCl, 0.745 g/L KCl, 3.6 g/L $MgSO_4$. And the sea water in 10-fold concentration was prepared with 292.5 g/L NaCl, 7.45 g/L KCl, 36 g/L $MgSO_4$. This sea water was renewed every 7 days during the curing process. Solutions of 50 g/L Na_2SO_4 and 50 g/L $MgSO_4$ were prepared with distilled water.

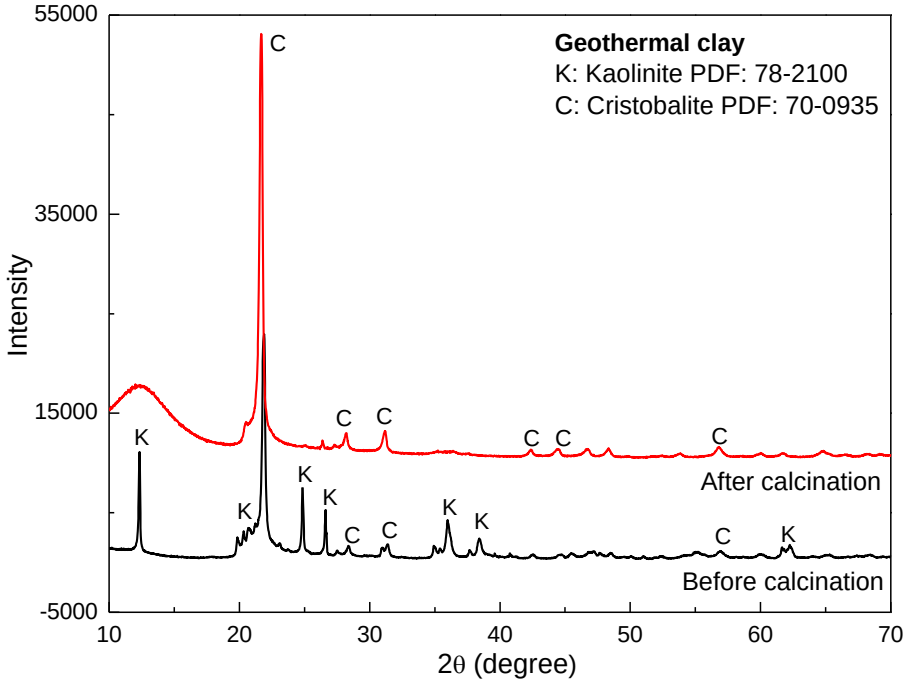

1) geothermal clay before and after calcination

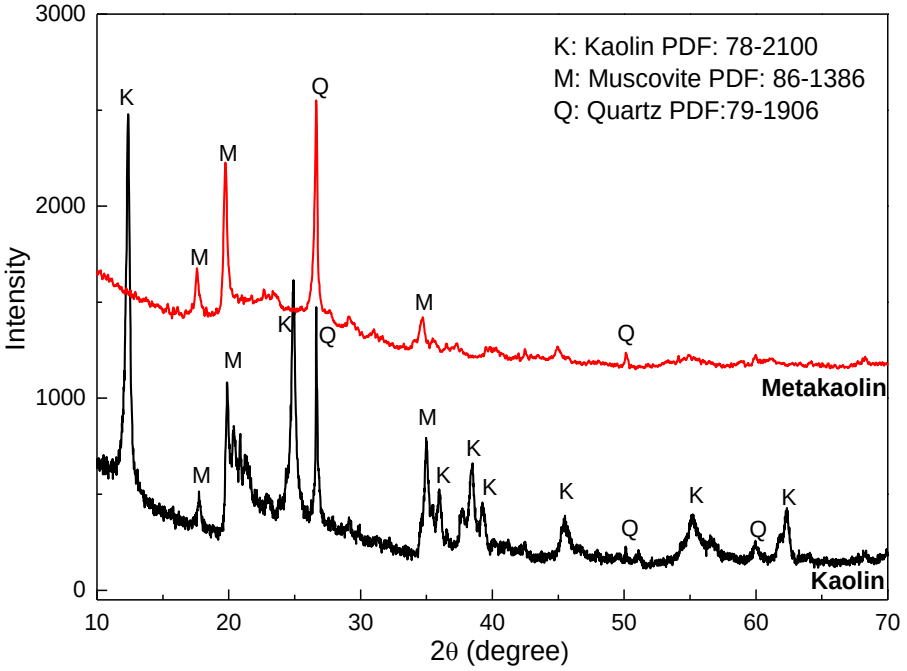

2) kaolin and metakaolin

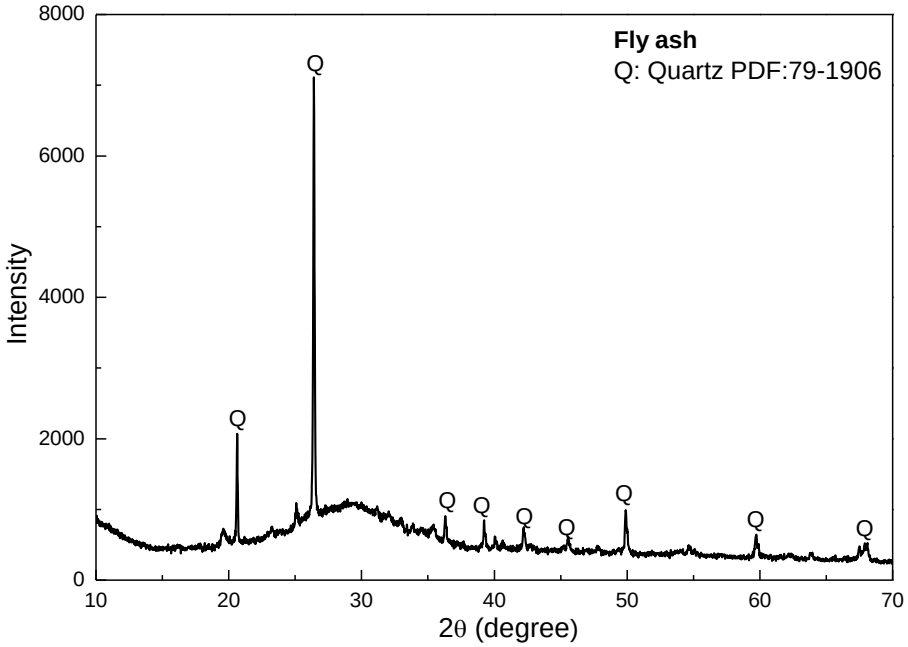

3) fly ash

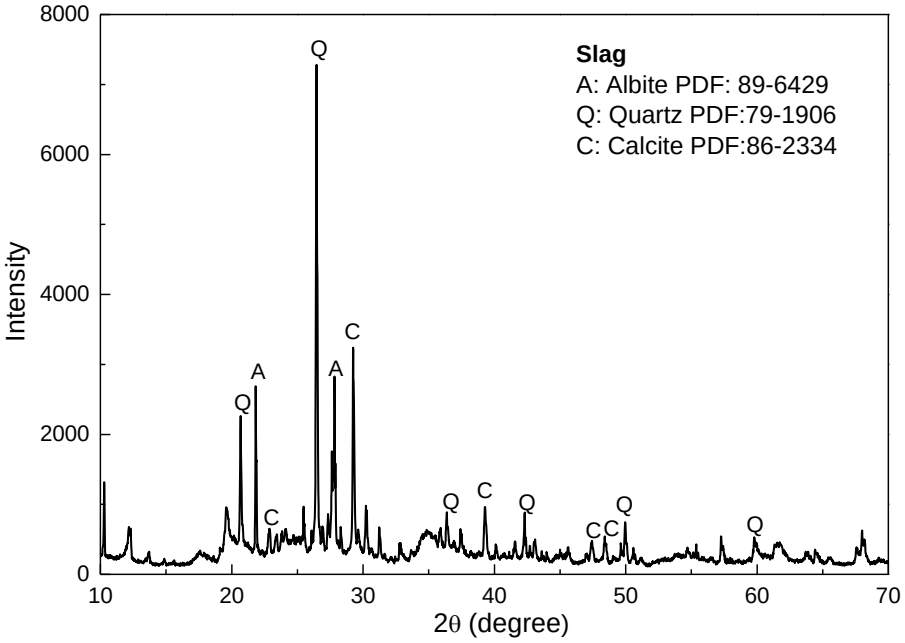

4) slag

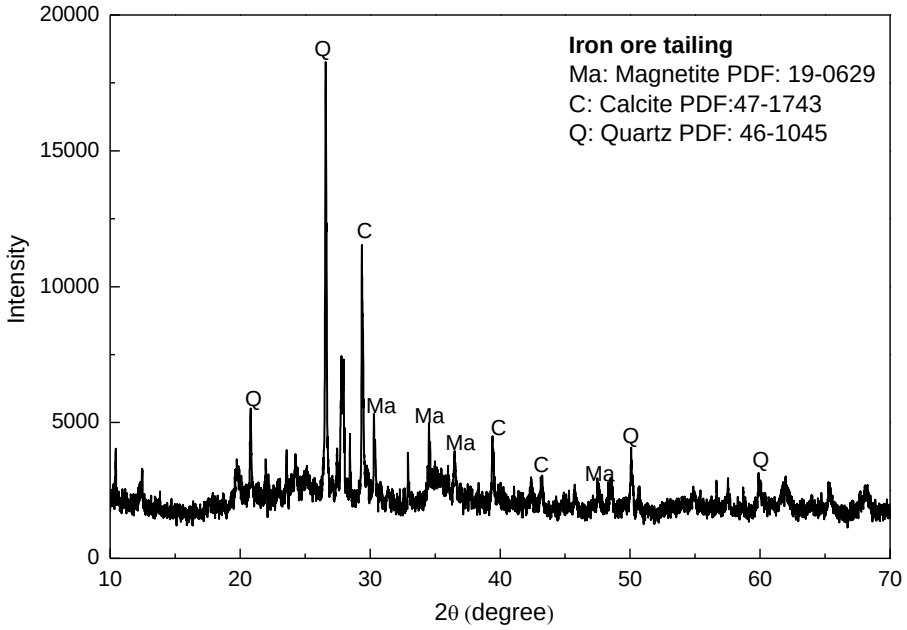

5) iron ore tailing

Figure 3.1. XRD patterns of the raw materials.

3.2 Synthesis and curing condition

In a typical synthesis, alkaline solution was first prepared and then mixed with the raw materials. The mixture was poured into a cubic steel mold (50 × 50 × 50 mm or 40 × 40 × 160 mm) and vibrated on a vibration table for 3 min to liberate the air bubbles. After that, the mold was sealed for the curing process.

Table 3.2. Preparation regimen of geothermal clay-based geopolymer concretes.

Samples	Mixtures		Steel fibers (volume fraction)	Na_2SiO_3 (mol)	NaOH (mol)	H_2O (mol)	Na/Al
	Geothermal clay (mass %)	Silica sand (mass %)					
SGC-0	100	0	0	0.50	0.25	8	1.8
SGC-1	90	10	0	0.45	0.225	7.2	1.8
SGC-2	80	20	0	0.40	0.20	6.4	1.8
SGC-3	70	30	0	0.35	0.175	5.6	1.8
SGC-4	60	40	0	0.30	0.15	4.8	1.8
SGC-5	50	50	0	0.25	0.125	4.0	1.8
SGC-5.5	45	55	0	0.225	0.113	3.6	1.8
SGC-6	40	60	0	0.20	0.10	3.2	1.8
SFGC-1	60	40	1%	0.30	0.15	4.8	1.8
SFGC-2	60	40	2%	0.30	0.15	4.8	1.8
SFGC-3	60	40	3%	0.30	0.15	4.8	1.8

In the synthesis of geothermal clay-based geopolymer, the precursor included given amounts (220 g) of geothermal clay and silica sand. As shown in Table 3.2, the Na/Al ratio in the mixture was kept at 1.8:1. In the first part, the geopolymers (SGC) were prepared with different additions of silica sand at 0, 10%, 20%, 30%, 40%, 50%, 55% and 60% additions, respectively. In the second part, the ratio of 60% geothermal clay and 40% of silica sand were selected, and 1%, 2% and 3% steel fiber were added to prepare the steel fiber geopolymer concrete (SFGC). The samples were cured at 60 °C for 6 h and room temperature for 7 days.

Table 3.3. Preparation regimen of geopolymer and curing conditions.

Sample ID	Precursor (g)	Alkaline activators(g)			Si/Na	Na/Al	Solid/liquid	Curing condition
		NaOH	Na_2SiO_3	H_2O				
M-In	Metakaolin (222)	0	122	162	1:1	1.3:1	2.1:1	-
MA								in air
MS								in sea water
MDW								in dry-wet cycles
MHC								in heat-cool cycles
G-In	Geothermal clay (222)	10	61	216	1:1	1.8:1	1.4:1	-
GA								in air
GS								in sea water
GDW								in dry-wet cycles
GHC								in heat-cool cycles

For studying the anticorrosion of metakaolin based geopolymer and geothermal clay based geopolymer in sea water, dry-wet cycle and heat-cool cycle. To obtain the optimal compressive strengths, metakaolin-based geopolymers and geothermal clay-based geopolymers were synthesized with different mix ratios. And the preparations are presented in the Table 3.3. The samples were cured at 60 °C for 6 h and room temperature for 7 days to obtain the initial strength (M-In and G-In). Then some of the specimens were analyzed as the initial geopolymer; others were exposed to one of four conditions: 1) curing in air: the geopolymer samples were kept in air at room temperature; 2) curing in sea water: the geopolymer samples were cured in artificial sea water (25±2 °C); 3) curing with dry-wet cycles of sea water: the geopolymer (MDW) samples and geothermal clay-based geopolymer (GDW) samples were cured with cycles of 12 h in air (25±2 °C) and 12 h in artificial sea water (25±2 °C); 4) curing with heat-cool cycles of sea water: the geopolymer (MHC) samples and geothermal clay-based geopolymer (GHC) samples were cured with cycles of 12 h in freezer (−15±2 °C) and 12 h in artificial sea water (25±2 °C); For each curing condition, the compressive strengths and the microstructures of the geopolymers were measured at 30, 60 and 90 days, respectively.

In the synthesis of alkali activated metakaolin, alkali activated fly ash and alkali activated slag, different dosages of alkali activator (Na_2SiO_3) were used to obtain the maximum compressive strength for the three binders, As shown in Table 3.4, the Ca/Si mole ratios were 0, 0.2:1 and 1.6:1 for the metakaolin, fly ash and slag-based binders. The samples were sealed and cured at 60 ℃ for 6 h and then slowly cooled about 18 h to room temperature (RT). Subsequently, the

binders were de-molded and exposed to three types of conditions: 1) in air at RT; 2) in 50 g/L Na_2SO_4 solution and 3) in 50 g/L $MgSO_4$ solution. For each exposure condition, the compressive strengths and the microstructures of the samples were characterized at 7, 21, 45, 60, 75 and 90 days, respectively.

Table 3.4. Preparation regimens of the alkali-activated binders and exposure conditions.

ID	Precursor (g)	Alkali activator (g)		Si/Al	Ca/Si	Liquid/ solid	Exposure conditions
		Na_2SiO_3	H_2O				
M-A	Metakaolin (222)	122	162	1:1	0	0.48	Air
M-Na							Na_2SO_4 solution
M-Mg							$MgSO_4$ solution
FA-A	Fly ash (222)	122	198	1.4:1	0.2:1	0.58	Air
FA-Na							Na_2SO_4 solution
FA-Mg							$MgSO_4$ solution
S-A	Slag (222)	36.6	54	2.8:1	1.6:1	0.21	Air
S-Na							Na_2SO_4 solution
S-Mg							$MgSO_4$ solution

Table 3.5. Preparation regimens of the alkali-activated metakaolin/iron ore tailing.

Sample ID	Precursor (g)		Tailing/ (tailing+metakaolin)	Si/Al	Ca/Si	Alkaline activators (g)	
	Metakaolin	Tailing				Na_2SiO_3	H_2O
M10T0	222	0	0	1:1	0	122	306
M8T2	177.6	44.4	0.2	1.2:1	0.06:1		
M6T4	133.2	88.8	0.4	1.4:1	0.13:1		
M4T6	88.8	133.2	0.6	1.6:1	0.21:1		

In the synthesis of alkali-activated metakaolin and iron ore tailing, the same dosage of alkali activator (Na_2SiO_3) was used. As shown in Table 3.5, the samples of M10T0, M8T2, M6T4 and M4T6 represented the mixtures of 100%, 80%, 60% and 40% of metakaolin, respectively. They were sealed and cured at 60 ℃ for 6 h and room temperature for 28 days to obtain enough mechanical property and compact microstructure. The series of samples of 50 × 50 × 50 mm were prepared for measurements in mechanical property, while the samples of 40 × 40 × 160 mm were reinforced with a rebar embedded in their centre and used for electrochemical measurements and microstructure, as shown in Figure 3.2 (a). The exposed length and surface area of rebar were 130 mm and 2449.2 mm^2, respectively. For the measurements, a copper wire was soldered to one end of the reinforcement. Epoxy coating was covered on the ends of the rebar to reduce crevice corrosion.

Figure 3.2 (b) presented the system of accelerated corrosion. The samples were immersed in seawater and connected with the external cathode. A stainless steel plate was contacted with the external anode in direct current (DC) power supply. A sustaining voltage of 3 V between the

external anode and the external cathode was applied in order to accelerate the migration of chloride ions. The accelerated corrosion lasted for 160 days. Prior to electrochemical measurements, power supply was temporarily interrupted for 24 h in order to achieve a stable steel surface condition. As shown in Figure 3.2 (c), the classical three-electrode system was employed for the electrochemical measurements in Chi760 Potentiostat (Chenhua, Shanghai, China). A saturated calomel electrode (SCE) and a stainless steel plate were used as the reference electrode and the counter electrode, respectively. The linear polarization test uses a potentiodynamic polarization method with a scan range of -10 mV to +10 mV and a scan rate of 10 mV/min. Through the test, the linear polarization curve of the steel bar electrode in the mortar sample can be obtained. The polarization resistance value R_p can be obtained by linearly fitting and calculating the curve. Thereby the corrosion current density i_{corr} is calculated as the Stern-Geary equation (Stern and Geary; 1957).

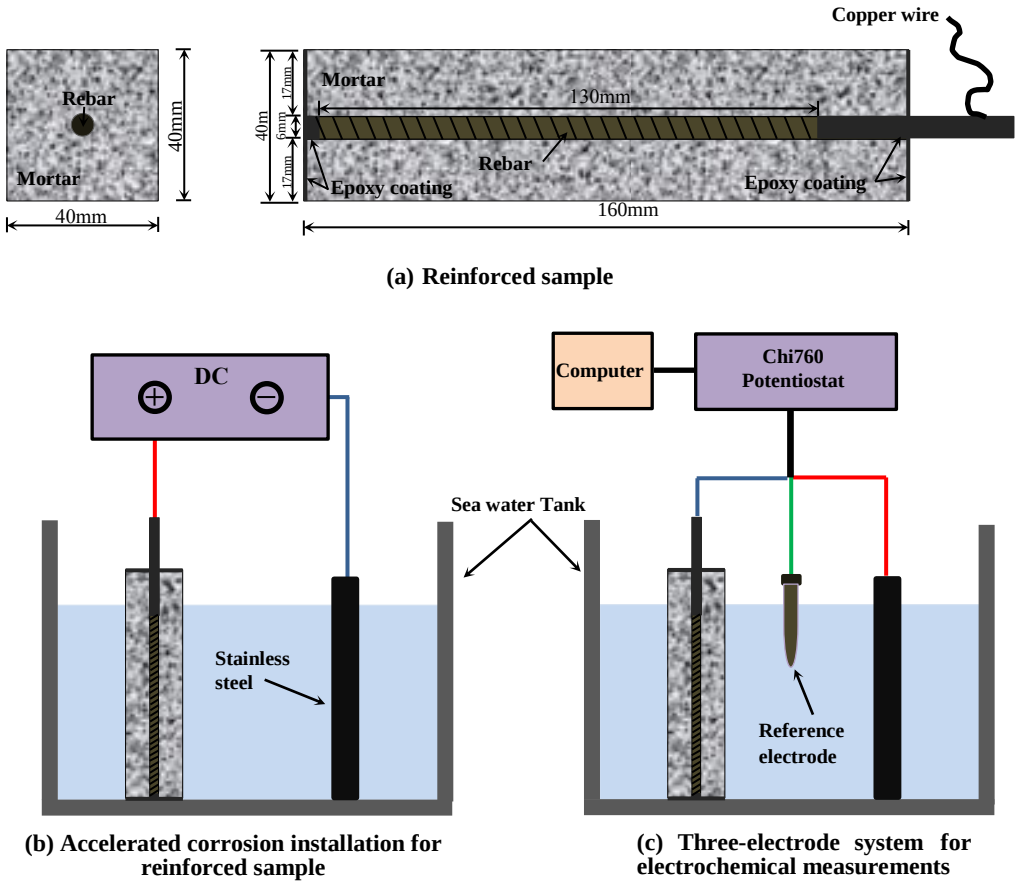

Figure 3.2. Schematic diagrams of electrochemical measurement

3.3 Characterization

The compressive strength values of the alkali-activated material samples were measured with Zwick/Roell, Zwick Z100 mechanical tester from Zwick/Roell Zwick GmbH & Co. KG, Germany. In each group of measurements, the average value was obtained from at least three samples. pH values was measured by pH-meter (FE28-standard, Mettler Toledo, Switzerland). Fourier-transform infrared (FTIR) spectroscopy (Nexus, Thermo Nicolet, USA) was used to

identify the geopolymer gel in the binders. The transmittance spectra were gathered over a wave number range of 40 to 4000 cm^{-1} with a resolution of 2 cm^{-1}. Scanning electron microscope (SEM, JEOL JSM-5610LV) equipped with energy dispersive X-ray (EDX) analyzer was used to observe the microstructure of the geopolymers. The multipoint Brunauer, Emmett, and Teller (BET) surface area, pore volume and pore size of the geopolymers were measured using a fully automated analyzer from Quantachrome Instruments, USA of model Nova Touch 1 F. ^{29}Si nuclear magnetic resonance (NMR) spectra of geopolymers were obtained by using a NMR spectroscopy (Bruker AVANCE III) at 79.49 MHz. The powder specimens were packed into 7 mm ZrO_2 rotors. Spectra were acquired at spinning speeds of 5 kHz with peak positions referenced to an external standard of tetramethylsilane (TMS) and recorded with 5 s delay time.

4. Results and Discussion

4.1. Effects of aggregates on the mechanical properties and microstructure of geothermal metakaolin-based geopolymers

4.1.1 Role of silica sand in the geothermal metakaolin-based geopolymers

Figure 4.1.1 gives the compressive strength of the geopolymers synthesized with various silica sand additions. Without silica sand, the compressive strength was 37.89 MPa. It suggests that geothermal clay possesses higher activity than normal clay (e.g., kaolinite) in alkaline activation reactions, because limited calcination (200 ℃ for 6 h) induced satisfactory compressive strength for the binder. With addition of 10% silica sand, compressive strength of the geopolymer decreased slightly to 35.66 MPa. And then, the compressive strength kept a plateau as increasing silica sand to 50%. These results indicate that geothermal clay-based geopolymers was formed through the incorporation of silica sand into geopolymer gel. However, the compressive strength decreased sharply to 26.67 and 19.6 MPa as increasing silica sand additions to 55% and 60%, respectively. At silica sand additions higher than 50%, the formed geopolymer gel was not enough to maintain high compressive strength of the binders.

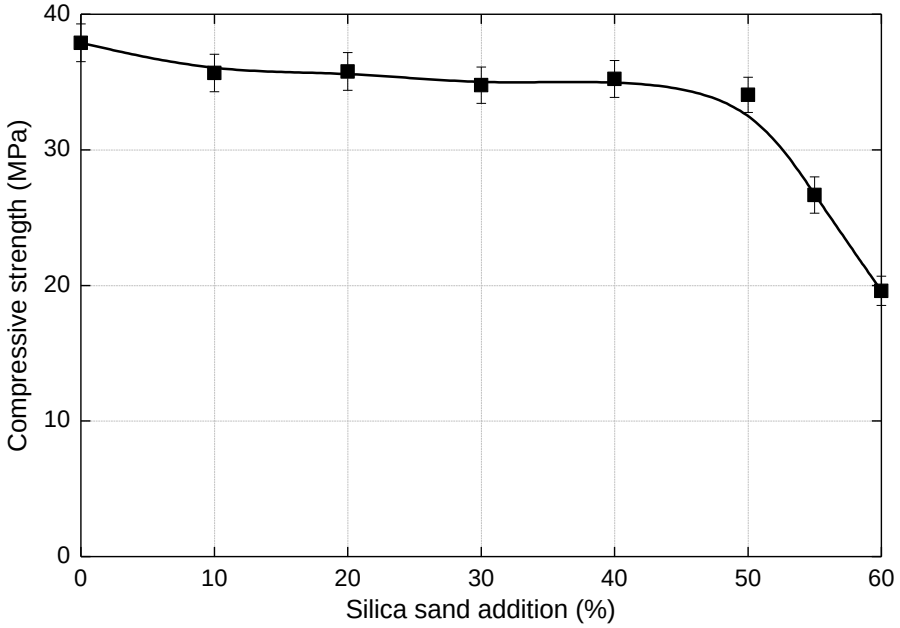

Figure 4.1.1. Compressive strengths of geothermal metakaolin-based geopolymers at various silica sand additions.

Figure 4.1.2 shows the XRD patterns of the geopolymers synthesized with various silica sand additions. Without silica sand, the concrete presents featureless amorphous diffraction pattern with one hump centered at approximately 27-29° 2θ, which represents the geopolymer gel, as well as some peaks of cristobalite and alunite, which are from the geothermal clay. With addition of moderate silica sand (20% and 50%), the peak of quartz becomes distinct and that of albite appears, suggesting that silica sand is not dissolved in alkaline activation reactions. With high amounts of silica sand additions (55% and 60%), the geopolymer gel hump becomes unclear, suggesting that the ratio of formed geopolymer gel decreased sharply. Furthermore, trona was formed at high silica sand additions (50%, 55% and 60%), which suggests the excess of alkalis in these conditions. In summary, silica sand is undissolved during the alkaline activation reactions,

so that a high amount of silica sand addition results in low ratio of geopolymer gel, leading to the excess of alkalis and a sharp decrease of the compressive strength (Figure 4.1.1).

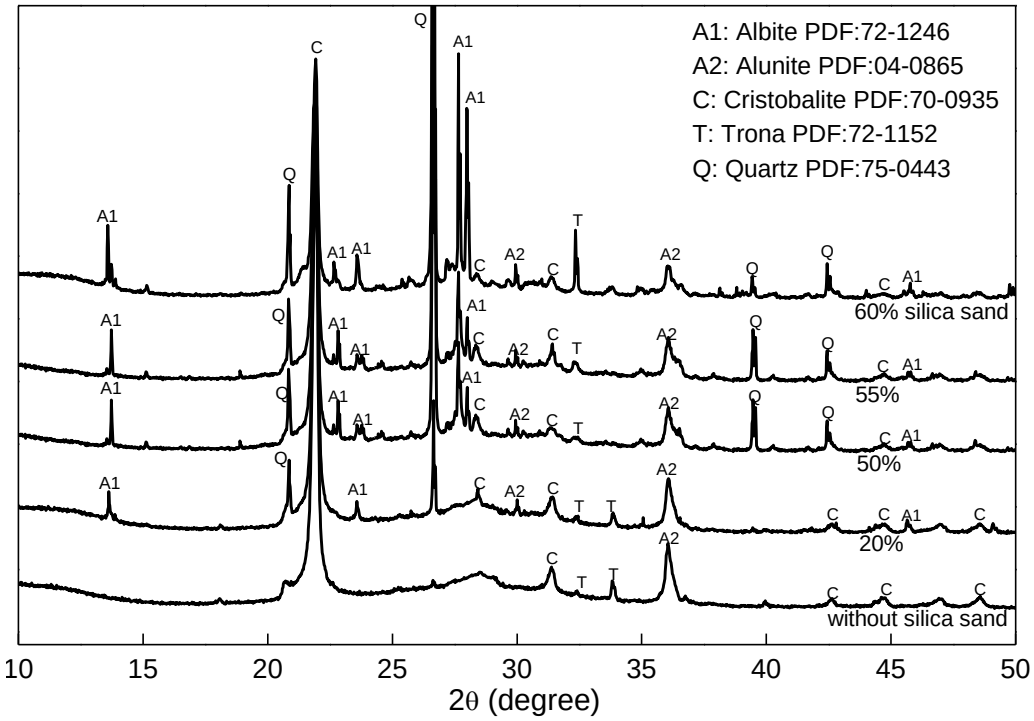

Figure 4.1.2. XRD patterns of the geothermal metakaolin-based geopolymers synthesized with various silica sand additions.

The change in compressive strength of the geopolymers synthesized with different silica sand additions may be attributed to their porous structure. Table 4.1.1 presents the porous characteristics of the geopolymers with various silica sand additions. The pore radius increased as increasing silica sand additions, and macropores were formed at 55% and 60% of silica sand. As increasing silica sand from 0 to 50%, specific surface area and pore volume of the concrete increased slightly, suggesting that silica sand induced pores in the geopolymers, so the compressive strength decreased on a small scale. As increasing silica sand continually to 55% and 60%, the specific surface area and pore volume decreased dramatically because of the formation of macropores, which also caused the sharp decrease in compressive strength (Figure 4.1.1).

Table 4.1.1. Physical characteristics of geothermal metakaolin-based geopolymers synthesized with various silica sand additions.

Samples	SGC-0	SGC-2	SGC-5	SGC-5.5	SGC-6
Silica sand (mass %)	0	20	50	55	60
Specific surface area ($m^2\ g^{-1}$)	10.10	11.23	13.81	6.37	3.21
Pore volume ($cm^3\ g^{-1}$)	0.0798	0.0937	0.1358	0.0279	0.0222
Pore radius (nm)	14.60	40.82	45.12	62.09	71.81

Figure 4.1.3 shows morphologically the porous structure of the geopolymers synthesized with various silica sand additions in SEM images. Holes were formed in all images after shedding the cristobalite and silica sand particles in preparing the specimens. And in comparison, geopolymer of homogeneous binder structure was formed without silica sand addition. With increasing silica sand addition to 20% and 50%, pores and cracks are observed and increased. With silica sand addition of 55%, the cracks become larger and much obvious. It corresponds well with the physical characteristics of the geopolymers.

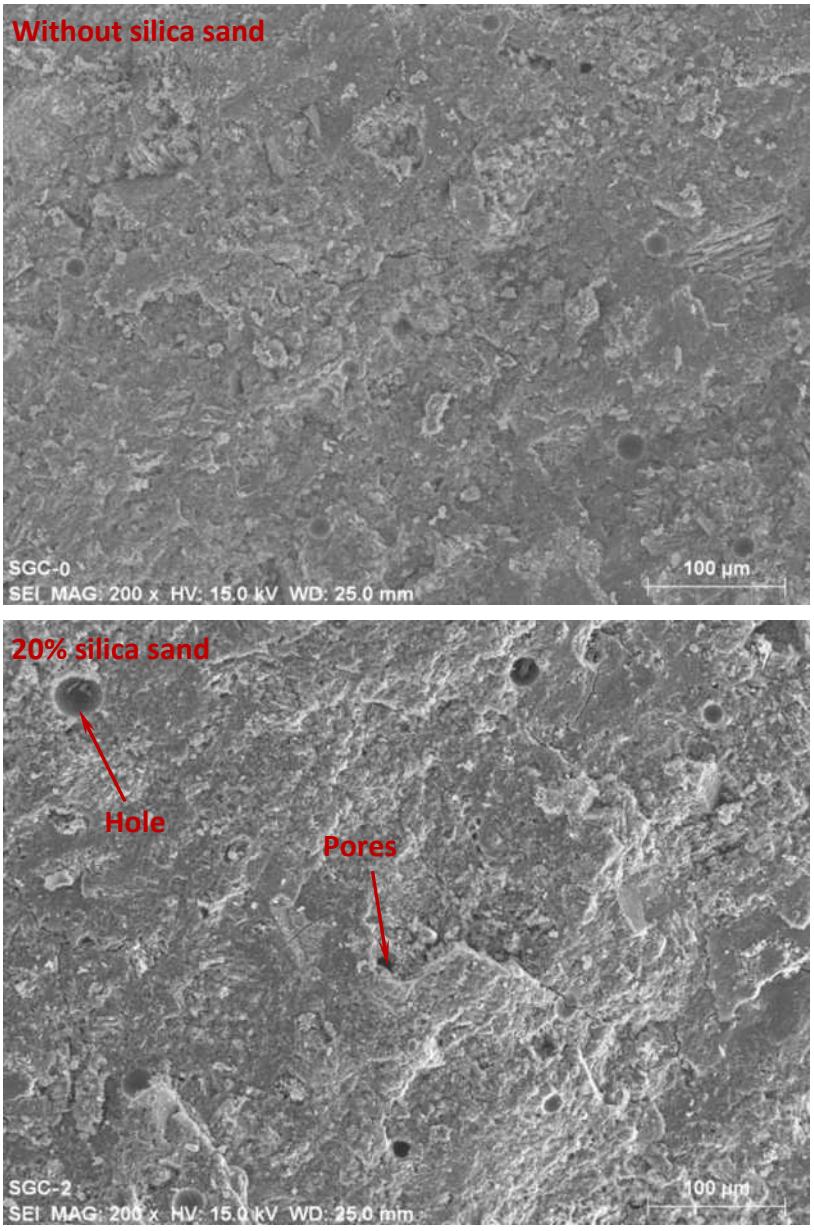

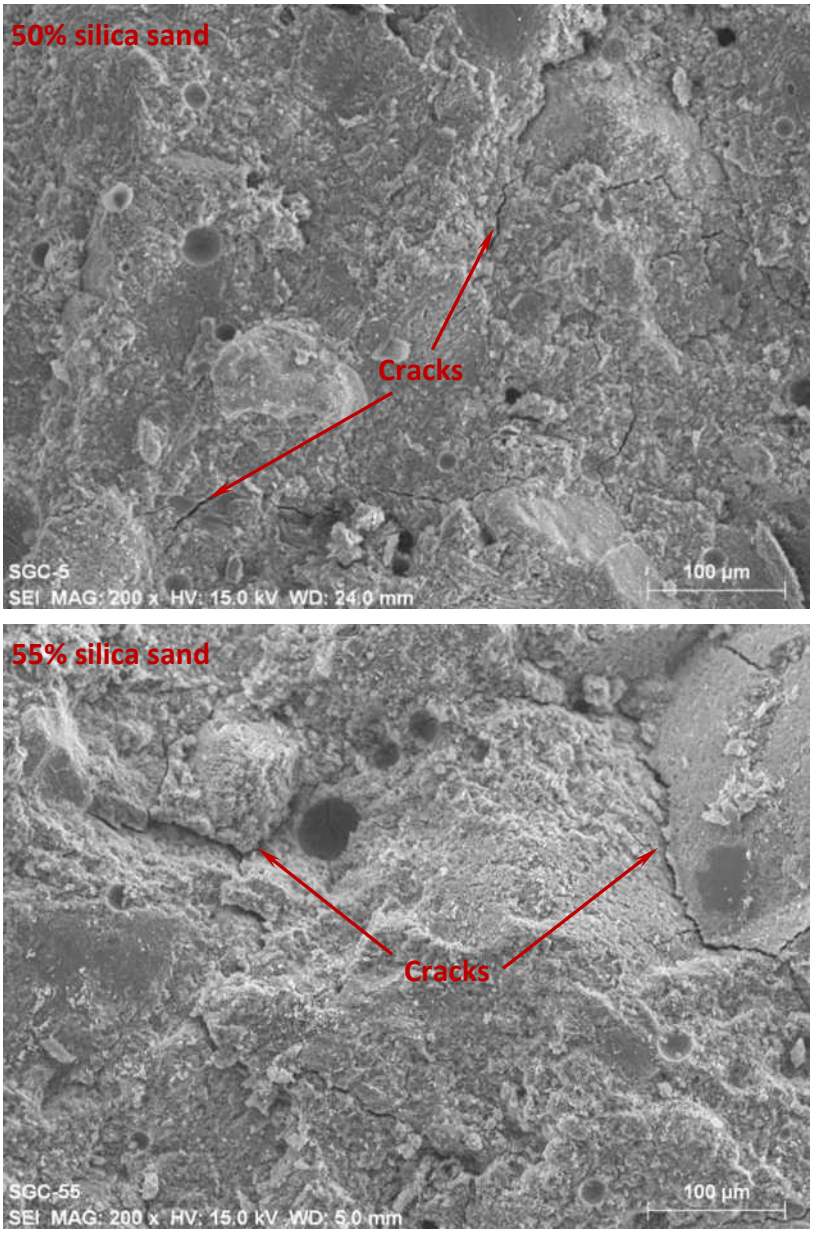

Figure 4.1.3. SEM images of geothermal metakaolin-based geopolymers synthesized with various silica sand additions.

Some reports stated that compressive strength of alkali-activated geopolymer concrete was enhanced by nano- and micro- silica sand (Kuenzel et al., 2013; Shaikh and Haque, 2017). But in this study, compressive strength of the geopolymer concrete decreased slightly with addition of silica sand (<50%). As reported previously (Wan et al., 2017b), silica sand of different size ranges induced different effects on the mechanical properties of metakaolin-based geopolymer. The dissolution of sand surface and the formation of polysiloxo (-Si-O-) combination associated it into geopolymer gel and reinforced the metakaolin-based geopolymer. This reinforcement was optimal at particles size range of 32-75 µm, while particles of big size (180-240 µm) are difficult to be combined into geopolymer gel because the formation of combination was in nanometers and insufficient to combine big particles. Therefore, the silica sand of size range in 0.3-0.6 mm induced a slight decrease in compressive strength of the concrete as increasing its ratio from 0 to

50%. However, the dissolution of silica sand and formation of combination can also be evidenced through NMR measurements. Figure 4.1.4 gives the ^{29}Si NMR spectra of the geopolymer gel and their deconvolution, which adopted Gaussian peak deconvolution to separate and quantify $Q^n(mAl)$ species ($0 \leq m \leq n \leq 4$) (Lee and Stebbins, 1999). In geopolymer gel, all the silicon and aluminum site were in tetrahedral coordination, so n = 4 (Rahier et al., 1996). And the resonance of a $Q^4(mAl)$ center with the replacement of each aluminum by silicon is an approximate -5 ppm chemical shift, with $Q^4(4Al)$, $Q^4(3Al)$, $Q^4(2Al)$, $Q^4(1Al)$, $Q^4(0Al)$ resonating at approximately -84, -89, -93, -99 and -108 ppm, respectively (Engelhardt and Michel, 1987). Without silica sand, the *$Q^4(4Al)$*, sum of *$Q^4(3Al)$*, *$Q^4(2Al)$* and *$Q^4(1Al)$*, and *$Q^4(0Al)$* in geopolymer gel were 9%, 71.4% and 19.6%, respectively. With increasing silica sand to 60%, the *$Q^4(0Al)$* kept almost the same at around 20%. While the *$Q^4(4Al)$* were converted into *$Q^4(3Al)$*, *$Q^4(2Al)$* and *$Q^4(1Al)$*, of which the *$Q^4(4Al)$* decreased to 8.4%, 5.7%, 5.4% and 3.9% at 20%, 50%, 55% and 60% of silica sand, respectively. It suggests that more tetrahedral silicon was formed as increasing silica sand, which is attributed to the dissolution of silica sand and combination formation on its surface.

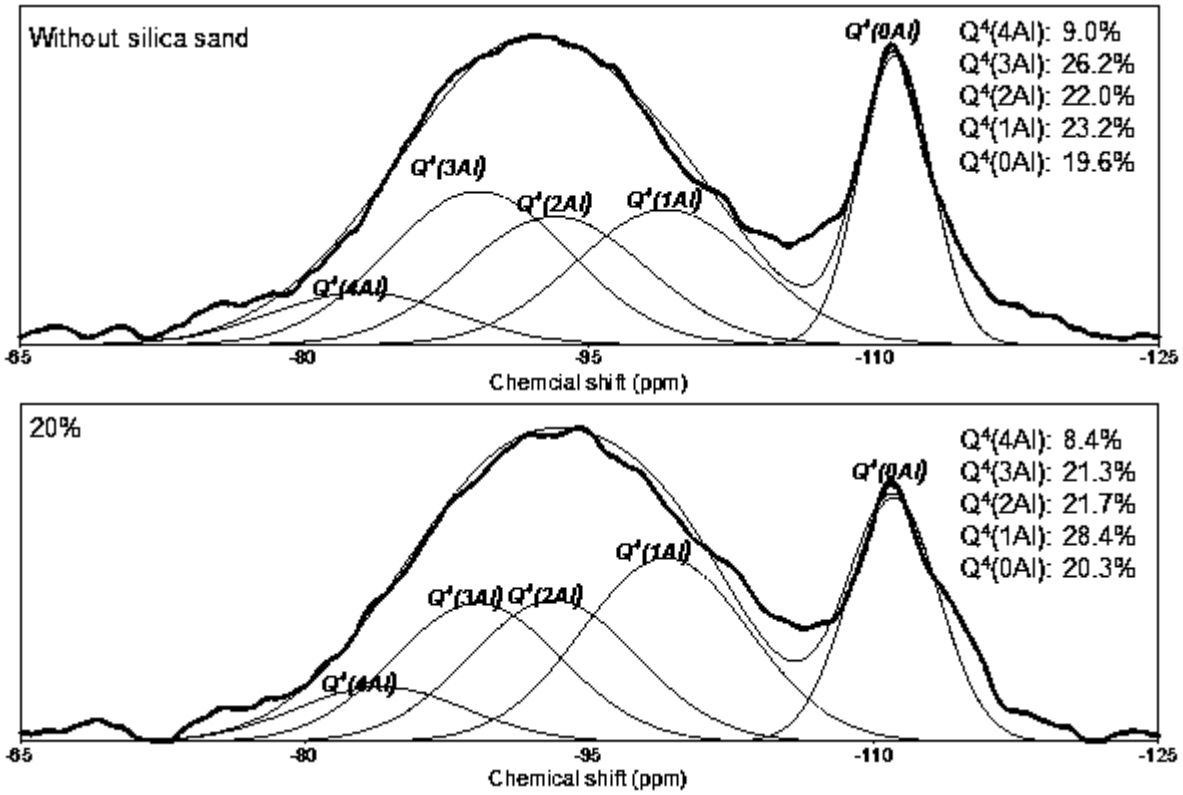

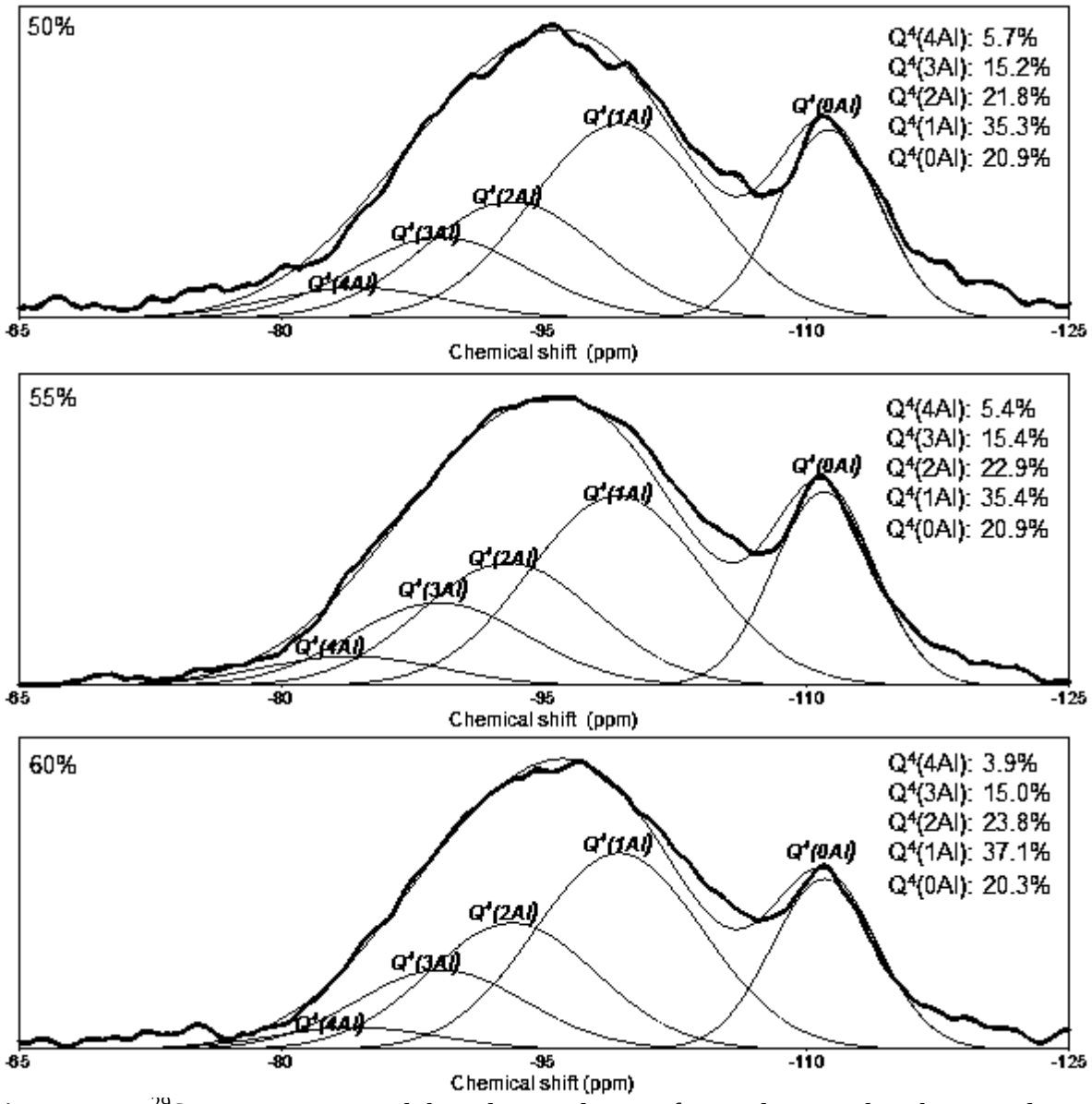

Figure 4.1.4. ^{29}Si NMR spectra and their deconvolution of geopolymer gel in the geopolymers synthesized with various silica sand additions.

4.1.2 Role of steel fiber in geothermal metakaolin-based geopolymers

Table 4.1.2 gives the mechanical properties of the geopolymers synthesized with various steel fiber additions. Compressive strength of the geopolymers remained around 35 MPa with additions of 1%, 2% and 3% steel fiber in volume fractions, indicating that steel fiber has negligible effect on compressive strength of the geopolymers. While the flexural strength increased steadily from 3.1 MPa to 3.19, 3.36 and 3.6 MPa as increasing steel fiber from 0 to 1%, 2% and 3% in volume fractions, respectively. However, because of the short curing time (7 days) of the geopolymers, this increase was small compared with the reported study elsewhere (Bernal et al., 2010).

Table 4.1.2. Mechanical properties of the geopolymer concrete with various steel fiber additions (the standard deviation is about ±10%).

Steel fiber (vol%) / Mechanical properties	0	1	2	3
Compressive strength (MPa)	35.33	34.65	35.22	34.01
Flexural strength (MPa)	3.1	3.19	3.36	3.6

Figure 4.1.5 gives the FTIR spectra of geothermal metakaolin-based geopolymers synthesized with various steel fiber additions. The absorption peaks at 3450 cm^{-1}, 1650 cm^{-1} and 1454 cm^{-1} are OH- stretching vibrations, H-OH bonds of free water and asymmetric stretching of O-C-O bonds in CO_3^{2-} groups, corresponding to the adsorbed water and carbonation during curing process (Wan et al., 2017a). The plural at 795 cm^{-1}, 696 cm^{-1}, 621 cm^{-1} and 476 cm^{-1} represent O-Si-O bonds in quartz, Si-O and Al-O bonds in unreacted kaolinite, and zeolite framework in the geopolymer (Hajimohammad et al., 2008; Mostafa et al., 2001). And the band around 1000 cm^{-1} represents the Si-O-T bonds (T is tetrahedral Si or Al) in geopolymer gel, showing tiny difference at different steel fiber additions. It suggests that steel fiber affect negligibly the geopolymer gel formation in the geopolymers, so does the compressive strength (Table 4.1.2).

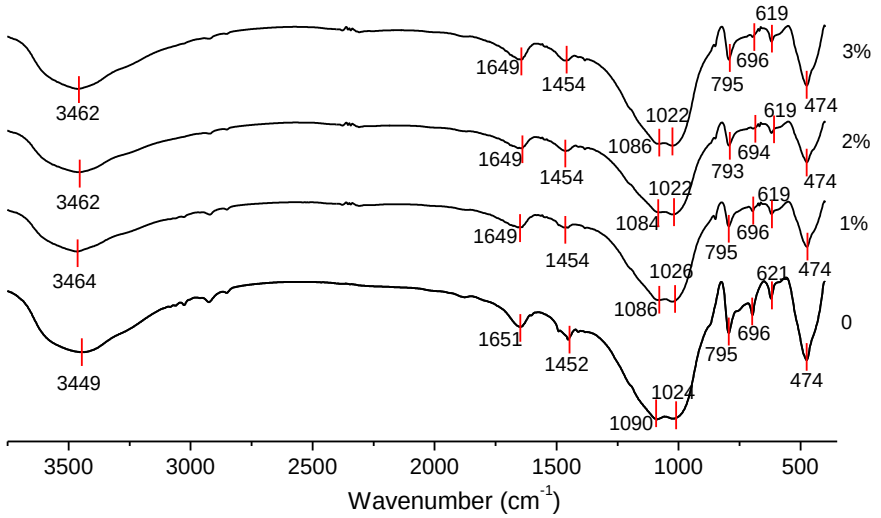

Figure 4.1.5. FTIR spectra of the geopolymer synthesized with 0, 1%, 2% and 3% steel fiber in volume fractions.

Figure 4.1.6 shows morphologically the incorporation of silica sand, geopolymer gel and steel fiber in the geopolymer in SEM image, in which the component materials were determined by element analysis through EDX. The geopolymer gel functions as binder material for silica sand and steel fiber. And cracks along with steel fiber are larger than those with sand. It can be observed the formation of combination on silica sand surface.

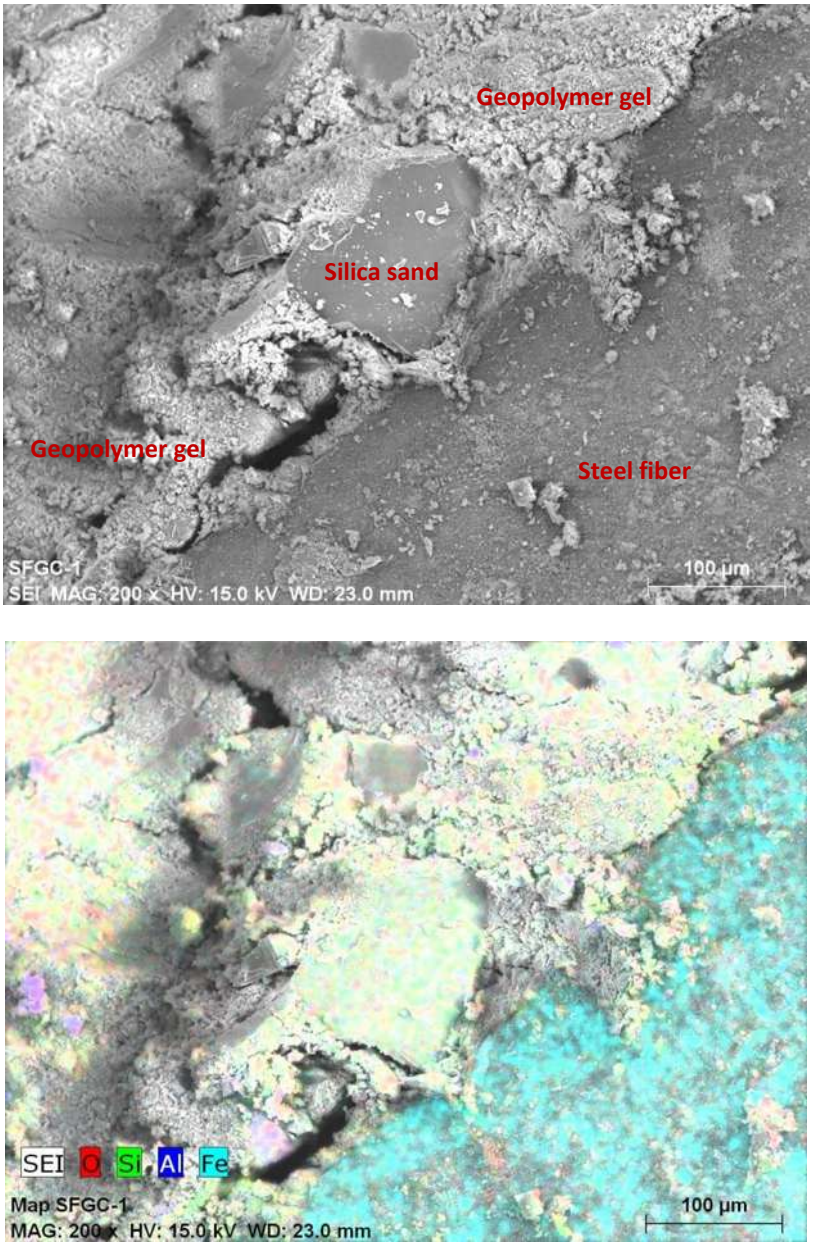

Figure 4.1.6. SEM images of silica sand, geopolymer gel and steel fiber in the geopolymer.

Figure 4.1.7 shows the load-deflection of geothermal metakaolin-based geopolymers synthesized at various steel fiber additions. The ultimate load and deflection increase as increasing steel fiber fractions and the post curves tend towards gently, which indicates the failure mode of the geopolymers was changed from brittle to ductile. It is in good agreement with the load-deflection curves in synthesizing steel fiber reinforced OPC concrete and fly ash-based geopolymers with micro steel fiber (Barr et al., 1982; Ranjbar et al., 2016). And the total area under the load-deflection curve increases with the addition of steel fiber. According to ASTM C1018-85 (USA), this area represents the flexural fracture toughness of the concrete. Therefore, the toughness of geothermal clay-based geopolymer concrete was reinforced by steel fiber, which might be attributed to the formation of bridge in the crack and more tortuous crack propagation path.

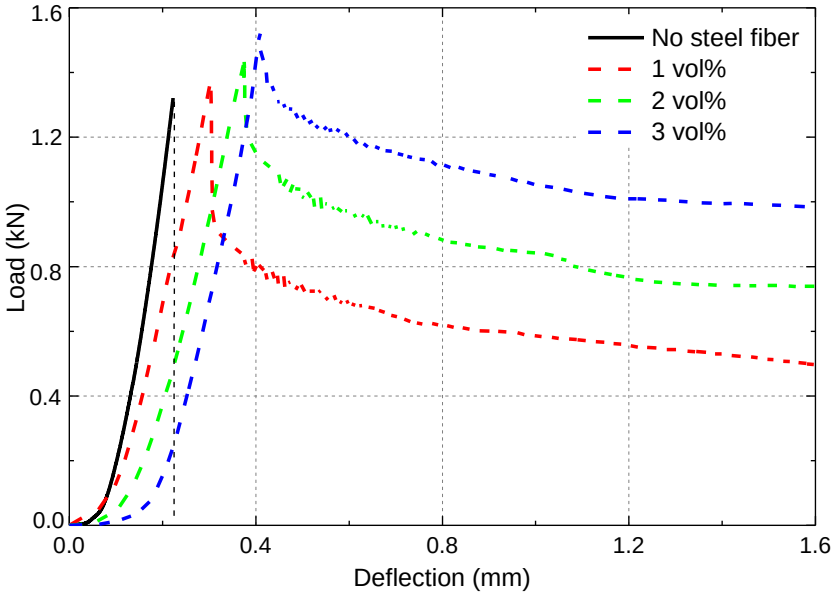

Figure 4.1.7. Load-deflection of the geopolymers at various steel fiber additions.

4.2. Deterioration in the microstructure of metakaolin-based geopolymers in marine environment

Figure 4.2.1 gives the compressive strength of the geopolymers exposed in various conditions. The initial geopolymers cured at 7 days had a compressive strength of 48.7 MPa. For the exposure in air, the compressive strength increased steadily to 54.5, 58.4 and 59.4 MPa at 30, 60 and 90 days, respectively. Such a high compressive strength suggests that metakaolin obtained through the calcination of geothermal clay has a high activity in the geopolymerization reactions (Wan et al., 2017c; Pandey et al., 2017). For the exposure in sea water, the compressive strength decreased significantly to 32.1 MPa at 30 days, which may be attributed to the dilution effect of sea water in geopolymerization reactions (Zhang et al., 2010a; Bascarevic et al., 2015; Bakharev, 2005; Rashad et al., 2018). Then it increased slightly to 33.6 and 35.0 MPa at 60 and 90 days, respectively, indicating the slow rate of geopolymerization reactions in sea water. For the exposure in dry-wet cycle, compressive strength of the geopolymers decreased steadily to 43.3, 41.4 and 38.9 MPa at 30, 60 and 90 days, respectively. For the exposure in heat-cool cycle, the compressive strength decreased more than that in dry-wet cycle, which was eventually of 33.1 MPa at 90 days. The compressive strengths of dry-wet and heat-cool cycles suggest the deterioration in mechanical properties of the metakaolin-based geopolymers in simulated marine conditions, which is in agreement with the report of OPC concrete (Liu et al., 2015).

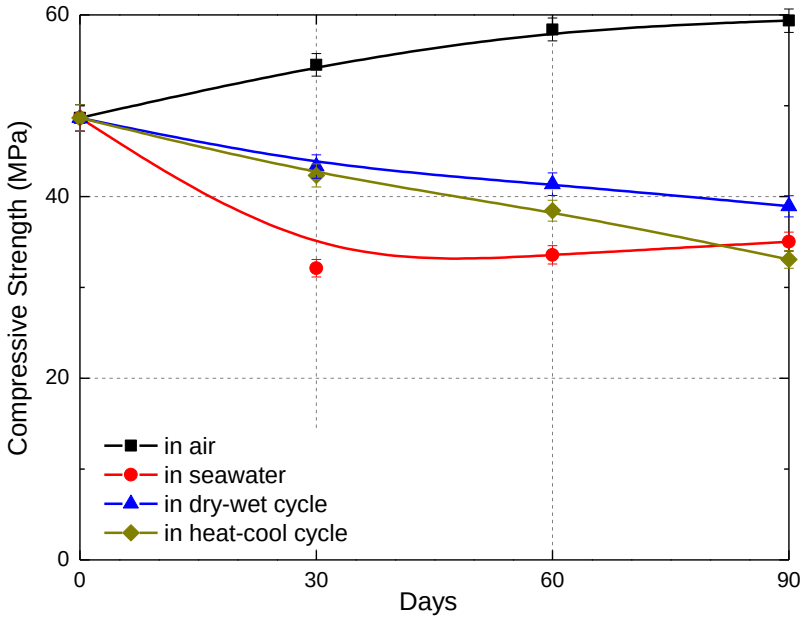

Figure 4.2.1. Compressive strengths of the metakaolin-based geopolymers exposed differently.

Figure 4.2.2 shows the SEM images of the geopolymers exposed in air, sea water, dry-wet and heat-cool cycles for 90 days. All the geopolymers show homogeneous binder structures, suggesting the sea water environment only influence the formation of metakaolin-based geopolymers moderately. However, halite precipitation is observed on the geopolymer exposed in sea water. The geopolymer exposed in dry-wet cycle shows small cracks along the cristobalite particle, and the geopolymer exposed in heat-cool cycle shows larger cracks in binder. The precipitation of halite and the formation of cracks may be the reasons for the lower compressive strengths of the geopolymers (Figure 4.2.1).

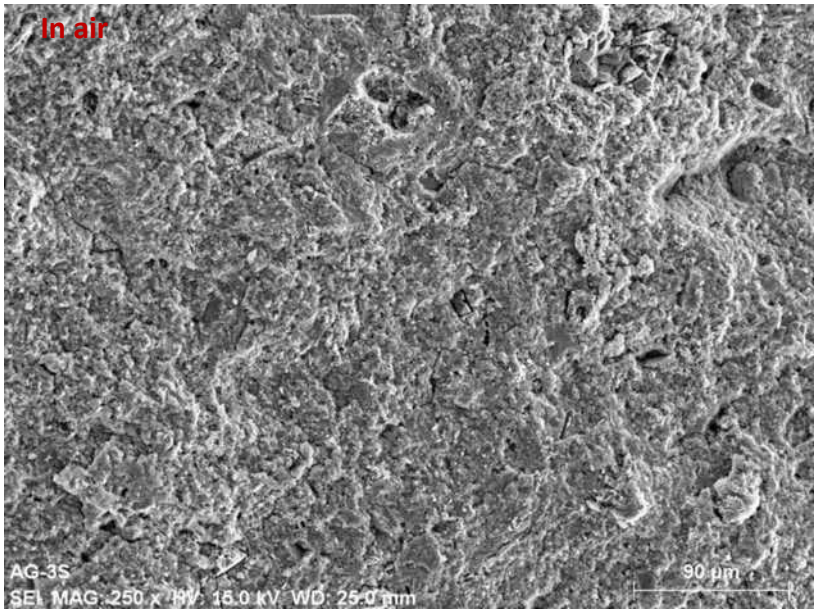

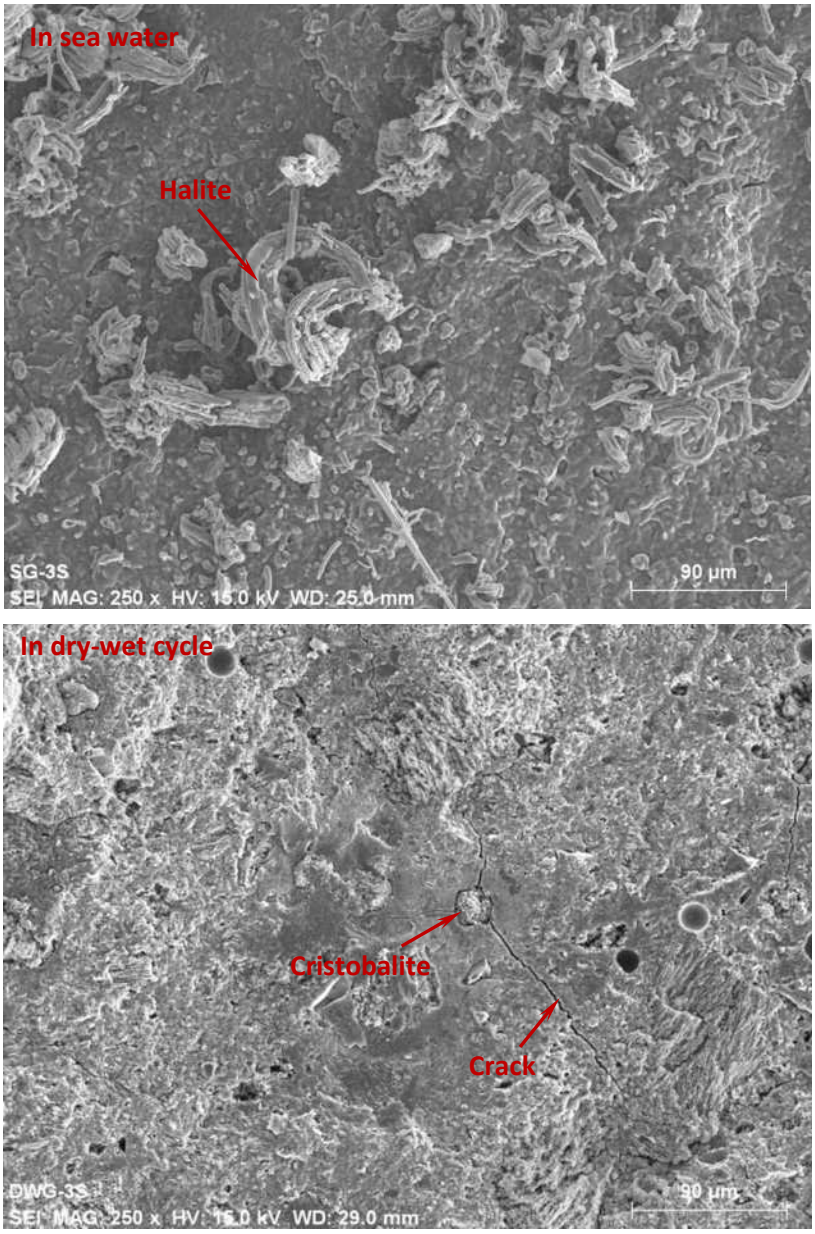
In sea water
Halite
SG-3S
SEI MAG: 250 x HV: 15.0 kV WD: 25.0 mm
90 μm
In dry-wet cycle
Cristobalite
Crack
DWG-3S
SEI MAG: 250 x HV: 15.0 kV WD: 29.0 mm
90 μm

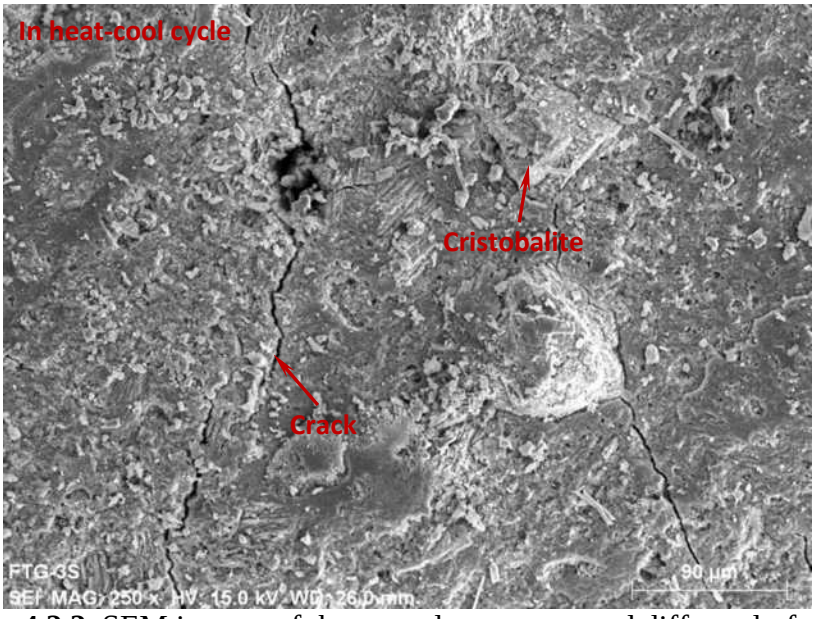

Figure 4.2.2. SEM images of the geopolymers exposed differently for 90 days.

Figure 4.2.3 presents the XRD patterns of the geopolymers exposed differently for 90 days, in which the XRD pattern of the initial geopolymer is given as a comparison. The hump of geopolymer gel centered at approximately 27-29 °2θ is featureless for these geopolymers, which may be attributed to the noise of high cristobalite content in the geothermal clay. The cristobalite and the trona are observed in the initial geopolymer. The cristobalite in the raw geothermal clay maintain after 90-days exposure in the four types of conditions, indicating its inert property in geopolymerization reactions. The formation of trona is attributed to the high alkali concentration and carbonation in the syntheses. It therefore disappears after exposure under sea water, dry-wet and heat-cool cycles of sea water, because of the dilution of the alkali by the sea water. However, halite is observed in the exposure conditions with sea water, which is in good agreement with SEM images (Figure 4.2.2). It indicates that substantial salts are formed when the geopolymers were exposed in sea water.

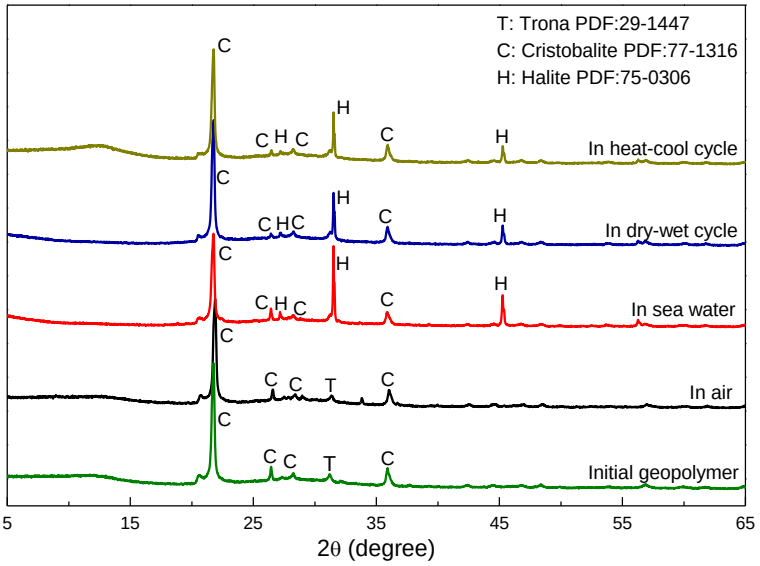

Figure 4.2.3. XRD patterns of the geopolymers cured differently for 90 days.

The ^{29}Si nuclear magnetic resonance (NMR) spectra had found great success in studying the microstructures of geopolymers, particularly their short-range ordering and molecular structure (Klinowski, 1984). The lack of spectral resolution for silicon has been overcome by adopting Gaussian peak deconvolution to separate and quantify Q^n(mAl) species ($0 \leq m \leq n \leq 4$, m, n = integer) (Engelhardt and Michel, 2005). In the geopolymer gel, it has been reported that all silicon and aluminum sites are in tetrahedral coordination, thus n=4 (Barbosa et al., 2000; Rahier et al., 1996; Duxson et al., 2005). And the resonance of a Q^4(mAl) center with the replacement of each aluminum by silicon is an approximate -5 ppm difference in δ, with Q^4(4Al), Q^4(3Al), Q^4(2Al), Q^4(1Al) and Q^4(0Al) resonating at approximately -84, -89, -93, -99 and -108 ppm, respectively (Engelhardt and Michel, 2005). Figure 4.2.4 gives the ^{29}Si NMR spectra and the deconvolution of the geopolymers exposed differently for 30, 60 and 90 days, in which the spectrum of the initial geopolymer is given as a comparison. The spectra not only show a broad peak of geopolymer gel, but also show sub-peaks that represent the formation of silicate derivatives. These silicate derivatives show structures of single tetrahedral structure from the monosilicates (Q^0) to the end groups (Q^1), to the chain middle groups (Q^2), to the layers and the branching sites (Q^3), and finally to the three-dimensional networks (Q^4). Here the resonances of Q^1, Q^2 and Q^3 resonate at approximately -79, -85 and -95 ppm, respectively, and the resonance of Q^4 is the same as the Q^4(0Al) of the geopolymer gel (Singh et al., 2005). In addition, the peak with resonance at -112 ppm is attributed to the remained cristobalite in the geopolymers (Fernandez-Jimenez et al., 2006). After deconvolution, all units of the species are shown by bars in the bottom of Figure 4.2.4. The bars are centered at the deconvoluted peaks of the species, and their lengths represent the widths of the peaks.

Figure 4.2.4 shows the main peak of the geopolymer gel is centered at δ of -91 ppm for the initial geopolymer, while that for the geopolymers exposed for a period of days is centered at a δ less than -91 ppm. Because the Q^4(4Al), Q^4(3Al), Q^4(2Al), Q^4(1Al), Q^4(0Al) resonate at approximately -84, -89, -93, -99 and -108 ppm, respectively, the lower values in δ suggest the formation of less sites of tetrahedral aluminum linking with the tetrahedral silicon. With considering the high Si/Al ratio of 3.7 in the raw materials, this result suggests that geopolymerization reactions are started with aluminum precursors and last for a long time (Duxson et al., 2005). However, the geopolymers exposed in sea water have the peaks that are centered at the δ of much lower ppm, than that exposed in air. For example, the geopolymer exposed in heat-cool cycle of sea water for 90 days has the peak centered at the δ of -95 ppm, while that exposed in air is -93 ppm. It indicates that the marine conditions inhibit the geopolymerization reactions.

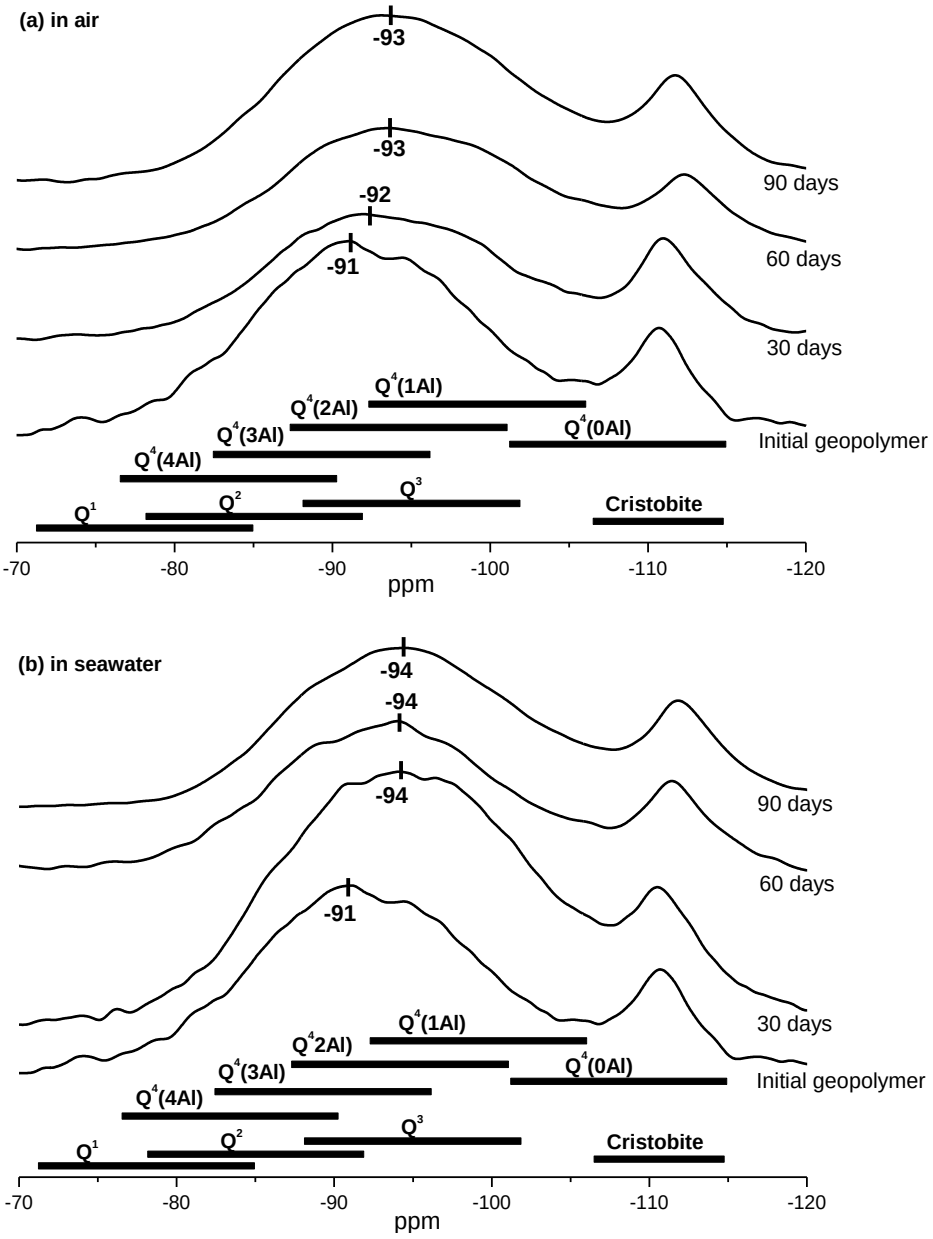
(a) in air
-93
-93
-92
-91
90 days
60 days
30 days
Initial geopolymer
Q4(1Al)
Q4(2Al)
Q4(3Al)
Q4(0Al)
Q4(4Al)
Q3
Q2
Q1
Cristobite
-70
-80
-90
-100
-110
-120
ppm
(b) in seawater
-94
-94
-94
-91
90 days
60 days
30 days
Initial geopolymer
Q4(1Al)
Q4 2Al)
Q4(3Al)
Q4(0Al)
Q4(4Al)
Q3
Q2
Q1
Cristobite
-70
-80
-90
-100
-110
-120
ppm

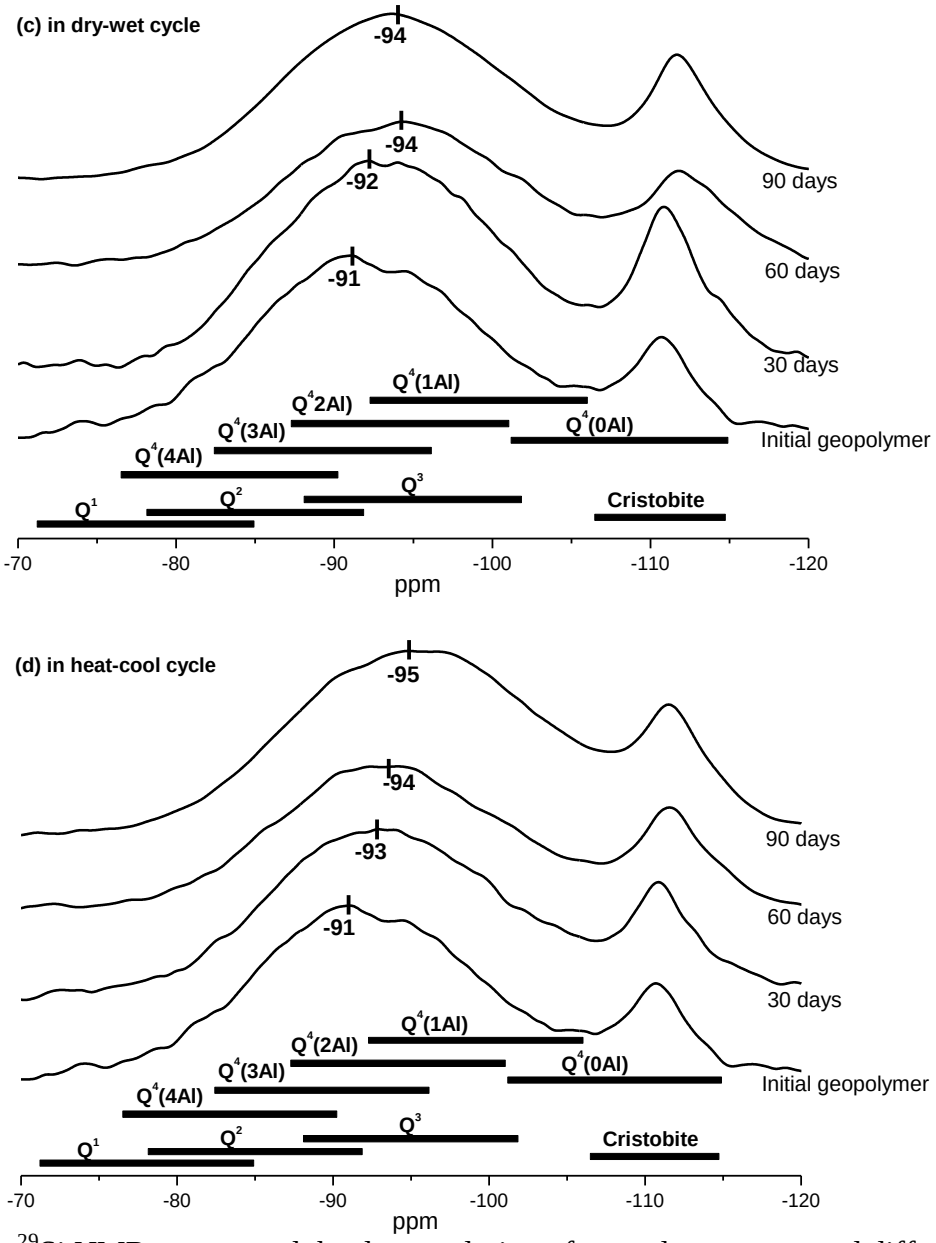

Figure 4.2.4. ^{29}Si NMR spectra and the deconvolution of geopolymers exposed differently for 30, 60 and 90 days.

Based on the deconvolutions of the spectra in Figure 4.2.4, the percentages of each species in the geopolymers are shown in Table 4.2.1. In the initial geopolymer, the sum of silicate derivatives (Q^1, Q^2 and Q^3) is 24.1%. As exposing the geopolymers for 30, 60 and 90 days, silicate derivatives are transformed into geopolymer gel. For example, as exposing in air for 90 days, silicate derivatives decrease to 3.8%, while the geopolymer gel increases from 67.5% to 86.5%. It suggests that the geopolymerization reactions proceed for a long time. In addition, the sum of Q^4(4Al), Q^4(3Al) and Q^4(2Al) is 47% for exposing in air of 90 days, while they are 44.6%, 44.8% and 42.3% for exposing in sea water, dry-wet and heat-cool cycles in sea water. It suggests again that the marine conditions inhibit the geopolymerization reactions.

Table 4.2.1. ^{29}Si NMR spectral deconvolution of the geopolymer samples (**Figure 4.2.4**)

samples		Q^1	Q^2	Q^3	$Q^4(4Al)$	$Q^4(3Al)$	$Q^4(2Al)$	$Q^4(1Al)$	$Q^4(0Al)$
Curing condition	**Curing time (days)**								
Initial geopolymer	7	4.0%	10.1%	10.0%	0.8%	23.3%	18.2%	15.8%	9.4%
In air	30	1.2%	3.8%	5.8%	2.2%	23.0%	17.6%	23.5%	10.4%
	60	0.9%	1.3%	4.6%	3.3%	19.4%	20.2%	27.5%	13.0%
	90	0.4%	0.7%	2.7%	4.7%	20.6%	21.6%	27.0%	12.6%
In sea water	30	2.3%	2.5%	7.3%	3.3%	21.3%	18.1%	26.2%	13.2%
	60	2.0%	3.7%	3.4%	4.1%	21.5%	18.2%	26.1%	12.9%
	90	0.1%	0.8%	3.7%	2.6%	19.2%	22.8%	27.2%	13.0%
In dry-wet cycle	30	1.4%	7.1%	6.5%	2.9%	16.0%	22.5%	21.4%	9.6%
	60	1.1%	2.5%	7.9%	3.6%	17.8%	20.7%	23.4%	12.7%
	90	0.9%	1.1%	3.6%	4.1%	17.0%	25.7%	24.0%	11.1%
In heat-cool cycle	30	1.8%	6.8%	6.9%	1.9%	19.4%	20.7%	21.0%	11.5%
	60	1.9%	5.0%	6.5%	2.6%	18.2%	21.7%	21.0%	12.1%
	90	0.6%	0.9%	4.0%	4.0%	17.2%	21.1%	28.4%	14.4%

4.3. Effect of cristobalite on the mechanical behaviour of metakaolin-based geopolymer in artificial sea water

Figure 4.3.1 shows the changes of the compressive strength values of geopolymer samples exposed to different conditions. The starting compressive strength of M-In is 27.11 MPa and that of G-In is 48.66 MPa. The compressive strength values of both MA and GA increase with time. After 90 days, the compressive strength value of MA is 33.65 MPa and that of GA is 59.37 MPa. The compressive strength of MS decreases to 18.03 MPa at 30 days, and then increases to 24.21 MPa at 90 days. These values are higher than those of MDW, which decreases to 11.33 MPa, then increases slightly to 15.13 MPa at 30 and 90 days, respectively. The compressive strength value of GS decreases to 32.12 MPa at 30 days, then increases to 35.04 MPa at 90 days. However, these values are lower than those of GDW, which decreases gradually to 38.93 MPa at 90 days.

It can be noted that: 1) the compressive strength values of samples exposed to sea water environment decrease. This may be associated with the dilution effect of sea water in geopolymerization reactions (Rashad et al., 2018; Zhang et al., 2010a). 2) the compressive strength values of the geothermal clay-based geopolymers are much higher than those of the metakaolin-based geopolymer. This is because the micron-size cristobalite enhance the

compressive strengths of the geopolymers. It is consistent with the reports of Wan et al., (2017c) and Shaikh and Haque (2017).

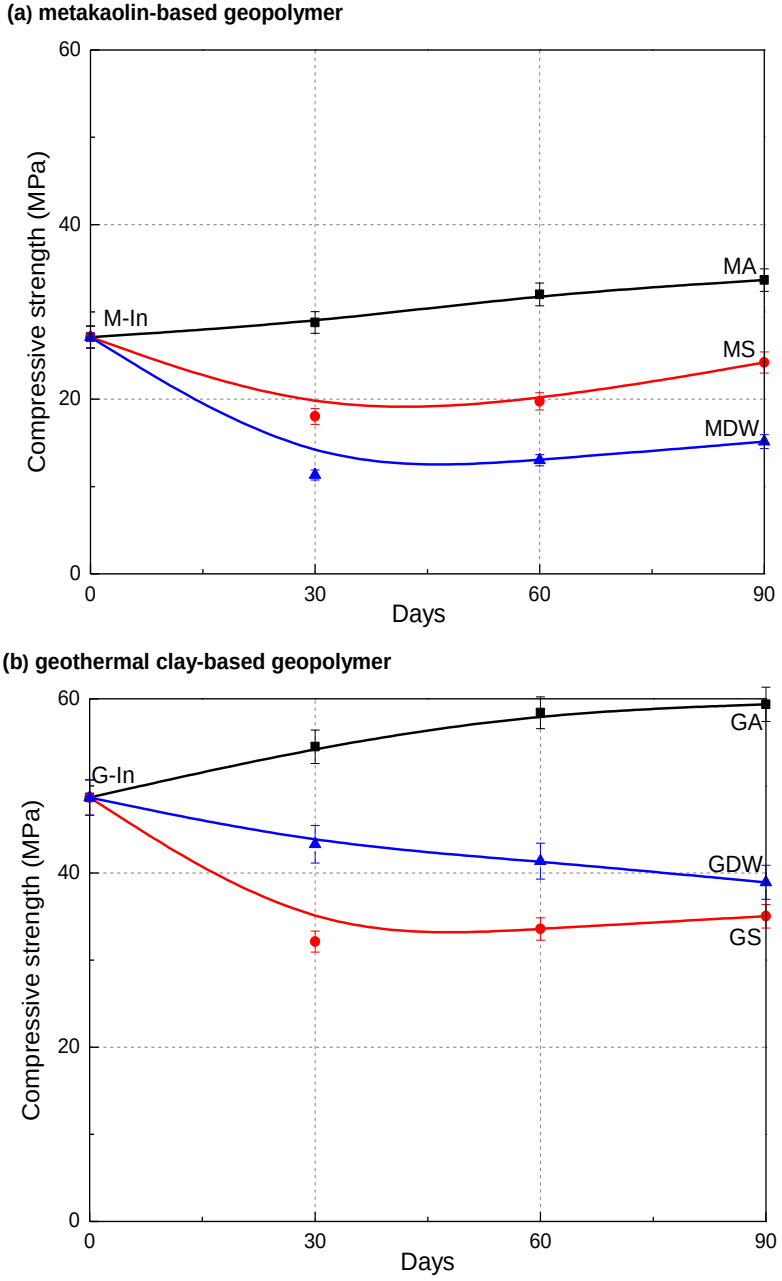

Figure 4.3.1. Compressive strengths of (a) metakaolin-based geopolymers and (b) geothermal clay-based geopolymers cured in different conditions.

Figure 4.3.2 shows the XRD analyses of the initial geopolymer mortars M-In and G-In, metakaolin-based geopolymer cured in air for 90 days (MA-3), in sea water for 90 days (MS-3) and in dry-wet cycle for 90 days (MDW-3), and geothermal clay-based geopolymer cured in air for 90 days (GA-3), in sea water for 90 days (GS-3) and cured in dry-wet cycle for 90 days (GDW-3). All the samples contain the phases originating from the starting raw materials: the muscovite and quartz in the metakaolin and the cristobalite in the geothermal clay. Meanwhile,

the formation of new phases due to the reactions with magnesium and sulfate ions is not indicated. The amorphous XRD patterns with one hump centred at approximately 27-29° 2θ are rarely observed in the MS-3, MDW-3, GS-3 and GDW-3 specimens, which indicate the sea water inhabited the formation of geopolymer gel. The trona appearing in M-In, MA-3, G-In and GA-3 is related to excessive alkali, and then it disappears in the MS-3, MDW-3, GS-3 and GDW-3 samples, it is relate to the dilution of the alkali by the sea water. Zeolites are formed in MS-3 and MDW-3 samples but not in GS-3 and GDW-3 samples, which may be attributed to the metakaolin-based geopolymer with low Si/Al ratio (2.1:1) in the sea water environment shows low reactivity (Yan et al., 2012; Yu et al., 2014). In addition, the dry-wet cycles of sea water seem to promote more zeolite formation in the metakaolin-based geopolymer. These zeolites hold substantial halite permeation in the samples. Therefore, the peak intensities of halite that appear in the MDW-3 specimens are higher. Meanwhile, many of these zeolites reduce the compressive strength of metakaolin-based geopolymer cured in dry-wet cycle greatly than those cured in sea water, which is agreement with the reports that increasing the amount of zeolite in the geopolymer reduces strength (Provis and Van Deventer, 2009; De Silva and Sagoe-Crenstil, 2008).

(a) metakaolin-based geopolymer

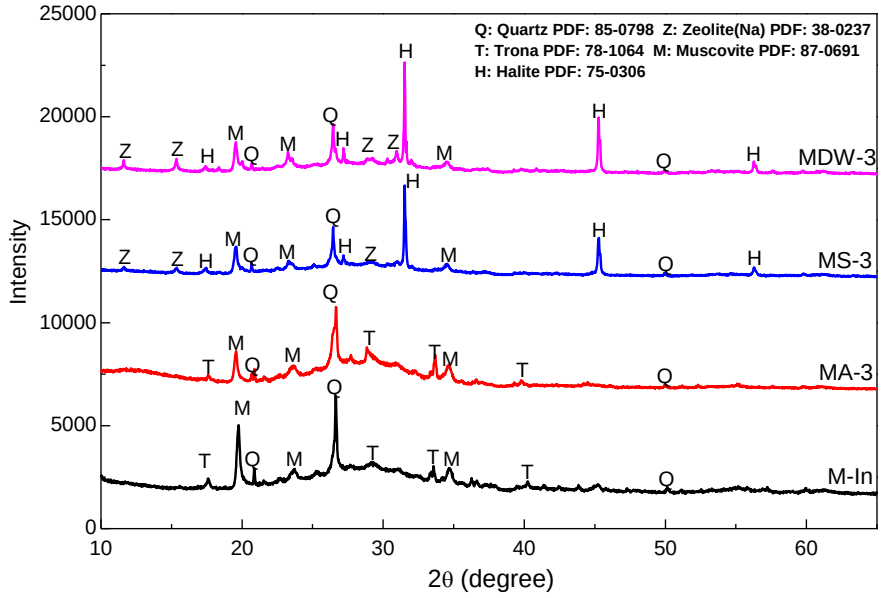

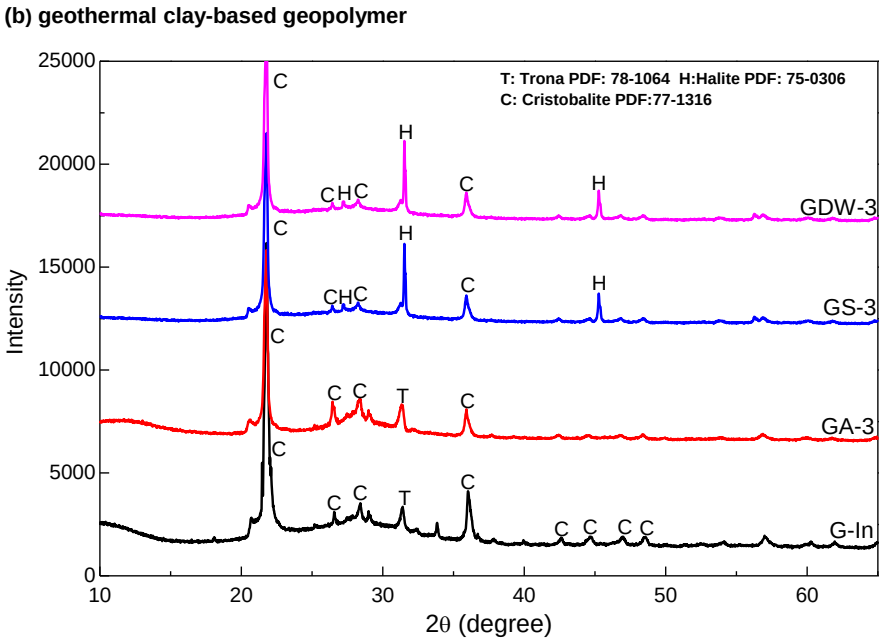

Figure 4.3.2. XRD patterns of (a) metakaolin-based geopolymers and (b) geothermal clay-based geopolymers exposed to different curing conditions for 90 days.

Figure 4.3.3 shows the SEM images of geopolymers synthesized with metakaolin and geothermal clay cured in dry-wet cycles of sea water for 90 days. For sample MDW-3, the geopolymer binder, halite and a number of zeolitic nuclei are observed. Most of these nuclei are not dispersed in the geopolymer binder. The cracks due to dry-wet cycles of sea water are not observed, because the zeolites could hold a lot of halite. For sample GDW-3, halite is not obvious. The cracks are presented in the geopolymer, and these cracks cause compressive strength of geothermal clay-based geopolymer to decrease gradually in the dry-wet cycles of sea water.

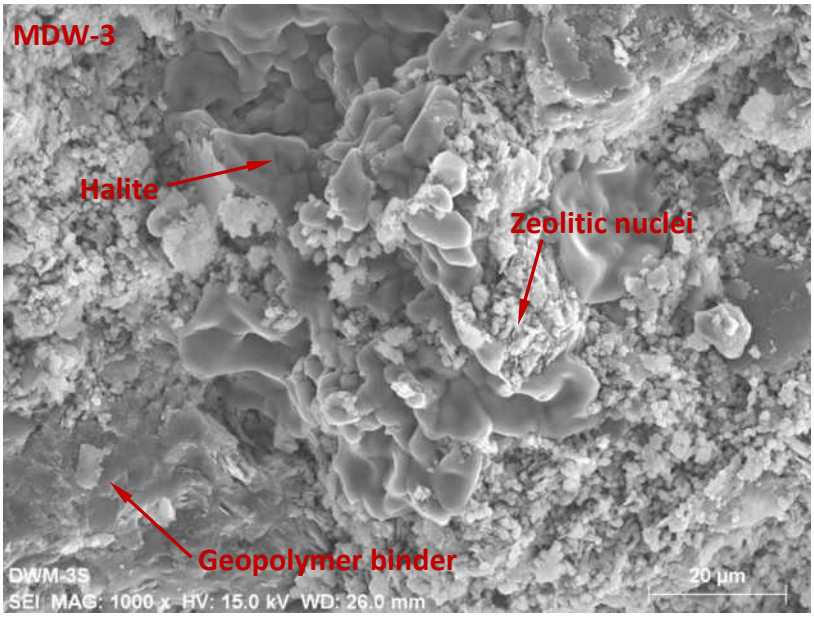

(a) metakaolin-based geopolymer

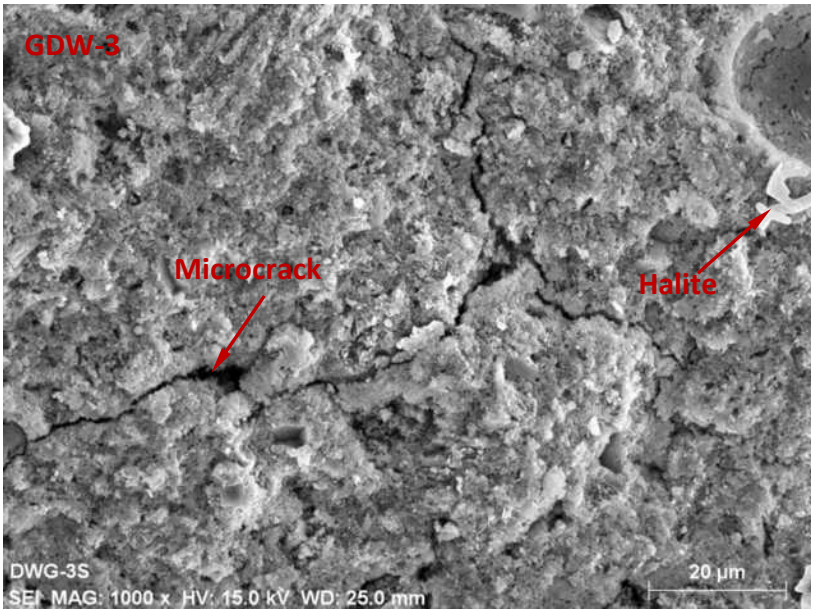

(b) geothermal clay-based geopolymer

Figure 4.3.3. SEM patterns of geopolymer cured in dry-wet cycles of sea water for 90 days.

^{29}Si MAS-NMR spectra are used to understand the evolution of geopolymer gel in this study. The ^{29}Si NMR spectra and their deconvolution of the metakaolin-based geopolymer and the geothermal clay-based geopolymer exposed to different conditions for 90 days are shown in Figure 4.3.4 and Figure 4.3.5. All the samples are deconvoluted by fitting the Gaussian peak of the $Q^n(mAl)$ ($0 \leq m \leq n \leq 4$, m, n = integer). It is reported that all the silicon sites are in tetrahedral coordination, thus n = 4 and Q^4(4Al), Q^4(3Al), Q^4(2Al), Q^4(1Al), Q^4(0Al) resonating at approximately -84, -89, -93, -99 and -108 ppm, respectively (Engelhardt and Michel; 1987). Meanwhile, the sub-peaks represent the formation of silicate derivatives. These silicate derivatives show structures of single tetrahedral structure of the monosilicates (Q^0) to the end groups (Q^1), to the chain middle groups (Q^2), to the layers and the branching sites (Q^3), and finally to the three-dimensional networks (Q^4). Here the Q^1, Q^2 and Q^3 resonate at approximately -79, -85 and -95 ppm, respectively, and the Q^4 is the same as the Q^4(0Al) of the geopolymer gel (Engelhardt and Michel; 1987). In addition, the MDW-3 shows two shoulders at approximately -88 and -95 ppm, which are associated with zeolite and Q^3 (Singh et al., 2005; Ramdas and Klinowski, 1984). The peak with resonance at -112 ppm in the geothermal clay-based geopolymer is attributed to the cristobalite (Fernandez-Jimenez et al., 2006).

From Figure 4.3.4 and Figure 4.3.5, the sum of $Q^4(4Al)$, $Q^4(3Al)$ and $Q^4(2Al)$ of M-In is 57.2%, and the sums of samples MA-3, MS-3 and MDW-3 are 61.3%, 58.7% and 57.7%, respectively. Meanwhile, the sum of $Q^4(4Al)$, $Q^4(3Al)$ and $Q^4(2Al)$ of G-In samples is 42.3%, and the sums of samples GA-3, GS-3 and GDW-3 are 47.0%, 44.6% and 46.8%, respectively. After curing for 90 days, all the sums of $Q^4(4Al)$, $Q^4(3Al)$ and $Q^4(2Al)$ increase, indicating that the formation of the geopolymer gel proceed for a long time. The sum of $Q^4(4Al)$, $Q^4(3Al)$ and $Q^4(2Al)$ in MA-3 is more than those of MS-3, MDW-3 and GA-3 is more than those of GS-3 and GDW-3, respectively, which suggests that the sea water environment delays the formation of the geopolymer gel. The sums of $Q^4(4Al)$, $Q^4(3Al)$ and $Q^4(2Al)$ of the metakaolin-based geopolymers are more than 57.2% while those of the geothermal clay-based geopolymer are less than 47.0%,

which is related to the large amounts of cristobalite present in geothermal clay hindering the formation of geopolymer gel.

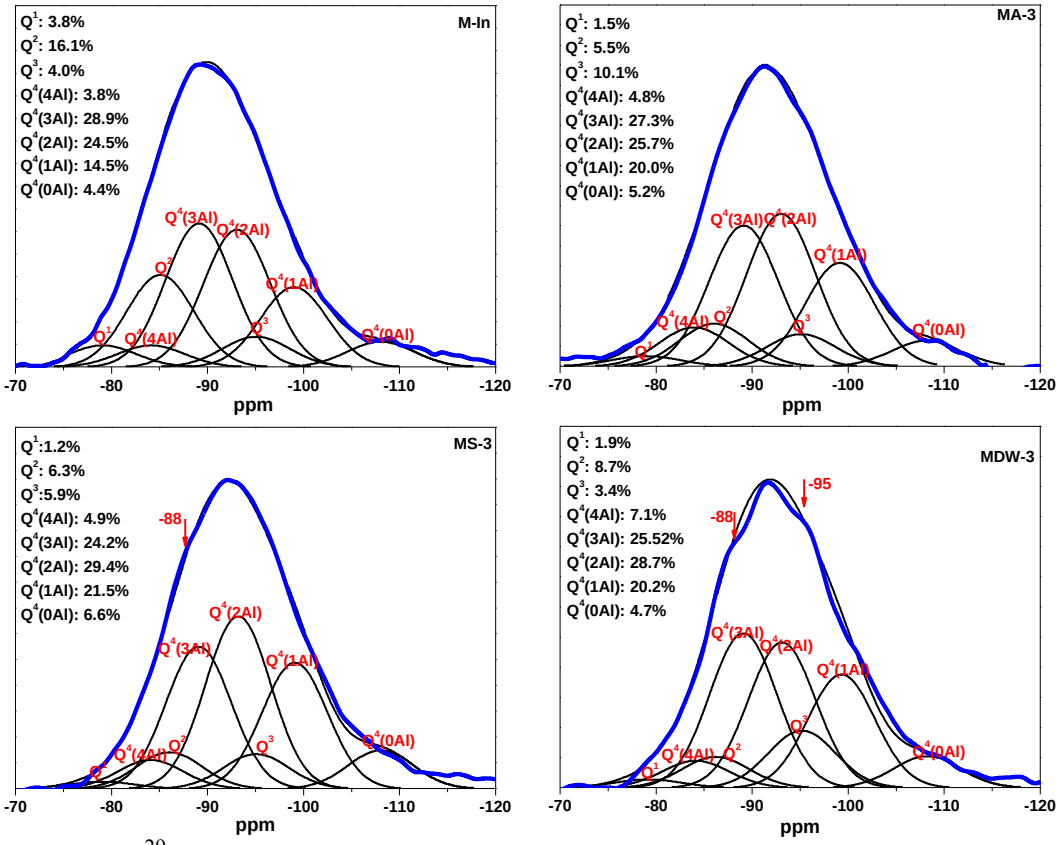

Figure 4.3.4. The ^{29}Si NMR spectra and their deconvolution of the metakaolin-based geopolymer gel cured in different curing conditions for 90 days.

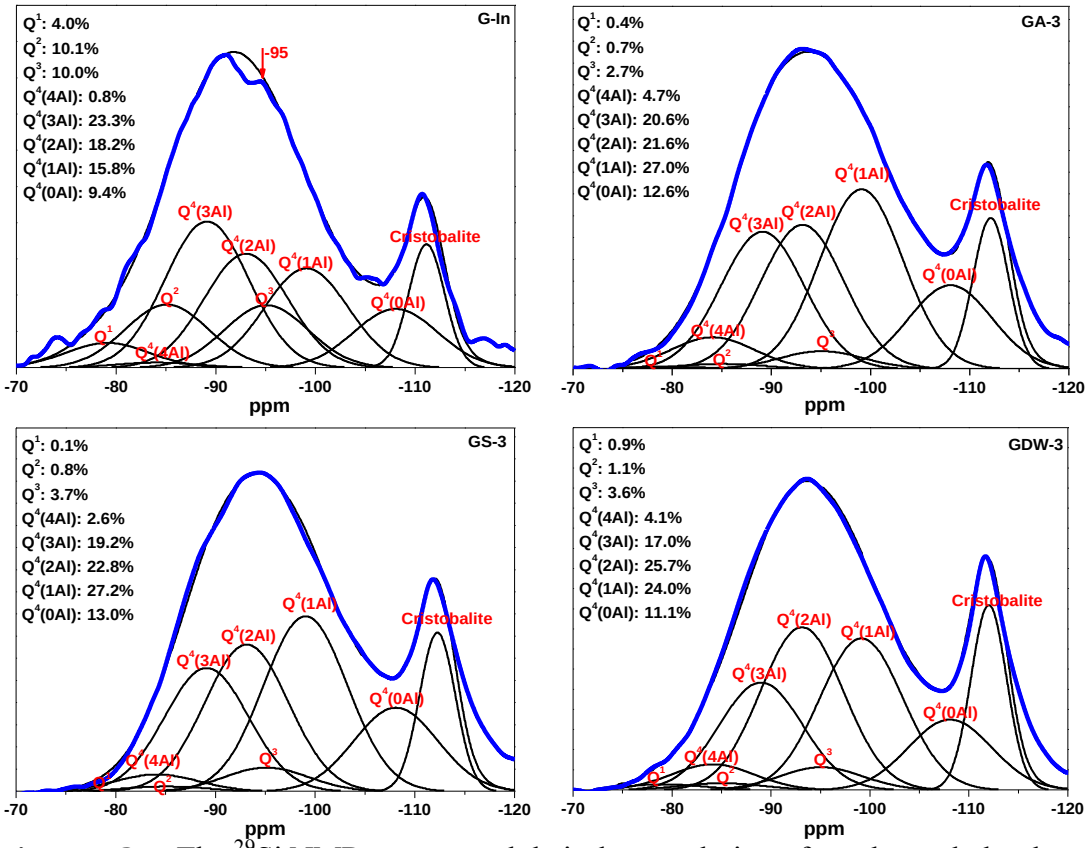

Figure 4.3.5. The ^{29}Si NMR spectra and their deconvolution of geothermal clay-based geopolymer gel cured in different curing conditions for 90 days

4.4. Microstructural evolution in sulfate solutions of alkali-activated binders synthesized at various calcium content

Figure 4.4.1 shows the compressive strength of the alkali-activated binders exposed in air, Na_2SO_4 and $MgSO_4$ solutions for 90 days. For the exposure in air, compressive strength of the metakaolin-based binder increased slightly from 46 to 51.1 MPa on 7 to 90 days. In comparison, the fly ash and slag-based binders showed a lower compressive strength, which increased slightly from around 19 to 23 MPa in curing for 90 days. It suggests the formation of geopolymer gel in the metakaolin-based binder, leading to superior mechanical property (Provis and Van Deventer, 2009).

For the exposure in Na_2SO_4 solution, compressive strength of the metakaolin-based binder decreased gradually from 40.8 to 15.7 MPa on 7 to 90 days. Compressive strength of the fly ash-based binder decreased from 17.1 to 11.1 MPa on 7 to 21 days, and then it kept a constant. The reduction of compressive strength suggests that the Na_2SO_4 solution dissolves alkalis in the binders, so that the alkaline activation process was weakened by deterioration of the N-A-S-H gel (Rajamane et al., 2012; Salami et al., 2017; Bakharev, 2005). However, compressive strength of the slag-based binders increased from 15.3 to 20.5 MPa on 7 to 21 days, and then remained constant. In the slag-based binders, high contents of C-A-S-H and C-S-H gels were formed, because of high CaO in the raw slag (Chindaprasirt et al., 2012). Therefore, the increase in compressive strength suggests that alkali dissolution affects less on the formation of C-A-S-H

and C-S-H gels (Mehta and Siddique, 2017; Alonso and Palomo, 2001; Van Deventer et al., 2007). Furthermore, Yip et al. (2008) reported that C-S-H gel worked as a micro-aggregate in the binder, resulting in homogeneous and dense structure.

For the exposure in $MgSO_4$ solution, compressive strength of metakaolin and fly ash-based binders decreased sharply from 33.5 and 16.9 MPa to 14.2 and 7.3 MPa on 7 to 21 days, respectively, and then they increased moderately to 23.6 and 9.87 MPa on 90 days, respectively. Compressive strength of the slag-based binder increased steadily from 8.9 to 18 MPa on 7 to 90 days. Compared to the exposure in Na_2SO_4 solution, precipitates of $Mg(OH)_2$ and $CaSO_4$ might be formed on surface of the binders, which protected them from the dissolution of alkalis, resulting in higher increases in compressive strength on 90 days (Yip et al., 2008; Kumar et al., 2010).

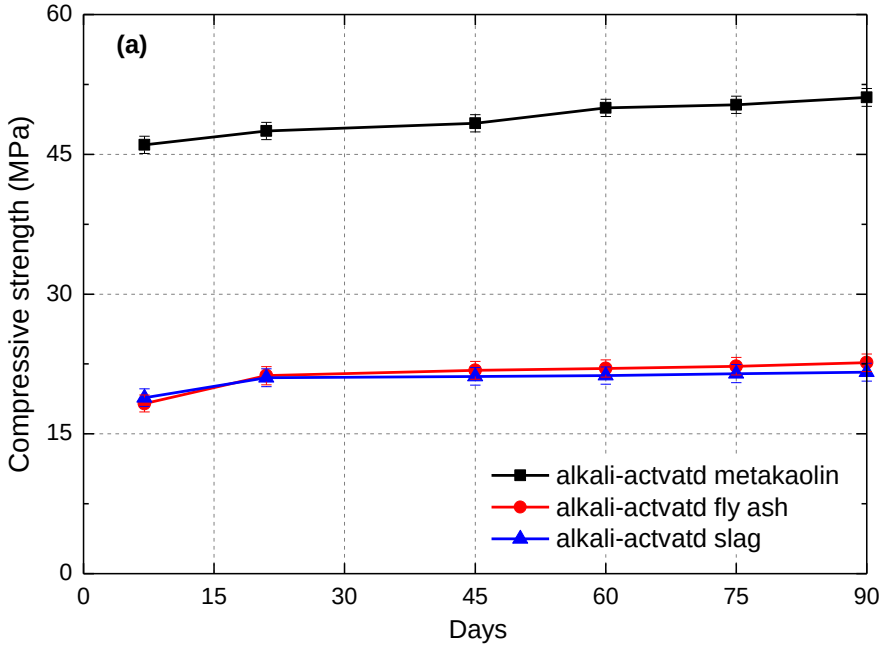

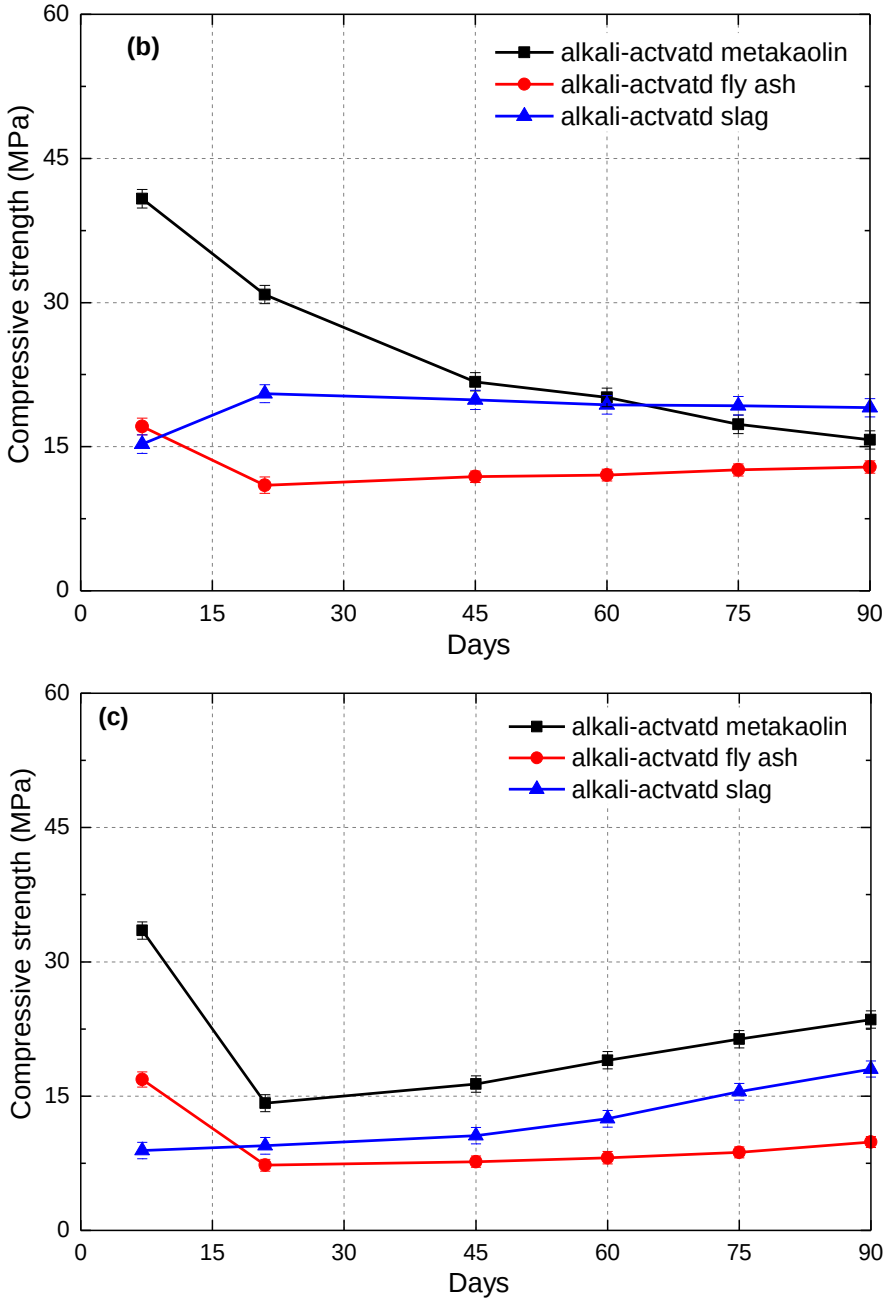

Figure 4.4.1. Compressive strengths of alkali-activated binders exposed in (a) air, (b) Na_2SO_4 and (c) $MgSO_4$ solutions.

Figure 4.4.2 shows photos of the alkali-activated binders exposed in Na_2SO_4 and $MgSO_4$ solutions for 90 days. In Na_2SO_4 solution, there is no macroscopic change on the binders' surface, indicating Na_2SO_4 attack is undetected in either the deterioration of the binder or the formation of precipitates. While in $MgSO_4$ solution, through XRD analysis (Figure 4.4.3), it was found that the white precipitates of brucite [$Mg(OH)_2$] and gypsum ($CaSO_4$) were formed on the surface of alkali-activated fly ash and alkali-activated slag. It is indicated that the Mg^{2+} ions not only precipitate with alkalis, but also promote the precipitation of $CaSO_4$. Table 4.4.1 gives the pH values of the sulfate solutions in 90 days. Initial pH of both the Na_2SO_4 and $MgSO_4$ solutions

were around 8.3. In Na_2SO_4 solution, it increased to pH 13.4 in 7 days and further to around pH 13.8 in 90 days for the exposure of the three binders. While in $MgSO_4$ solution, it increased to around pH 9.5 in 7 days and further to around pH 11 in 90 days. The increase of the pH suggests the dissolution of alkali from the binders (Bascarevic et al., 2015; Kumar et al., 2010), and the lower increase of pH in $MgSO_4$ solution is attributed to the fact that the precipitated brucite acted as an insoluble and protective layer for the binders (De Weerdt et al., 2014).

(a) Na_2SO_4

(b) $MgSO_4$

Figure 4.4.2. Photos of the alkali-activated binders exposed in (a) Na_2SO_4 and (b) $MgSO_4$ solutions for 90 days.

Table 4.4.1. pH values of the sulfate solutions after exposure of the alkali-activated binders.

Binders	Metakaolin-binders		Fly ash-binders		Slag-binders	
	Na_2SO_4	$MgSO_4$	Na_2SO_4	$MgSO_4$	Na_2SO_4	$MgSO_4$
0	8.37	8.31	8.37	8.31	8.37	8.31
7 days	13.41	9.46	13.45	9.40	13.45	9.40
90 days	13.84	10.53	13.73	11.02	13.78	10.50

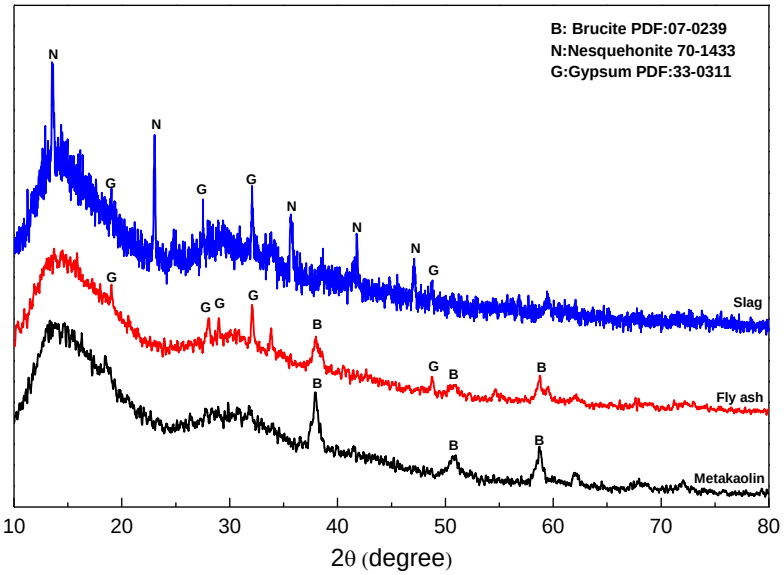

Figure 4.4.3 XRD of precipitates on the surfaces of samples for alkali-activated binders exposed in $MgSO_4$ solution.

Figure 4.4.4 shows the SEM images and corresponding elemental mapping of the fly ash and slag -based binders exposed in Na_2SO_4 and $MgSO_4$ solutions, respectively. Compared with the surface photos of the binders (Figure 4.4.2), their microstructural morphology shows homogeneous gel structure. It indicates that the sulfate attack merely affects the gel formation in the alkali-activated binders. In elemental mapping of both the fly ash and slag-based binders, the Ca, Al and Si elements are evenly distributed throughout. It suggests that the N-A-S-H, C-A-S-H and C-S-H gels were formed evenly in the binders.

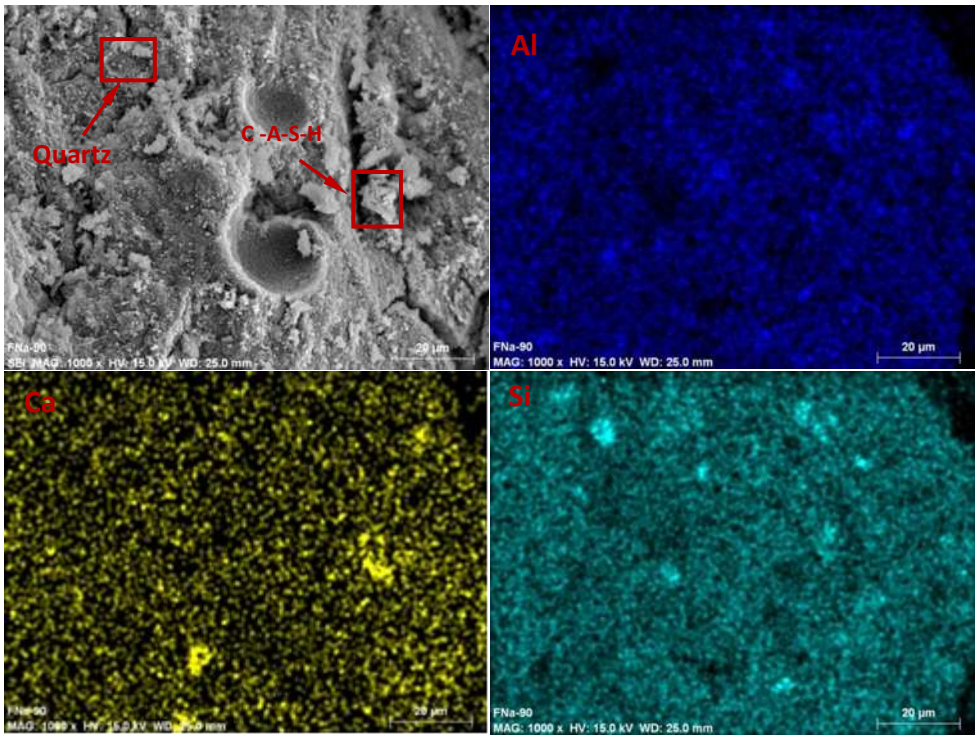

(a) Fly ash-based binder exposed in Na_2SO_4 solution for 90 days

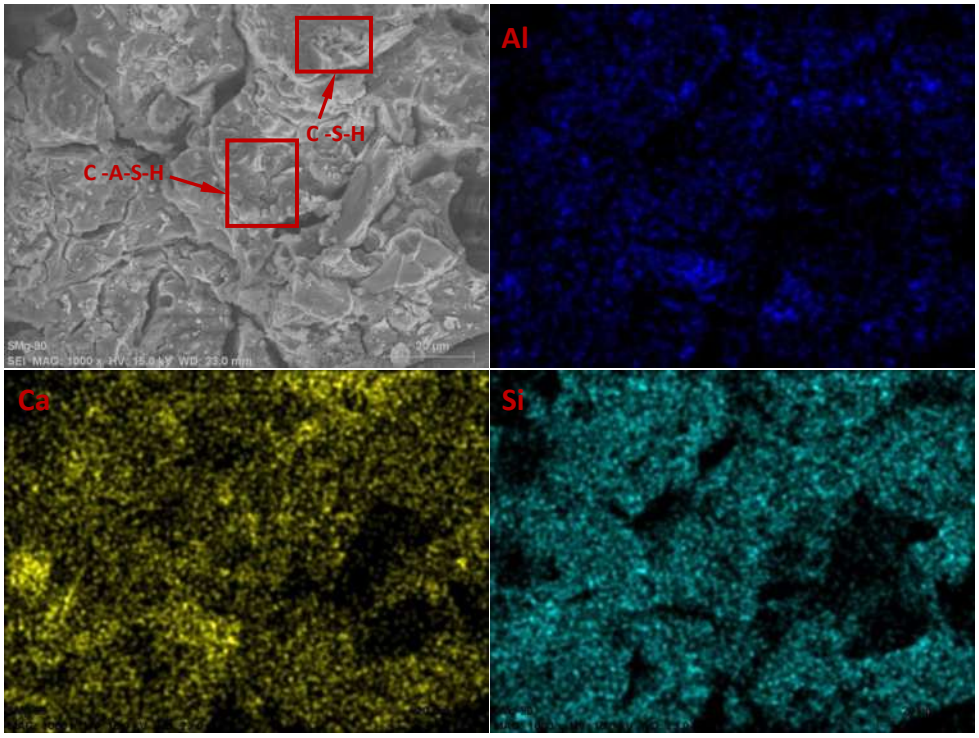

(b) Slag-based binder exposed in $MgSO_4$ solution for 90 days

Figure 4.4.4. SEM images and corresponding elemental mapping of the binders.

Figure 4.4.5 presents the XRD patterns of the metakaolin, fly ash and slag-based binders exposed differently for 90 days. For the metakaolin-based binders, impurities of quartz and muscovite were observed because they are inert minerals in alkaline activation process. The binder exposed in air shows featherless amorphous XRD pattern with one hump centered at approximately 2θ = 27-29 °, which suggests the formation of geopolymer N-A-S-H gel (Duxson et al., 2005). However, the binder exposed in Na_2SO_4 solution presents the characteristic peaks of zeolite, which is attributed to the dissolution of alkalis (Duxson et al., 2005). The zeolite crystals weaken the formation of N-A-S-H gel, leading to the decrease in mechanical property of the binders (Provis and Van Deventer, 2009; De Silv and Sagoe-Crenstil, 2008), which is in agreement of the compressive strength results (Figure 4.4.1). While the binders exposed in $MgSO_4$ solution show amorphous XRD pattern without zeolite peaks, which might be due to precipitated brucite delaying the dissolution of alkalis. For the fly ash-based binders, quartz is originated from the raw materials. Zeolite forms in the three exposure conditions, which is attributed to higher content of unreacted material and higher Si/Al ratio of gel (Fernández-Jiménez and Palomo, 2005). In addition, the C-S-H gel is observed when exposing in Na_2SO_4 and $MgSO_4$ solutions, which indicates that the diluted alkali from the binder leads to the formation of C-S-H gel (Sukmak et al., 2014). For the slag-based binders, zoisite, calcite, quartz and maghemite are from the raw materials. The C-S-H gel is observed in the three exposing conditions. Gypsum and ettringite form in the alkali-activated slag cured in Na_2SO_4 and $MgSO_4$ solution. And no obvious peaks of brucite and hydrotalcite are observed. It is suggested that a small amount of Mg ions diffuse into of the samples.

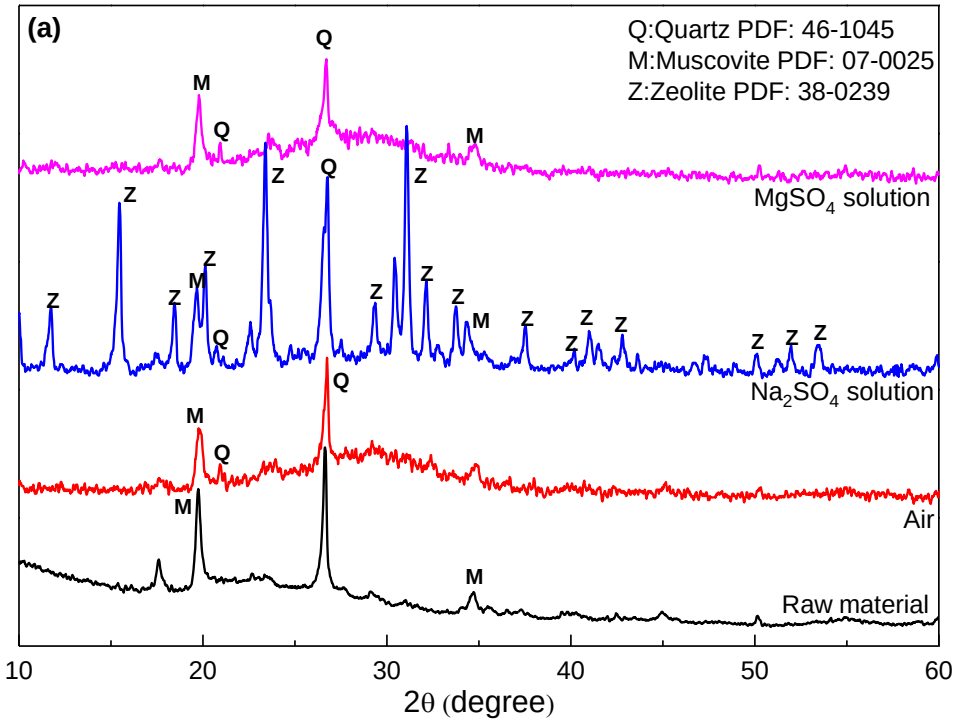
(a)
Q:Quartz PDF: 46-1045
M:Muscovite PDF: 07-0025
Z:Zeolite PDF: 38-0239
MgSO4 solution
Na2SO4 solution
Air
Raw material
10
20
30
40
50
60
2θ (degree)

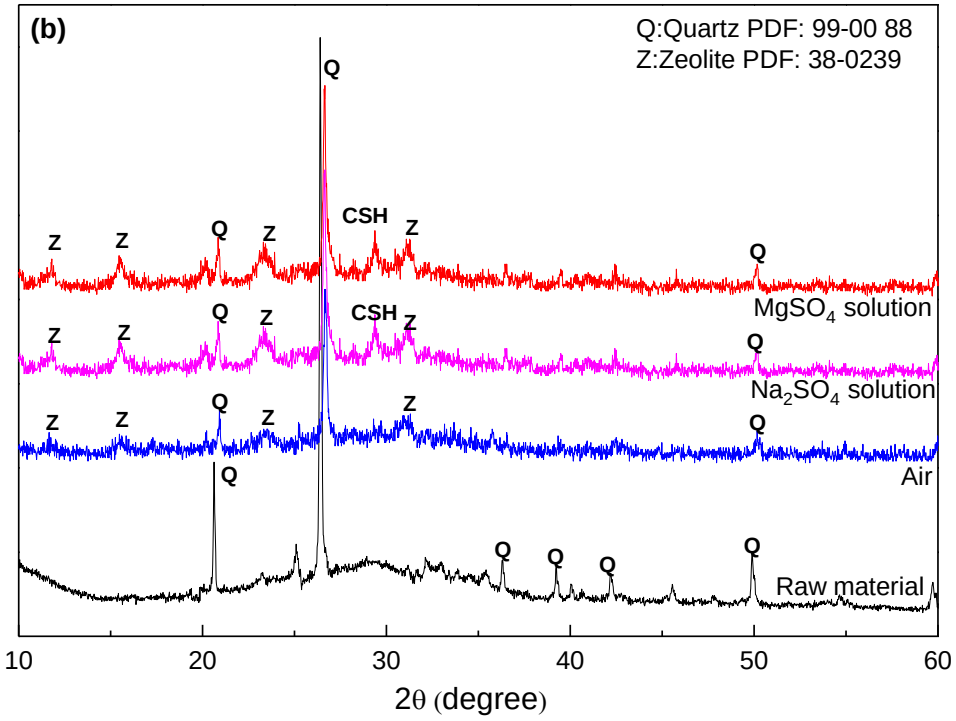
(b)
Q:Quartz PDF: 99-00 88
Z:Zeolite PDF: 38-0239
CSH
MgSO4 solution
Na2SO4 solution
Air
Raw material
10
20
30
40
50
60
2θ (degree)

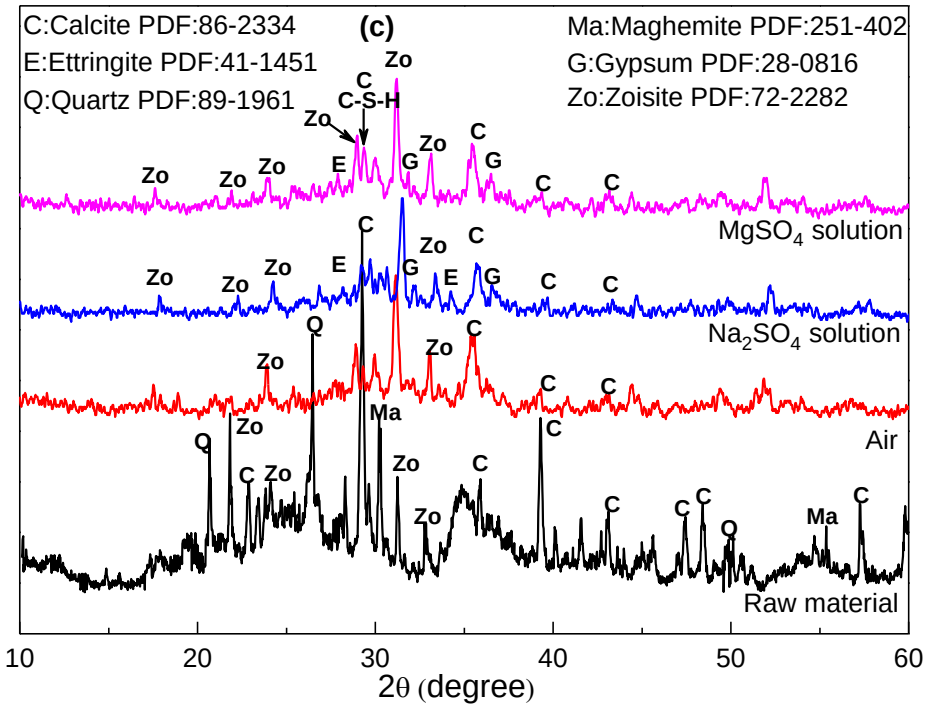

Figure 4.4.5. XRD patterns of the (a) metakaolin, (b) fly ash and (c) slag-based binders exposed differently for 90 days.

In studying the microstructure of alkali-activated binders, short-range ordering and molecular structure have been investigated with great success using NMR spectroscopy (Youngman, 2018). The lack of spectral resolution for Si in the binders has been overcome by adopting Gaussian peak deconvolution to separate and quantify $Q^n(mAl)$ species ($0 \leq m \leq n \leq 4$, m, n = integer) (Lee and Stebbins, 1999). In geopolymer N-A-S-H gel, it is reported that all the Si sites are in tetrahedral coordination, thus n = 4 and the $Q^4(4Al)$, $Q^4(3Al)$, $Q^4(2Al)$, $Q^4(1Al)$, $Q^4(0Al)$ resonate at approximately -84, -89, -93, -99 and -108 ppm, respectively (Engelhardt and Michel, 1987). In the C-A-S-H and C-S-H gels, the silicate derivatives show structures of the end groups (Q^1), the chain middle groups (Q^2), the layers and the branching sites (Q^3) (Richardson, 1999). Here the Q^1, Q^2 and Q^3 resonate at approximately -70, -79, -85 and -95 ppm, respectively, the peak at -74 and -84 represent $Q^1(1Al)$, $Q^2(1Al)$ when Al is involved, respectively. Figure 4.4.6 presents the ^{29}Si NMR spectra and their deconvolution of the alkali-activated binders exposed in different conditions. For the metakaolin-based binders, the spectra of the binders exposed in air and $MgSO_4$ solution show a broad peak, while that exposed in Na_2SO_4 solution shows several peaks in the spectrum. It corresponds well with the XRD results (Figure 4.4.5) that only the binder exposed in Na_2SO_4 solution showed high contents of zeolite. For the fly ash-based binders, the spectra show several peaks in air, Na_2SO_4 and $MgSO_4$ solutions, corresponding well to the observation of zeolite in XRD patterns (Figure 4.4.5). For the slag-based binders, high CaO in the raw slag leads to the one broad peak spectra when exposing in air and in $MgSO_4$ solution, and to the several peaks in the spectrum when exposing in Na_2SO_4 solution.

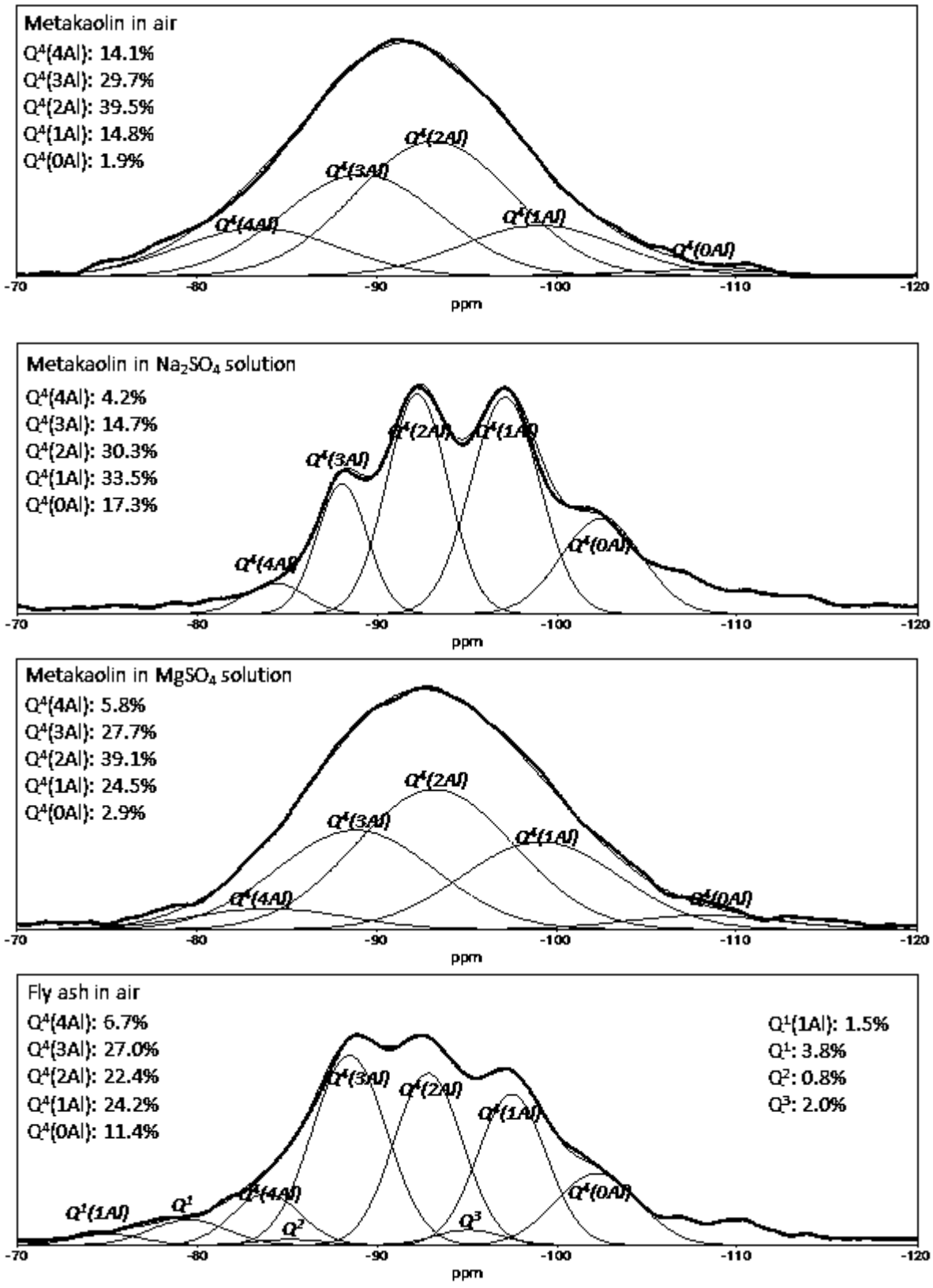
Metakaolin in air
Q4(4Al): 14.1%
Q4(3Al): 29.7%
Q4(2Al): 39.5%
Q4(1Al): 14.8%
Q4(0Al): 1.9%
Q4(4Al)
Q4(3Al)
Q4(2Al)
Q4(1Al)
Q4(0Al)
-70
-80
-90
-100
-110
-120
ppm
Metakaolin in Na2SO4 solution
Q4(4Al): 4.2%
Q4(3Al): 14.7%
Q4(2Al): 30.3%
Q4(1Al): 33.5%
Q4(0Al): 17.3%
Q4(4Al)
Q4(3Al)
Q4(2Al)
Q4(1Al)
Q4(0Al)
-70
-80
-90
-100
-110
-120
ppm
Metakaolin in MgSO4 solution
Q4(4Al): 5.8%
Q4(3Al): 27.7%
Q4(2Al): 39.1%
Q4(1Al): 24.5%
Q4(0Al): 2.9%
Q4(4Al)
Q4(3Al)
Q4(2Al)
Q4(1Al)
Q4(0Al)
-70
-80
-90
-100
-110
-120
ppm
Fly ash in air
Q4(4Al): 6.7%
Q4(3Al): 27.0%
Q4(2Al): 22.4%
Q4(1Al): 24.2%
Q4(0Al): 11.4%
Q1(1Al): 1.5%
Q1: 3.8%
Q2: 0.8%
Q3: 2.0%
Q1(1Al)
Q1
Q4(4Al)
Q4(3Al)
Q4(2Al)
Q4(1Al)
Q4(0Al)
Q2
Q3
-70
-80
-90
-100
-110
-120
ppm

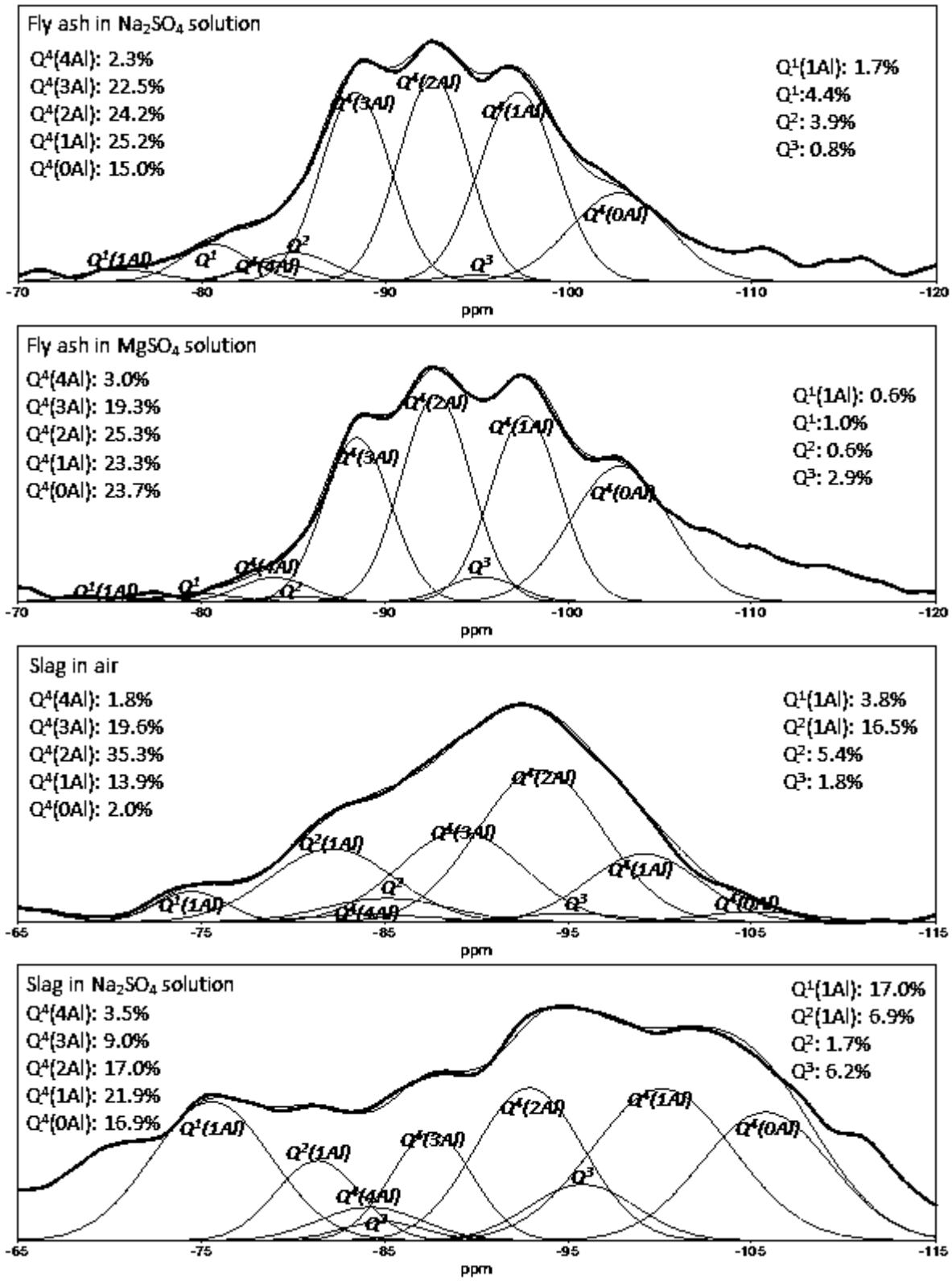
Fly ash in Na_2SO_4 solution
Q^4(4Al): 2.3%
Q^4(3Al): 22.5%
Q^4(2Al): 24.2%
Q^4(1Al): 25.2%
Q^4(0Al): 15.0%
Q^1(1Al): 1.7%
Q^1:4.4%
Q^2: 3.9%
Q^3: 0.8%
Q^1(1Al)
Q^1
Q^4(4Al)
Q^2
Q^4(3Al)
Q^4(2Al)
Q^4(1Al)
Q^3
Q^4(0Al)
-70
-80
-90
-100
-110
-120
ppm
Fly ash in $MgSO_4$ solution
Q^4(4Al): 3.0%
Q^4(3Al): 19.3%
Q^4(2Al): 25.3%
Q^4(1Al): 23.3%
Q^4(0Al): 23.7%
Q^1(1Al): 0.6%
Q^1:1.0%
Q^2: 0.6%
Q^3: 2.9%
Q^4(2Al)
Q^4(1Al)
Q^4(3Al)
Q^4(0Al)
Q^4(4Al)
Q^3
Q^1(1Al)
Q^1
Q^2
-70
-80
-90
-100
-110
-120
ppm
Slag in air
Q^4(4Al): 1.8%
Q^4(3Al): 19.6%
Q^4(2Al): 35.3%
Q^4(1Al): 13.9%
Q^4(0Al): 2.0%
Q^1(1Al): 3.8%
Q^2(1Al): 16.5%
Q^2: 5.4%
Q^3: 1.8%
Q^4(2Al)
Q^2(1Al)
Q^4(3Al)
Q^4(1Al)
Q^2
Q^1(1Al)
Q^3
Q^4(4Al)
Q^4(0Al)
-65
-75
-85
-95
-105
-115
ppm
Slag in Na_2SO_4 solution
Q^4(4Al): 3.5%
Q^4(3Al): 9.0%
Q^4(2Al): 17.0%
Q^4(1Al): 21.9%
Q^4(0Al): 16.9%
Q^1(1Al): 17.0%
Q^2(1Al): 6.9%
Q^2: 1.7%
Q^3: 6.2%
Q^1(1Al)
Q^2(1Al)
Q^4(3Al)
Q^4(2Al)
Q^4(1Al)
Q^4(0Al)
Q^3
Q^4(4Al)
Q^2
-65
-75
-85
-95
-105
-115
ppm

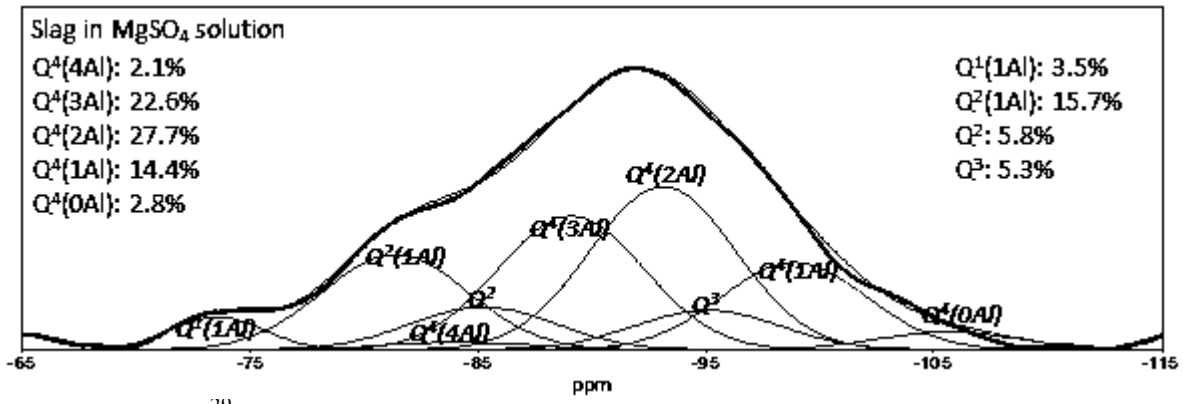

Figure 4.4.6. ^{29}Si NMR spectra and deconvolution of the alkali-activated binders cured differently.

Table 4.4.2 gives the summary of N-A-S-H, C-A-S-H and C-S-H gels in the alkali-activated binders after deconvolution. For the metakaolin-based binders, only N-A-S-H gel is formed. For the fly ash -based binders, about 91.8%, 89.3% and 91.3% N-A-S-H gel formed in the binders exposed in air, Na_2SO_4 and $MgSO_4$ solutions, respectively. For the slag-based binders, about 72.6%, 68.3% and 67.3% N-A-S-H gel are formed in the binders exposed in air, Na_2SO_4 solution, and $MgSO_4$ solution, respectively. It is suggested that N-A-S-H gel is the main gel in the alkali-activated binder. The sum of $Q^4(4Al)$, $Q^4(3Al)$ and $Q^4(2Al)$ in the N-A-S-H gel representing a better cross-linked aluminosilicate structure is also presented. It can be observed that the sums of alkali-activated binder cured in sulfate solution are lower than them cured in air. It is suggested that sulfate solutions inhibit the geopolymerization through dissolving the alkalinity of the samples.

Table 4.4.2. Summary of N-A-S-H, C-A-S-H and C-S-H gels in the alkali-activated binders after deconvolution.

Binders		N-A-S-H gel		C-A-S-H and C-S-H gels
		Q^4(mAl)	sum of Q^4(4Al), Q^4(3Al) and Q^4(2Al)	(Q^1+Q^2+Q^3)
Metakaolin	Air	100%	83.3%	0
	Na_2SO_4	100%	49.7%	0
	$MgSO_4$	100%	72.6%	0
Fly ash	Air	91.8%	56.2%	8.2%
	Na_2SO_4	89.3%	49.1%	10.7%
	$MgSO_4$	91.3%	45.9%	8.7%
Slag	Air	72.6%	56.7%	27.4%
	Na_2SO_4	68.3%	29.2%	31.7%
	$MgSO_4$	69.7%	52.4%	30.3%

4.5. Effect of calcium content on the microstructure and chloride corrosion of alkali-activated reinforced mortars

Figure 4.5.1 shows the compressive strength of alkali-activated mortars after 28 days in sealed. Without tailing, the compressive strength is 25.0 MPa, and then it increases to 30.2 MPa, 36.5

MPa and 41.3 MPa as increasing the contents of tailing to 20%, 40% and 60%, respectively. With the addition of iron mine tailings, C-A-S-H and C-S-H gels are formed in the mortars, which enhance the mechanical property of the mortars (Buchwald et al., 2009; Bernal, 2015; Chen et al., 2018). It corresponds well with the report elsewhere that the C-A-S-H gel in N-A-S-H gel promotes the formation of more cross-linked binding products and a denser microstructure (Ismail et al., 2014)

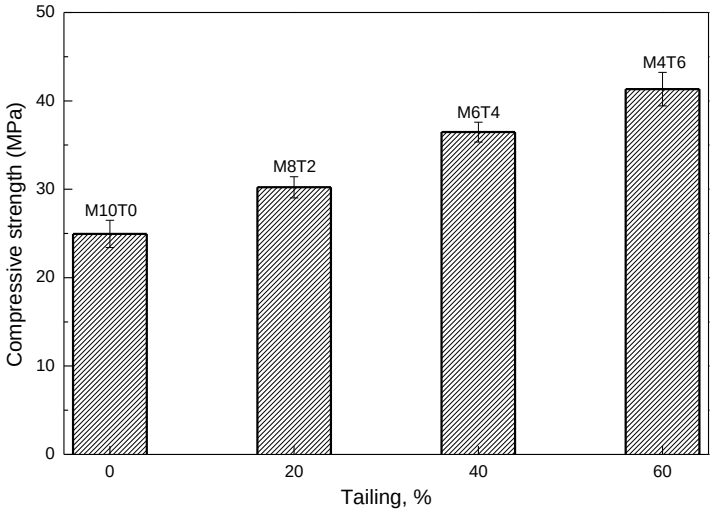

Figure 4.5.1. The compressive strength of AAMs after 28 days in sealed.

Figure 4.5.2 shows the ^{29}Si NMR spectra and their deconvolution of the binders in AAMs. The spectra are deconvoluted by fitting the Gaussian peak of the $Q^n(mAl)$ ($0 \leq m \leq n \leq 4$, m, n = integer). As reported elsewhere (Engelhardt and Michel, 1987), the N-A-S-H gel in alkali-activated metakaolin is described as $Q^4(mAl)$, namely $Q^4(4Al)$, $Q^4(3Al)$, $Q^4(2Al)$, $Q^4(1Al)$ and $Q^4(0Al)$, which resonate at approximately -84, -89, -93, -99 and -108 ppm, respectively. In addition, the silicon in the form of Q^1, Q^2 and Q^3 sites are presented in the C-A-S-H gel and C-S-H (Paradal et al., 2012; Burciaga-Díaz and Escalante-Garcia, 2013). Here the Q^1, Q^2 and Q^3 resonate at approximately -79, -85 and -95 ppm, respectively. The peak at about -73 ppm in M4T6 may be attributed to the unreacted silicate in iron ore tailing. Without iron ore tailing, the N-A-S-H gel is 100% in M10T0. As increasing the content of iron ore tailing to 20%, 40% and 60%, the N-A-S-H gel decreases to 82.1%, 73.2% and 69.7%, respectively. It suggests that the main gel in alkali-activated metakaolin-iron ore tailing is N-A-S-H gel. The content of C-A-S-H and C-S-H gel in M8T2, M6T4 and M4T6 are 17.9%, 26.8% and 26.3%, respectively. These gels raised the compressive strength of the AAMs.

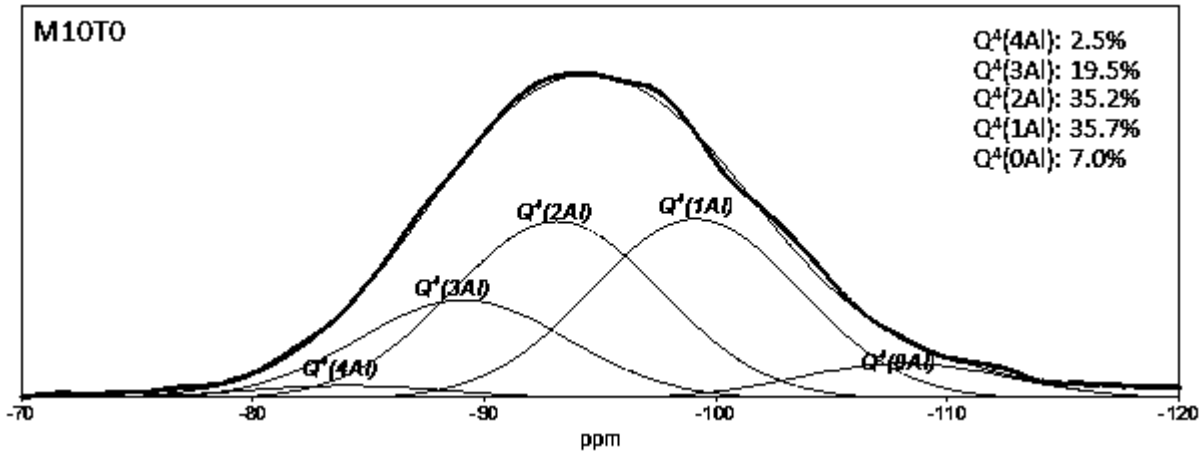
M10T0
Q⁴{4Al}: 2.5%
Q⁴{3Al}: 19.5%
Q⁴{2Al}: 35.2%
Q⁴{1Al}: 35.7%
Q⁴{0Al}: 7.0%
Q⁴(2Al)
Q⁴(1Al)
Q⁴(3Al)
Q⁴(4Al)
Q⁴(0Al)
-70
-80
-90
-100
-110
-120
ppm

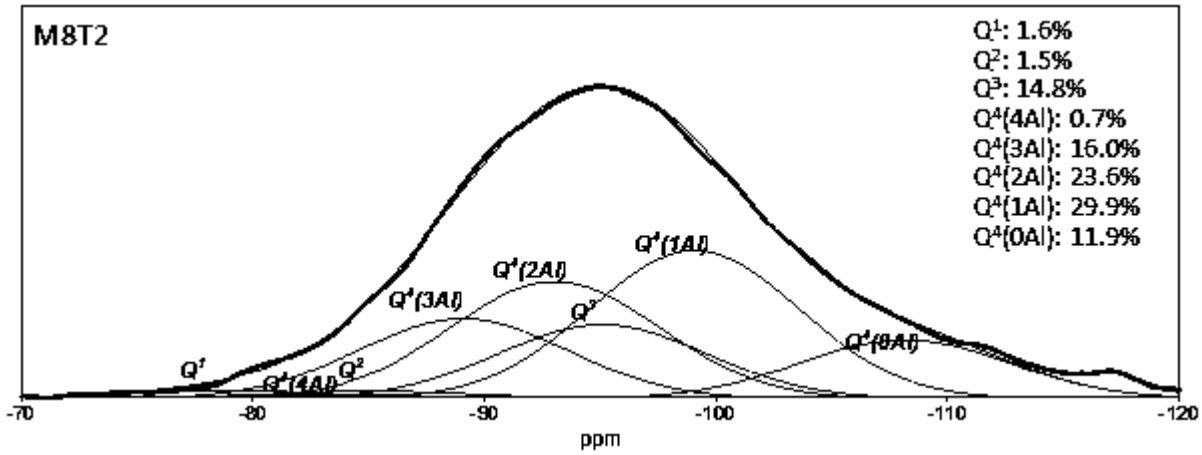
M8T2
Q¹: 1.6%
Q²: 1.5%
Q³: 14.8%
Q⁴{4Al}: 0.7%
Q⁴{3Al}: 16.0%
Q⁴{2Al}: 23.6%
Q⁴{1Al}: 29.9%
Q⁴{0Al}: 11.9%
Q⁴(1Al)
Q⁴(2Al)
Q⁴(3Al)
Q³
Q⁴(0Al)
Q¹
Q⁴(4Al)
Q²
-70
-80
-90
-100
-110
-120
ppm

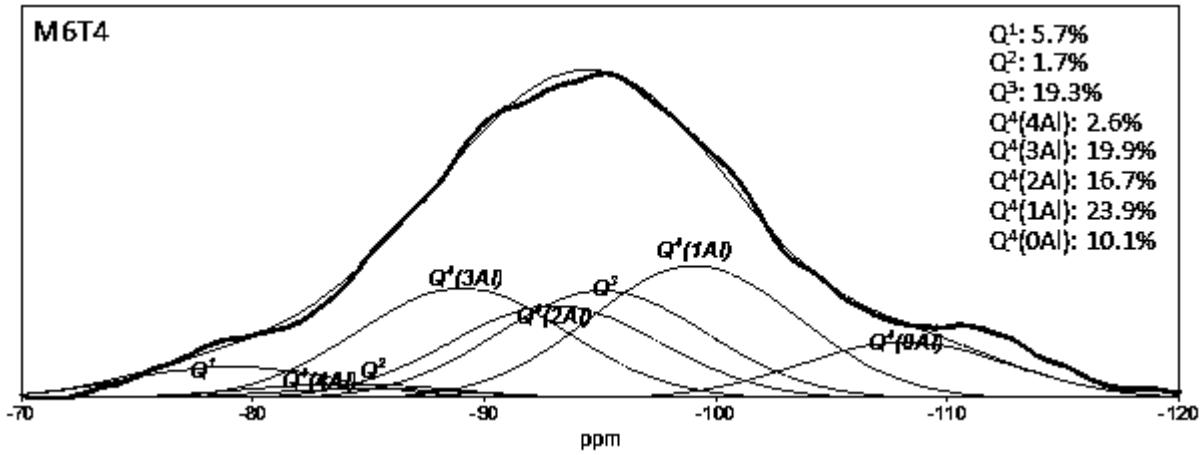
M6T4
Q¹: 5.7%
Q²: 1.7%
Q³: 19.3%
Q⁴{4Al}: 2.6%
Q⁴{3Al}: 19.9%
Q⁴{2Al}: 16.7%
Q⁴{1Al}: 23.9%
Q⁴{0Al}: 10.1%
Q⁴(1Al)
Q⁴(3Al)
Q²
Q⁴(2Al)
Q⁴(0Al)
Q¹
Q⁴(4Al)
Q²
-70
-80
-90
-100
-110
-120
ppm

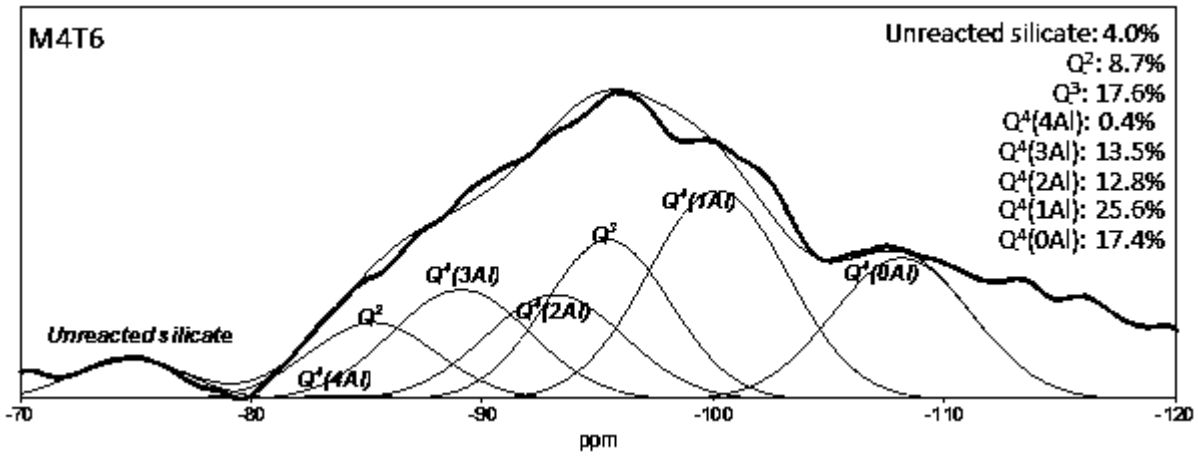

Figure 4.5.2. Deconvolution results for ^{29}Si NMR spectra of binders in the AAMs after accelerated corrosion.

Figure 4.5.3 shows the surface morphology of the reinforcement after accelerated corrosion for 160 days. All the reinforcements show the corrosion products. Part of the passivation film still remains on the surface of the reinforcement in M10T0, indicating relatively low corrosion. Some loose and porous corrosion products peel off from the reinforcements in the M8T2 and M6T4. A visible corrosion trace along the reinforcement in M4T6 mortar is attributed to strong corrosion reaction. Table 4.5.1 displays the quality loss of the reinforcement in mortar specimens. The quality loss of reinforcements in M10T0, M8T2 and M6T4 are very low, which are 2.7%, 3.3% and 3.9%. But the quality loss of reinforcement in M4T6 is 18.9%. These results indicate that rebar in M4T6 is more corroded than others.

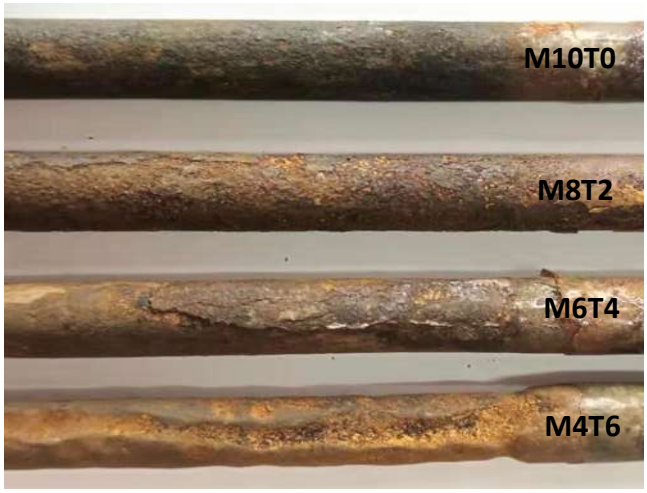

Figure 4.5.3. Surface morphology of reinforcement in mortar specimens at the end of accelerated corrosion.

Table 4.5.1. Quality loss of the reinforcement in mortar specimens.

Quality loss	M10T0	M8T2	M6T4	M4T6
Mass (wt %)	2.7%	3.3%	3.9%	18.9%

Figure 4.5.4 presents the results of corrosion density for the reinforcement in AAMs obtained by the electrochemical measurement of R_p. The reinforcement in M10T0 shows an extremely low i_{corr} around 0.1 μA cm^{-2}, indicating low corrosion rate or protection from corrosion. In 70 days corrosion, the reinforcements in M8T2, M6T4 and M4T6 also show low corrosion current, which might indicate the unstable passive film remain (Alhozaimy et al., 2014). Then, the i_{corr} of these reinforcement samples increases from 70 to 160 days of corrosion. While at 160 days, the reinforcements in M8T2 and M6T4 show the i_{corr} around 0.5 μA cm^{-2}, which is a low corrosion according to the Durar network specifications (1997), but the reinforcement in M4T6 gives the i_{corr} around 1.53 μA cm^{-2}, indicating high corrosion. These results correspond well with the surface morphology of reinforcements as shown in Figure 4.5.5. Therefore, the AAM without tailing or calcium shows very low corrosion in 160 days, while the AAMs with 20% and 40% tailings show a relative low corrosion, but the AAM with 60% tailings shows a high corrosion in 160 days.

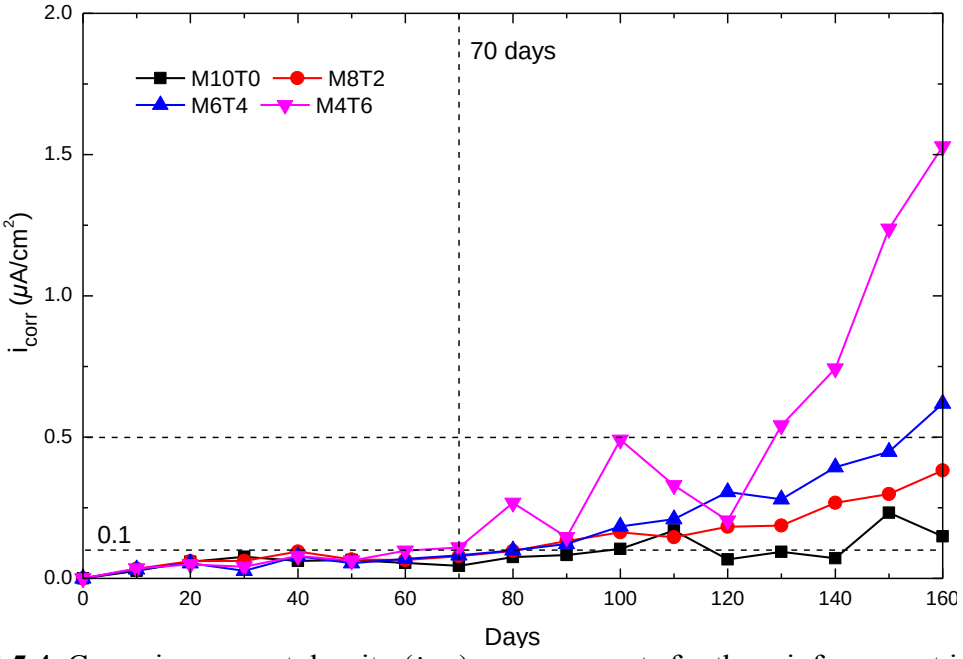

Figure 4.5.4. Corrosion current density (i_{corr}) measurements for the reinforcement in alkali-activated binders.

Figure 4.5.5 shows the microstructural morphology of M10T0 and M4T6 after accelerated corrosion. Based on the EDX analysis, halite is observed in both samples without calcium and with high calcium contents. Compared to the M10T0, crack is observed in M4T6. The halite distributes mainly along the crack in M4T6, however, it distributes evenly in the binder of M10T0 mortar. The distribution of halite in M10T0 suggests micropores in the structure.

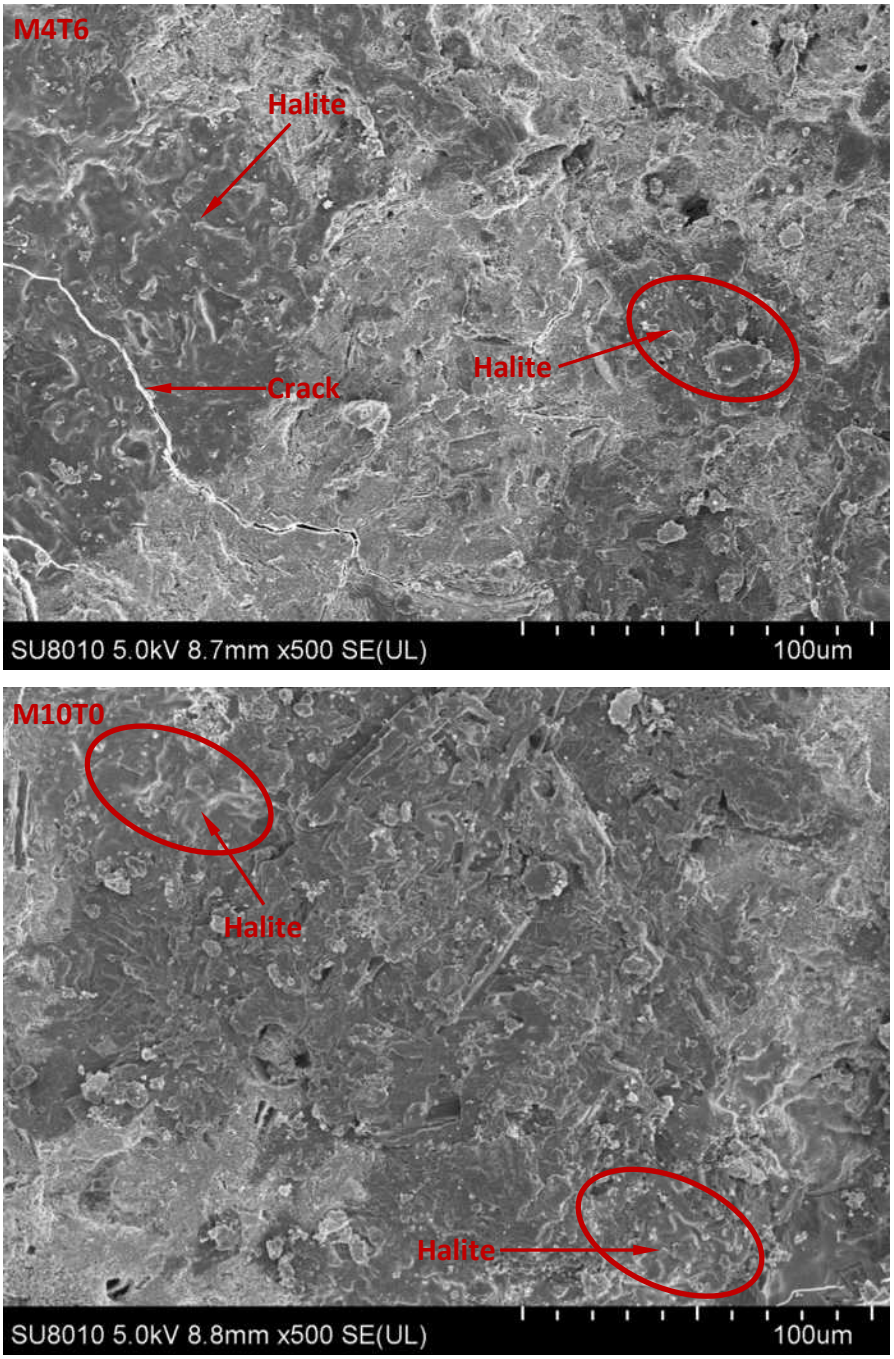

Figure 4.5.5. Microstructural morphology of the AAMs after 160 days accelerated corrosion.

Figure 4.5.6 shows the diffractograms of the AAMs near the reinforcements. An amorphous XRD pattern with one hump centered at approximately 27-29° 2θ is observed in all mortars, which suggests the formation of N-A-S-H gel (Duxson et al., 2005). As increasing the tailing content, the hump attenuates and the characteristic peaks of C-S-H enhances. The quartz, muscovite and calcite are from the raw materials of metakaolin and iron ore tailing. After 160 days accelerated corrosion in sea water, the precipitates of gypsum and ettringite form in the AAMs (M8T2, M6T4 and M4T6). It reveals that sulfate ions invade the mortar and react with calcium in binder. As discussed by Komljenovic et al. (2013), the gypsum and ettringite could induce the structural

changes of alkali-activated binder with calcium. Especially ettringite can induce disruptive expansion in the mortar, which reduces the corrosion resistance of the sample (Gollop et al., 1996). Therefor it can be observed that more corrosion products, such as goethite (α-FeOOH) and magnetite (Fe_3O_4), form in M4T6 (Duff ó et al., 2004). Once the ettringite causes crack, lots of chloride ions invade into the surface of rebar instead of penetrating. When the rebar is corroded, the expanded corrosion products further lead to more cracks. Therefore, an obvious corrosion trace is observed in M4T6 (Figure 4.5.3 and 4.5.4).

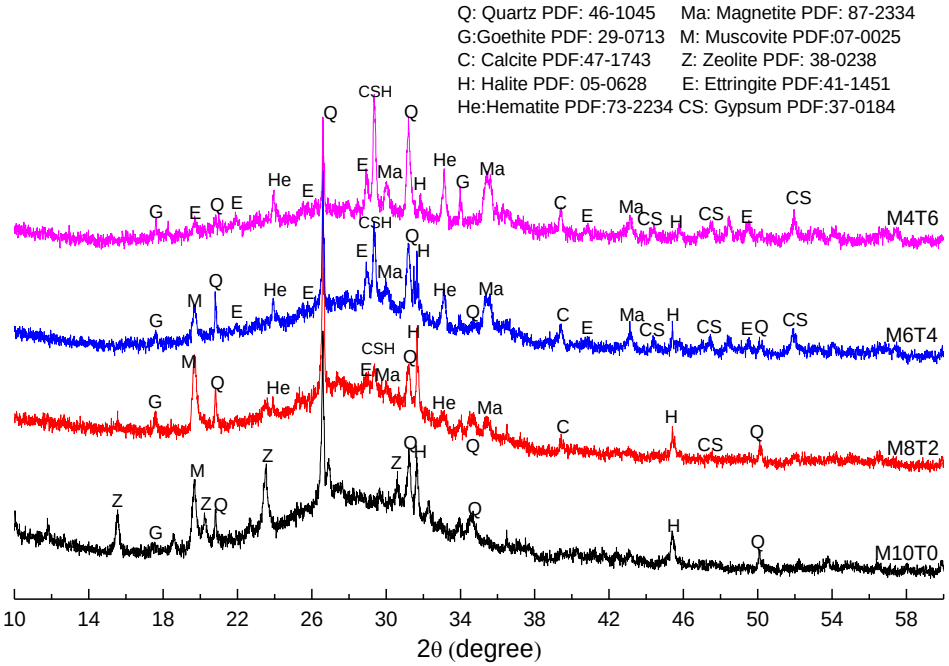

Figure 4.5.6. XRD patterns of the AAMs after accelerated corrosion.

5. Conclusion

1) Alkali-activated materials can be synthesized by metakaolin, geothermal clay, fly ash, slag and tailing. The initial values of compressive strength are about 20 ~ 60 MPa. After cured in various corrosive environments, the values of compressive strength can be still more than 10 MPa.

2) The replacement of silica sand induces porous structure in the geopolymer binders and decreases the compressive strength. Steel fiber gives negligible effect on compressive strength of the geopolymers, but it enhances their flexural strength and flexural fracture toughness.

3) Cracks and salts such as halite are formed in the metakaolin-based geopolymers exposed in seawater, leading to the decrease in compressive strength. Seawater environments inhibit the geopolymerization reactions.

4) Cristobalite enhances the compressive strength of geothermal clay-based geopolymer cured in sea water environment. They also improve the Si/Al ratio to prevent the formation of zeolite.

5) The deterioration of the alkali-activated materials exposed in sulfate solution is attributed to the dissolution of alkalis. Zeolite formation in the binders cured in Na_2SO_4 solution leads to their compressive strength decreases. A layer of precipitated minerals (e.g., brucite) formed on the surface of the binders cured in $MgSO_4$ solution, which inhibits the deterioration of the binders.

6) The 60% replacement of iron ore tailing in alkali-activated metakaolin (M4T6) greatly improves compressive strength. It is attributed to the presence of C-S-H gel and C-A-S-H gel. After 160 days accelerated corrosion by sea water, the reinforcement in M4T6 shows high corrosion because the low reactively and sulfate attack.

Recommendations for future work

The degradation mechanism of alkali activated materials exposed in sea water under the action of multiple factors has become a focus of current research. We have conducted some laboratory research on the durability of alkali-activated materials individually influenced by freeze-thaw and dry-wet cycles, sulfate corrosion and chloride penetration. However, the factors of carbonization, load and abrasion have not yet been amply investigated in this work, which is expected as our further research work.

References

Albitar, M., Ali, M.S.M., Visintin, P., Drechsler, M., 2017. Durability evaluation of geopolymer and conventional concretes. Construction and Building Materials. 136, 374-385.

Alhozaimy, A., Hussain, R.R., Al-Negheimish, Al-Zaid, A., R., Singh, D.D.N., 2014. Effect of simulated concrete pore solution chemistry, chloride ions, and temperature on passive layer formed on steel reinforcement. ACI Materials Journal. 111.

Alonso, S. and Palomo, A., 2001. Alkaline activation of metakaolin and calcium hydroxide mixtures: influence of temperature, activator concentration and solids ratio. Materials Letters. 47, 55-62.

Arbi, K., Nedeljkovic, M., Zuo, Y., Ye, G., 2016. A review on the durability of alkali-activated fly ash/slag systems: advances, issues, and perspectives. Industrial and Engineering Chemistry Research. 55(19), 5439-5453.

Astutiningsih, S., Nurjaya, D.M., Ashadi, HW., Swastika, N., 2010. Durability of Geopolymer Concretes upon Seawater Exposure. Advances in Science and Technology. 69, 92-96.

Bakharev, T., 2005. Durability of geopolymer materials in sodium and magnesium sulfate solutions. Cement and Concrete Research. 35(6), 1233-1246.

Bakharev, T., 2005. Resistance of geopolymer materials to acid attack. Cement and Concrete Research. 35(4), 658-670.

Bascarevic, Z., Komljenovic, M., Miladinovic, Z., Nikolic, V., Marjanovic, N., Petrovic, R., 2015. Impact of sodium sulfate solution on mechanical properties and structure of fly ash based geopolymers. Materials and Structures. 48, 683-697.

Barbosa, V.F.F., MacKenzie, K.J.D., 2000. Thaumaturgo C. Synthesis and characterisation of materials based on inorganic polymers of alumina and silica: sodium polysialate polymers. International Journal of Inorganic Materials. 2(4), 309-317.

Barr, B.I.G., Liu, K., Dowers, R.C., 1982. A toughness index to measure the energy absorption of fibre reinforced concrete. International Journal of Cement Composites and Lightweight Concrete. 4, 221-227.

Bayuaji, R., Darmawan, M.S., Wibowo, B., Husin, N.A., Subekti, S., 2016. Utilization of high calcium content fly ash: flexural strength of geopolymer concrete beams in sea water environment. The Open Civil Engineering Journal. 10, 782-793.

Ben Haha, M., Lothenbach, B., Le Saout, G.L., Winnefeld F., 2011. Influence of slag chemistry on the hydration of alkali-activated blast-furnace slag-Part I: Effect of MgO. Cement and Concrete Research. 41, 955-963.

Bernal, S., De Gutierrez, R., Delvasto, S., Rodriguez, E., 2010. Performance of an alkali-activated slag concrete reinforced with steel fibers. Construction and building Materials. 24(2), 208-214.

Bernal, S.A., De Gutierrez, R.M., Provis, J.L., Rose, V., 2010. Effect of silicate modulus and metakaolin incorporation on the carbonation of alkali silicate-activated slags. Cement and Concrete Research. 40, 898-907.

Bernal, S.A., Provis, J.L., Rose, V., De Gutierrez, R.M., 2011. Evolution of binder structure in sodium silicate-activated slag-metakaolin blends. Cement and Concrete Composites. 33(1), 46-54.

Bernal, S.A., Provis, J.L., De Gutiérrez, R.M., van Deventer, J.S.J., 2015. Accelerated carbonation testing of alkali-activated slag/metakaolin blended concretes: effect of exposure conditions. Materials and Structures. 48, 653-669.

Bernal, S.A., 2015. Effect of the activator dose on the compressive strength and accelerated carbonation resistance of alkali silicate-activated slag/metakaolin blended materials. Construction and Building Materials. 98, 217-226.

Binici, H., Aksogan, O., Görür, E.B., Kaplan, H., Bodur, M.N., 2008. Performance of ground blast furnace slag and ground basaltic pumice concrete against seawater attack. Construction and Building Materials. 22, 1515-1526.

Bonk, F., Schneider, J., Cincotto, M.A., Panepucci, H., 2003. Characterization by multinuclear high-resolution NMR of hydration products in activated blast-furnace slag pastes. Journal of the American Ceramic Society. 86, 1712-1719.

Bortnovsky, O., Dedecek, J., Tvaružková, Z., Sobalík, Z., Šubrt, J., 2008. Metal ions as probes for characterization of geopolymer materials. Journal of the American Ceramic Society. 91, 3052-3057.

Buchwald, A., Tatarin, R., Stephan, D., 2009. Reaction progress of alkaline-activated metakaolin-ground granulated blast furnace slag blends. Journal of materials science. 44, 5609-5617.

Buenfeld, N.R., Newman, J.B., 1986.The development and stability of surface layers on concrete exposed to sea-water. Cement and Concrete Research. 16(5),721-732.

Burciaga-Díaz, O., Escalante-García, J.I., 2013. Structure, mechanisms of reaction, and strength of an alkali-activated blast-furnace slag. Journal of the American Ceramic Society. 96, 3939-3948.

Chen, X., Sutrisno, A., Struble, L.J., 2018. Effects of calcium on setting mechanism of metakaolin-based geopolymer. Journal of the American Ceramic Society. 101, 957-968.

Cheng, T.W, and Chiu, J.P., 2003. Fire-resistant geopolymer produced by granulated blast furnace slag. Minerals Engineering, 16, 205-210.

Chindaprasirt, P., Silva, P.D., Crentsil, K.S., Hanjitsuwan, S., 2012. Effect of SiO_2 and Al_2O_3 on the setting and hardening of high calcium fly ash-based geopolymer systems. Journal of materials science. 47, 4876-4883.

Chindaprasirt, P., Chalee, W., 2014. Effect of sodium hydroxide concentration on chloride penetration and steel corrosion of fly ash-based geopolymer concrete under marine site. Construction and Building Materials. 63, 303-310.

Criado, M., Fernández-Jiménez, A., de la Torre, A.G., Aranda, M.A.G., Palomo, A., 2007. An XRD study of the effect of the SiO_2/Na_2O ratio on the alkali activation of fl y ash. Cement and Concrete Research. 37(5), 671-679.

Davidovits J., 1984. Synthetic mineral polymer compound of the silicoaluminates family and preparation process. US Patent :4472199.

Davidovits, J., 1989. Geopolymers and geopolymeric materials. Journal of Thermal Analysis and Calorimetry. 35(2), 429-441.

Davidovits, J., 1994. Properties of geopolymer cements. In First international conference on alkaline cements and concretes. Kiev State Technical University, Ukraine: Scientific Research Institute on Binders and Materials.

De Silva, P., Sagoe-Crenstil, K., 2008. Medium-term phase stability of Na_2O-Al_2O_3-SiO_2-H_2O geopolymer systems. Cement and Concrete Research. 38(6), 870-876.

De Weerdt, K., Justnes, H., Geiker, M.R., 2014. Changes in the phase assemblage of concrete exposed to sea water. Cement and Concrete Composites. 47, 53-63.

Diaz-Loya, E.I., Allouch, E.N., Vaidya, S., 2011. Mechanical properties of fly-ash based geopolymer concrete. ACI Materials Journal. 108, 300-306.

Duffó, G.S., Morris, W., Raspini, I., Saragovi, C., 2004. A study of steel rebars embedded in concrete during 65 years. Corrosion Science. 46, 2143-2157.

DURAR NETWORK, 1997. Manual inspection evaluation and assessment of corrosion in reinforced concrete structures, CYTED Program, Rio de Janeiro.

Duxson, P., Provis, J.L., Lukey, G.C., Separovic, F., van Deventer, J.S. 2005. ^{29}Si NMR study of structural ordering in aluminosilicate geopolymer gels. Langmuir. 21(7), 3028-3036.

Duxson, P., Fernández-Jiménez, A., Provis, J.L., Lukey, G.C., Palomo, A., van Deventer, J.S.J., 2007. Geopolymer technology: the current state of the art. Journal of materials science. 42 (9), 2917-2933

Engelhardt, G., and Michel, D., 1987. High-resolution solid-state NMR of silicates and zeolites. United States.

Escalante-García, J.I., Fuentes A.F., Gorokhovsky, A., Fraire-Luna, P.E., Mendoza-Suarez, G., 2003. Hydration Products and Reactivity of Blast-Furnace Slag Activated by Various Alkalis. Journal of the American Ceramic Society. 86, 2148-2153.

Fernández-Jiménez, A., Puertas, F., Sobrados, I., Sanz, J., 2003. Structure of calcium silicate hydrates formed in alkaline-activated slag: influence of the type of alkaline activator. Journal of the American Ceramic Society. 86, 1389-1394.

Fernández-Jiménez, A., Palomo, A., 2005a. Microstructure development of alkali-activated fly ash cement: a descriptive model. Cement and Concrete Research. 35, 1204-1209.

Fernández-Jiménez, A., and Palomo, A., 2005b. Composition and microstructure of alkali activated fly ash binder: Effect of the activator. Cement and Concrete Research. 35, 1984-1992.

Fernández-Jiménez, A., Palomo, A., Sobrados, I., Sanz, J., 2006. The role played by the reactive alumina content in the alkaline activation of fly ashes. Microporous and Mesoporous materials. 91(1-3), 111-119.

Ganesan, N., Abraham, R., Raj, S.D., 2015. Durability characteristics of steel fibre reinforced geopolymer concrete. Construction and Building Materials. 93, 471-476.

Gao, X., Yu, Q.L., Brouwers, H.J.H., 2017. Apply ^{29}Si, ^{27}Al MAS NMR and selective dissolution in identifying the reaction degree of alkali activated slag-fly ash composites. Ceramics International. 43, 12408-12419.

Gjorv, O.E., 1994. Steel corrosion in concrete structures exposed to Norwegian marine environment. Concrete International, 16(4), 35-39.

Glad, B.E., Kriven, W.M., 2013. Optimization of gas adsorption porosimetry for geopolymer analysis. Journal of the American Ceramic Society. 96, 3643-3649

Glukhovsky, V.D., Rostovskaja, G.S., Rumyna, G.V, 1980. High strength slag-alkaline cements. Proceedings of the seventh international congress on the chemistry of cement. 3, 164-168.

Glukhovsky, V.D., 1994. Ancient, modern and future concretes. In Proceedings of the 1st International Conference on Alkaline Cements and Concretes, P. (V. Krivenko, Ed.), Kiev, Ukraine: VIPOL Stock Company. 1-9.

Gollop, R.S., Taylor, H.F.W., 1996. Microstructural and microanalytical studies of sulfate attack. V. Comparison of different slag blends. Cement and Concrete Research. 26, 1029-1044.

Gomez-Zamorano, L.Y., Vega-Cordero, E., Struble, L., 2016. Composite geopolymers of metakaolin and geothermal nanosilica waste. Construction and Building Materials. 115, 269-276.

Hu, X., Shi, C., Shi, Z., Zhang, L., 2019. Compressive strength, pore structure and chloride transport properties of alkali-activated slag/fly ash mortars. Cement and Concrete Composites. 104, 103392.

Ismail, I., Bernal, S.A., Provis, J.L., San Nicolas, R., Hamdan, S., van Deventer, J.S.J., 2014. Modification of phase evolution in alkali-activated blast furnace slag by the incorporation of fly ash. Cement and Concrete Composites. 45, 125-135.

Jaya, N.A., Abdullah, M.M.A.B., Li, L.Y., Sandu, A.V., Hussin, K., Ming, L.Y., 2017. Durability of metakaolin geopolymers with various sodium silicate/sodium hydroxide ratios against seawater exposure. AIP Conference Proceedings. AIP Publishing. 1887(1), 020063.

Khale, D., Chaudhary, R., 2007. Mechanism of geopolymerization and factors influencing its development: a review. Journal of Materials Science. 42, 729-746.

Klinowski, J., 1984. Nuclear magnetic resonance studies of zeolites. Prog Nucl Magn Reson Spectrosc. 16, 237-309.

Komljenovic, M., Bascarevic, Z., Marjanovic, N., Nikolic, V., 2013. External sulfate attack on alkali-activated slag. Construction and Building Materials. 49, 31-39.

Krivenko, P., 2017. Why alkaline activation-60 years of the theory and practice of alkali-activated materials, Journal of Ceramic Science and Technology. 8, 323-333.

Kuenzel, C., Grover, L.M., Vandeperre, L., Boccaccini, A.R., Cheeseman, C.R., 2013. Production of nepheline/quartz ceramics from geopolymer mortars. Journal of the European Ceramic Society. 33(2), 251-258.

Kukko, H., Mannonen, R., 1982. Chemical and mechanical properties of alkali-activated blast furnace slag (F-concrete). Nordic Concrete. Research.

Kumar, R., Kumar, S., and Mehrotra, S.P., 2007. Towards sustainable solutions for fly ash through mechanical activation. Resources Conservation & Recycling, 52, 157-179.

Kumar, S., Kumar, R., Mehrotra, S.P., 2010. Influence of granulated blast furnace slag on the reaction, structure and properties of fly ash based geopolymer. Journal of materials science. 45(3), 607-615.

Kumar, S. and Kumar, R., 2011. Mechanical activation of fly ash: Effect on reaction, structure and properties of resulting geopolymer. Ceramics International. 37, 533-541.

Kupwade-Patil, K., Allouche, E.N., 2013. Examination of chloride-induced corrosion in reinforced geopolymer concretes. Journal of Materials in Civil Engineering. 25, 1465-1476.

Kwan, W.H., Cheah, C.B., Ramli, M., Chang, K.Y., 2018. Alkali-resistant glass fiber reinforced high strength concrete in simulated aggressive environment. Materiales de Construcción. 68(329), 147.

Lee, S.K., Stebbins, J.F., 1999. The degree of aluminum avoidance in aluminosilicate glasses. American Mineralogist. 84(5-6), 937-945.

Li, G., Zhang, A., Song, Z., Shi, C., Wang, Y., Zhang, J., 2017. Study on the resistance to seawater corrosion of the cementitious systems containing ordinary Portland cement or/and calcium aluminate cement. Construction and Building Materials. 157, 852-859.

Li, X., Rao, F., Song, S., Corona-Arroyo, M.A., Ortiz-Lara, N., Aguilar-Reyes, E.A., 2018. Effects of aggregates on the mechanical properties and microstructure of geothermal metakaolin-based geopolymers. Results in Physics. 11, 267-273.

Liu, Z., Diao, B., Zheng, X., 2015. Effects of seawater corrosion and freeze-thaw cycles on mechanical properties of fatigue damaged reinforced concrete beams. Advances in Materials Science and Engineering. 536487.

Long, T., Wang, Q., Guan, Z., Chen, Y., Shi, X. 2017. Deterioration and microstructural evolution of the fly ash geopolymer concrete against $MgSO_4$ solution. Advances in Materials Science and Engineering. 4247217.

Lothenbach, B., Gruskovnjak, A., 2007. Hydration of alkali-activated slag: thermodynamic modelling. Advances in cement research. 19(2), 81-92.

Luukkonen, T., Abdollahnejad, Z., Yliniemi, J., Kinnunen, P., Illikainen, M., 2018. One-part alkali-activated materials: A review. Cement and Concrete Research. 103, 21-34.

Mas, A., Guisseau, D., Mas, P.P., Beaufort, D., Genter, A., Sanjuan, B., Girard, J.P., 2006. Clay minerals related to the hydrothermal activity of the Bouillante geothermal field (Guadeloupe). Journal of Volcanology and Geothermal research. 158(3-4), 380-400.

Mehta, PK. 1990. Causes of deterioration of concrete in seawater. Concrete in the marine environment. Routledge.

Mehta, PK., 2005. Concrete in the marine environment. CRC Press.

Mehta, A., Siddique, R., 2017. Strength permeability and micro-structural characteristics of low-calcium fly ash based geopolymers. Construction and Building Materials. 141, 325-334.

Mather, B., 1964. Effects of sea water on concrete. Highway Research Record, Highway Research Board.

Myers, R.J., Bernal, S.A., San Nicolas, R,, Provis, J.L., 2013. Generalized structural description of calcium-sodium aluminosilicate hydrate gels: the cross-linked substituted tobermorite model. Langmuir. 29:5294-5306.

Myers, R.J., Bernal, S.A., Provis, J.L., 2014. Athermodynamicmodel for C-(N-)A-S-H gel: CNASH_ss. Derivation and validation. Cement and Concrete Research. 66, 27-47.

Mobili, A., Belli, A., Giosue, C., Bellezze, T., Tittarelli, F., 2016. Metakaolin and fly ash alkali-activated mortars compared with cementitious mortars at the same strength class. Cement and Concrete Research. 88, 198-210.

Montes, C., Allouche, E.N., 2012. Evaluation of the potential of geopolymer mortar in the rehabilitation of buried infrastructure. Structure and Infrastructure Engineering. 8(1), 89-98.

Moosberg-Bustnes, H., Lagerblad, B., Forssberg, E., 2004. The function of fillers in concrete. Materials and Structures. 37(2), 74.

Mostafa, N.Y., El-Hemaly, S.A.S., Al-Wakeel, E.I., El-Korashy, S.A., & Brown, P.W., 2001. Characterization and evaluation of the pozzolanic activity of Egyptian industrial by-products: I: Silica fume and dealuminated kaolin. Cement and Concrete Research. 31(3), 467-474.

Noushini, A., Castel, A., Aldred, J., Rawal, A., 2020. Chloride diffusion resistance and chloride binding capacity of fly ash-based geopolymer concrete, Cement and Concrete Composites. 105, 103290.

Muñiz-Villarreal, M. S., Manzano-Ramírez, A., Sampieri-Bulbarela, S., Gasca-Tirado, J. R., Reyes-Araiza, J. L., Rubio-Ávalos, J. C., Pérez-Bueno, J. J., Apatiga, L. M., Cadena, A. Z., and Borrás, V. A., 2011, The effect of temperature on the geopolymerization process of a metakaolin-based geopolymer. Materials Letters. 65, 995-998.

Osio-Norgaard, J., Gevaudan, J.P., Srubar III, W.V., 2018. A review of chloride transport in alkali-activated cement paste, mortar, and concrete. Construction and Building Materials. 186, 191-206.

Pacheco-Torgal, F., Abdollahnejad, Z., Camões, A.F., Jamshidi, M., Ding. Y., 2012. Durability of alkali-activated binders: a clear advantage over Portland cement or an unproven issue? Construction and Building Materials. 30, 400-405.

Pasupathy, K., Berndt, M., Sanjayan, J., Rajeev, P., Cheema, D.S., 2017. Durability of low-calcium fly ash based geopolymer concrete culvert in a saline environment. Cement and Concrete Research. 100, 297-310.

Palomo, A., Fernández-Jimenez, A., Kovalchuck, G., 2005. Some key factors affecting the alkali activation of fly ash. 2nd International Symposium of Non-Traditional Cement and Concrete, Brno, Czech Republic.

Phair, J. W., van Deventer, J. S. J., and Smith, J. D., 2000, Mechanism of polysialation in the incorporation of zirconia into fly ash-based geopolymers. Industrial & Engineering Chemistry Research. 39, 2925-2934

Phair, J.W., and van Deventer, J.S.J., 2001. Effect of silicate activator pH on the leaching and material characteristics of waste-based inorganic polymers. Minerals Engineering, 14, 289-304.

Phair, J.W., van Deventer, J.S.J., and Smith, J.D., 2004. Effect of Al source and alkali activation on Pb and Cu immobilization in fly-ash based ‘‘geopolymers’’. Applied Geochemistry. 19, 423-434.

Provis, J.L., Van Deventer, J.S.J., 2009. Geopolymers: structures, processing, properties and industrial applications. Elsevier.

Provis, J.L., Van Deventer J.S.J., 2013. Alkali activated materials: state-of-the-art report. Springer Science and Business Media.

Provis, J.L., Palomo, A., Shi, C., 2015. Advances in understanding alkali-activated materials. Cement and Concrete Research. 78, 110-125

Purdon, A.O, 1940. The action of alkalis on blast-furnace slag. Journal of the Society of Chemical Industry. 59(9), 191-202

Ramdas, S., Klinowski, J., 1984. A simple correlation between isotropic ^{29}Si-NMR chemical shifts and T-O-T angles in zeolite frameworks. Nature. 308(5959), 521-523.

Rahier, H., Van Mele, B., Biesemans, M., Wastiels, J., Wu, X. 1996. Low-temperature synthesized aluminosilicate glasses. Journal of Materials Science. 31(1), 71-79.

Ranjbar, N., Mehrali, M., Mehrali, M., Alengaram, U.J., Jumaat, M.Z., 2016. High tensile strength fly ash based geopolymer composite using copper coated micro steel fiber. Construction and Building materials. 112, 629-638.

Rajamane, N.P., Nataraja, M.C., Dattatreya, J.K., Lakshmanan, N., Sabitha, D., 2012. Sulphate resistance and eco-friendliness of geopolymer concretes. Indian Concrete Journal. 86(1), 13-22.

Rashad, A.M., Ouda, A.S., Sadek, D.M., 2018. Behavior of alkali-activated metakaolin pastes blended with quartz powder exposed to seawater attack. Journal of Materials in Civil Engineering. 30(8), 04018159.

Rao, F., Liu, Q., 2015. Geopolymerization and its potential application in mine tailings consolidation: a review. Mineral Processing and Extractive Metallurgy Review. 36(6), 399-409.

Richardson, I.G., 1999. The nature of CSH in hardened cements. cement and concrete research. 29(8), 1131-1147.

Salami, B.A., Johari, M.A.M., Ahmad, Z.A., Maslehuddin, M., 2017. Durability performance of palm oil fuel ash-based engineered alkaline-activated cementitious composite (POFA-EACC) mortar in sulfate environment. Construction and building materials. 131, 229-244.

Schilling, P.J., Butler, L.G., Roy, A., Eaton, H.C., 1994. ^{29}Si and ^{27}Al MAS-NMR of NaOH-activated blast-furnace slag. Journal of the American Ceramic Society. 77(9), 2363-2368.

Seon-Ju, K., Kyung-Sub, C., Tae-Hoon, K., Chan-Ki, K., Chae-yong, L., 2011. Characteristics of seawater-resistance for Geo-polymer type of grout agen. In 2011 PAN-AM CGS geotechnical conference. The Canadian Geotechnical Society and the International Society for Soil Mechanics and Geotechnical Engineering.

Shaikh, F., Haque, S., 2017. Effect of nano silica and fine silica sand on compressive strength of sodium and potassium activators synthesised fly ash geopolymer at elevated temperatures. Fire and Materials. 42(3), 324-335.

Shang, X., Zhang, Y., Qu, N., Tang, X., 2016. Electrochemical analysis of passivation film formation on steel rebar in concrete. International Journal of Electrochemical Science. 11(7), 5870-5876.

Silva, P.D., Sagoe-Crenstil, K., Sirivivatnanon, V., 2007. Kinetics of geopolymerization: Role of Al_2O_3 and SiO_2. Cement and Concrete Research, 37, 512-518

Skorina, T., 2014. Ion exchange in amorphous alkali-activated aluminosilicates: potassium based geopolymers. Applied Clay Science. 87, 205-211

Singh, P.S., Bastow, T., Trigg, M., 2005. Structural studies of geopolymers by ^{29}Si and ^{27}Al MAS-NMR. Journal of materials science. 40(15), 3951-3961.

Skvara, F., Jílek, T., Kopecký, L., 2005. Geopolymer materials based on fly ash. Ceramics-Silikaty 49(3), 195-204.

Stern, M., Geary, A.L., 1957. Electrochemical polarization I. A theoretical analysis of the shape of polarization curves. Journal of the Electrochemical Society. 104, 56-63.

Sukmak, P., De Silva, P., Horpibulsuk, S., Chindaprasirt, P., 2014. Sulfate resistance of clay-portland cement and clay high-calcium fly ash geopolymer. Journal of Materials in Civil Engineering. 27, 4014158.

Shi, C., Fernández-Jiménez, A., Palomo, A., 2011. New cements for the 21st century: the pursuit of an alternative to Portland cement. Cement and Concrete Research. 41, 750-763.

Temuujin, J., Williams, R.P., and van Riessen, A., 2009. Effect of mechanical activation of fly ash on the properties of geopolymer cured at ambient temperature. Journal of Materials Processing Technology. 209, 5276-5280.

Tennakoon, C., Shayan, A., Sanjayan, J.G., Xu, A., 2017. Chloride ingress and steel corrosion in geopolymer concrete based on long term tests. Materials and design. 116, 287-299.

Val, D.V., Stewart, M.G., 2003. Life-cycle cost analysis of reinforced concrete structures in marine environments. Structural Safety. 25, 343-362.

Van Deventer, J.S.J., Provis, J.L., Duxson, P., Lukey, G.C., 2007. Reaction mechanisms in the geopolymeric conversion of inorganic waste to useful products. Journal of hazardous materials. 139(3), 506-513.

Wan, Q., Rao, F., Song, S., García, R.E., Estrella, R.M., Patino, C.L., Zhang, Y., 2017a. Geopolymerization reaction, microstructure and simulation of metakaolin-based geopolymers at extended Si/Al ratios. Cement and Concrete Composites. 79, 45-52.

Wan, Q., Rao, F., Song, S., Cholico-González, D.F., Ortiz, N.L., 2017b. Combination formation in the reinforcement of metakaolin geopolymers with quartz sand. Cement and Concrete Composites. 80, 115-122.

Wan, Q., Rao, F., Song, S., León-Patiño, C.A., 2017c. Geothermal clay-based geopolymer binders: Synthesis and microstructural characterization. Applied Clay Science. 146, 223-229.

Wan, Q., Rao, F., Song, S., 2017d. Reexamining calcination of kaolinite for the synthesis of metakaolin geopolymers-roles of dehydroxylation and recrystallization. Journal of Non-Crystalline Solids. 460, 74-80.

Wang, S.D., Pu, X.C., Scrivener, K.L., Pratt, P.L., 1995. Alkali-activated slag cement and concrete: a review of properties and problems. Advances in cement research. 7(27), 93-102.

Wang, H., Li, H., and Yan F., 2005. Synthesis and mechanical properties of metakaolinite-based geopolymer. Colloids and Surfaces A: Physicochemical and Engineering Aspects. 268, 1-6.

Wu, J., Li, H., Wang, Z., Liu, J., 2016. Transport model of chloride ions in concrete under loads and drying-wetting cycles. Construction and Building Materials. 112, 733-738.

Xu, H., van Deventer, J.S.J., 2000. The geopolymerisation of alumino-silicate minerals. International Journal of Mineral Processing, 59, 247-266.

Xu, H., van Deventer, J.S.J., 2002. Geopolymerisation of multiple minerals. Minerals Engineering. 15, 1131-1139.

Yan, H., Xue-min, C., Liu, L.P., Liu, X.D., Chen, J. Y. 2012. The hydrothermal transformation of solid geopolymers into zeolites. Microporous and mesoporous materials. 161, 187-192.

Yip, C.K., Lukey, G.C., Provis, J.L., van Deventer, J.S.J., 2008. Effect of calcium silicate sources on geopolymerisation. Cement and Concrete Research. 38, 554-564.

Youngman, R., 2018. NMR spectroscopy in glass science: a review of the elements. Materials. 11(4), 476.

Yu, Y., Li, X., Zou, X., Zhu, X., 2014. Effect of seawater salinity on the synthesis of zeolite from coal fly ash. Frontiers of Environmental Science and Engineering. 8(1), 54-61.

Zhang, Y.J., Zhao, Y. L., Li, H.H., 2008. Structure characterization of hydration products generated by alkaline activation of granulated blast furnace slag. Journal of materials science. 43(22), 7141-7147.

Zhang, Z., Yao, X., Zhu, H., 2010a. Potential application of geopolymers as protection coatings for marine concrete: I. Basic properties. Applied clay science. 49(1-2), 1-6.

Zhang, Z., Yao, X., Zhu, H., 2010b. Potential application of geopolymers as protection coatings for marine concrete II. Microstructure and anticorrosion mechanism. Applied clay science. 49(1-2), 7-12.

Zhang. J., Gao, Y., Han, Y., 2011. Interior humidity of concrete under dry-wet cycles. Journal of Materials in Civil Engineering.;24(3), 289-298.

Zhang, Z., Yao, X., Wang, H., 2012. Potential application of geopolymers as protection coatings for marine concrete III: Field experiment. Applied clay science. 67, 57-60.

Zhang, Y., Li, T., Hou, D., Zhang, J., Jiang, J., 2018. Insights on magnesium and sulfate ions' adsorption on the surface of sodium alumino-silicate hydrate (NASH) gel: a molecular dynamics study. Physical Chemistry Chemical Physics. 20(27), 18297-18310.

APPENDIX

List of Articles Published and Submitted During the P.h.D Study

1. Articles published in international journals during the P.h.D study

1) **Li, X.,** Rao, F., Song, S., Corona-Arroyo, M.A., Ortiz-Lara, N., Aguilar-Reyes, E.A., 2018. Effects of aggregates on the mechanical properties and microstructure of geothermal metakaolin-based geopolymers. Results in Physics, 11, 267-273.

2) **Li, X.,** Rao, F., Song, S., Ma, Q., 2019. Deterioration in the microstructure of metakaolin-based geopolymers in marine environment. Journal of Materials Research and Technology, 8(3), 2747-2752.

3) **Li, X.,** Rao, F., Song, S., Ma, Q., 2020. Effect of cristobalite on the mechanical behaviour of metakaolin-based geopolymer in artificial seawater. Advances in Applied Ceramics, 119(1), 29-36.

4) **Li, X.,** Li, X.O., Rao, F., Song, S., Ortiz-Lara, N., Aguilar-Reyes, E.A., Microstructural evolution in sulfate solutions of alkali-activated binders synthesized at various calcium contents. 9(5), 10377-10385

2. Articles submitted to international journals during the P.h.D study

1) **Li, X.,** Rao, F., Song, S., Ortiz-Lara, N., Aguilar-Reyes, E.A., Effect of calcium content on the microstructure and chloride corrosion of alkali-activated reinforced mortars. 2020.03

Results in Physics 11 (2018) 267–273

Contents lists available at ScienceDirect

Results in Physics

journal homepage: www.elsevier.com/locate/rinp

Effects of aggregates on the mechanical properties and microstructure of geothermal metakaolin-based geopolymers

Xing Li[a,b], Feng Rao[a,b,*], Shaoxian Song[c,*], Mario A. Corona-Arroyo[d], Noemi Ortiz-Lara[b], Ena A. Aguilar-Reyes[b]

[a] School of Zijin Mining, Fuzhou University, Fuzhou, Fujian 350108, China
[b] CONACYT Instituto de Investigación en Metalurgia y Materiales, Universidad Michoacana de San Nicolás de Hidalgo, Morelia, Michoacán 58030, Mexico
[c] School of Resources and Environmental Engineering, Wuhan University of Technology, Wuhan, Hubei 430070, China
[d] Departamento de Minas, Metalurgia y Geología, Universidad de Guanajuato, Guanajuato, Guanajuato 36020, Mexico

ARTICLE INFO

Keywords:
Geopolymer
Microstructure
Aggregates
Geothermal clay
Metakaolin

ABSTRACT

Geothermal clay rich in kaolinite was first prepared into geopolymers in the preparation of alkali-activated cementitious binders (AACBs). Effects of silica sand and steel fiber aggregates on the microstructure and mechanical strength of the geothermal-metakaolin-based geopolymer were studied. Measurements of compressive strength, X-ray diffraction (XRD), Fourier-transform infrared spectroscopy (FTIR), scanning electron microscopy (SEM), Brunauer-Emmett-Teller (BET) and nuclear magnetic resonance (NMR) were used to characterize the geopolymers. With the replacement of silica sand, combination between sand and geopolymer gel was formed, the geopolymers therefore showed compressive strength higher than 34 MPa with silica sand up to 50%. However, silica sand of coarse particle size (0.3–0.6 mm) caused porous structure in the geopolymers, hindering the increase in their compressive strength. With the replacement of steel fiber, the flexural strength and flexural fracture toughness of the geopolymers were greatly improved.

Introduction

Geopolymer has attracted extensive attention due to its mechanical properties in the replacement of ordinary Portland cement (OPC), but of low CO_2 emission in the synthesis [1–2]. Alkaline activation reactions in the synthesis of geopolymers involved mainly the dissolution of raw aluminosilicates into monomers in alkaline solution, reorientation and polymerization of the monomers into network, and condensation of the network [3]. Generally, calcination in the pre-treatment or to choose by-products after calcination is employed to obtain raw materials of high reactivity in the dissolution of monomers. Therefore, metakaolin and fly ash are mostly used in the syntheses of geopolymers. However, calcination stands on the opposite of low CO_2 emission of alkali-activated geopolymer concrete, which weakens the advantage of this concrete on environmental aspect. Thus, raw materials from industrial waste without or with limited calcination were studied in the synthesis of alkali-activated concrete in pursuing the commercialization of it as environmental friendly construction material. For example, bottom ash generated by incineration of municipal solid waste was used as additive in the synthesis of high calcium fly ash-based geopolymer, of which the maximum compressive strength was 52.8 MPa [4]. Palm oil fuel ash and granulated blast furnace slag were synthesized into geopolymer by using sodium silicate (Na_2SiO_3) and sodium hydroxide (NaOH) mixture as alkaline activator, optimal compressive strength (66 MPa) was achieved for the geopolymer concrete with 30% ash and 70% slag [5].

Clays related to geothermal activity in some regions, namely geothermal clay, are abundant in aluminosilicates and calcium minerals. Geothermal clay is a common industrial waste after drilling wells in geothermal energy exploitation. Because of the hydrothermal impact, geothermal clay may possess higher reactivity than usual clays [6]. Even so, geothermal clay is seldom studied in the preparation of geopolymer concrete. Our group tested the parameters of calcination on geothermal clay, Na_2SiO_3 and NaOH combination in alkaline activator, and water content in the synthesis of geothermal clay-based geopolymer paste [7]. Optimal paste of high percentages of $Q^4(2Al)$ and $Q^4(1Al)$, homogeneous geopolymer gel in microstructure, and 19.5 MPa in compressive strength was obtained at calcination temperature of 800 °C, and solid to liquid and Na/Al ratios in raw materials of 1.37 and 2.01, respectively. These results showed the potential of using geothermal clay to prepare geopolymer concrete with appropriate aggregates. Furthermore, geothermal silica from geothermal power plants, which is an analogous by-product to geothermal clay, has been

* Corresponding authors at: School of Zijin Mining, Fuzhou University, Fuzhou, Fujian 350108, China (F. Rao)
E-mail addresses: fengrao@umich.mx (F. Rao), shaoxian@uaslp.mx (S. Song).

https://doi.org/10.1016/j.rinp.2018.09.018
Received 14 August 2018; Received in revised form 7 September 2018; Accepted 7 September 2018
Available online 12 September 2018

used as additive in OPC and geopolymer syntheses. It was reported that nano-geothermal silica particles acted as nucleation sites consuming calcium hydroxide and promoted the formation of calcium-silicate-hydrate (C-S-H) gel in OPC pastes [8]. And geothermal silica was studied to replace metakaolin in geopolymer preparation. With the replacement ($\leq$20%), the usage of Na_2SiO_3 in alkaline activator was greatly reduced, while the compressive strength decreased slightly due to the formation of pores in the geopolymer [9].

In OPC concrete, aggregate materials of silica sand and steel fiber are commonly used in practices, and the incorporation behavior is fully reported [10]. However, the incorporation of aggregate materials in geopolymers is hypothesized to behave differently because of the alkaline activation process. For example, quartz sand was added in metakaolin-based geopolymer. Combination on quartz particle surface was found to form and associate them into geopolymer gel, so that the compressive strengths of geopolymers with only silicate and with silicate plus quartz sand were 31.2 and 52.2 MPa, respectively [11]. In another study, the drying shrinkage of metakaolin-based geopolymer was found to reduce from 8% to 1% with the replacement of silica sand (38 vol%) [12]. In a synthesis of alkali-activated slag concrete, the replacement of steel fiber (1.5 vol%) was found to improve 40% of its flexural strength [13]. The present study continues our previous work [7] in the synthesis of alkali-activated geothermal clay-based geopolymer. The effects of silica sand and steel fiber aggregates in the geopolymer concrete are discussed. It aims to find a new aluminosilicate in the formation of alkali-activated geopolymer concrete with limited calcination or without it, as well as to discuss the incorporation of aggregates in alkali-activated concrete.

Experimental

Materials

Geothermal clay rock was collected from the Los Azufres geothermal field, Michoacan, Mexico at the depth of 250 m where the temperature exceeds 150 °C. The rock was crushed and grinded into powder at 50% and 85% of cumulative undersize of 13.0 μm and 27.4 μm, respectively, which was measured from a Beckman Coulter (USA) particle size analyzer. Table 1 gives the chemical analysis of the geothermal clay measured by an X-ray fluorescence (XRF, PA Nalytical Axios), in which SiO_2 and Al_2O_3 were the main components and the Si/Al ratio was around 3.7:1. X-ray diffraction (XRD, Bruker D8) pattern of the geothermal clay (Fig. 1) showed main components of cristobalite, kaolinite and alunite. Steel fiber was purchased from Shangta plant in Shanghai, China, which was 8.5 mm in length, 0.2 mm in diameter, and specific gravity of 7.9. Silica sand was purchased from Zwick Roell Group, Mexico, which was in the size range of 0.3–0.6 mm and specific gravity of 2.9. Sodium silicate of the modulus 1 and sodium hydroxide (ACS reagent grade) grade were purchased from Sigma-Aldrich and used as alkaline activator in the syntheses.

Synthesis of geothermal metakaolin-based geopolymers

Limited calcination was applied to geothermal clay in this synthesis. Every 150 g powders of geothermal clay after grinded was calcined for 6 h at 200 °C, which increased the reactivity of geothermal clay. In a typical synthesis, alkaline activator solution was first prepared and

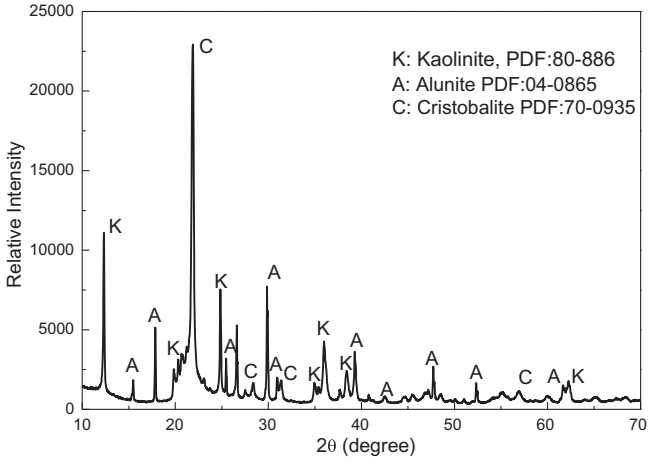

Fig. 1. XRD pattern of geothermal clay.

mixed with the raw material (220 g), which includes given amounts of geothermal clay, silica sand and steel fiber. The Na/Al ratio in the mixture was kept at 1.8:1. The mixture was then poured into steel cubic (50 × 50 × 50 mm) or cuboid molds (40 × 40 × 160 mm). The molds were vibrated on a vibration table for 3 min to liberate the air bubbles. After that, the molds were sealed and cured at 60 °C for 6 h and room temperature for 7 days. Table 2 gives the preparation regimen of the geothermal clay-based geopolymers. In the first part, the geopolymers (SGC) were prepared with different replacements of silica sand at 0, 10%, 20%, 30%, 40%, 50%, 55% and 60% replacements, respectively. In the second part, the ratio of 60% geothermal clay and 40% of silica sand was selected, and 1%, 2% and 3% steel fiber were added to prepare the steel fiber geopolymer concrete (SFGC).

Characterization

Compressive strength (50 × 50 × 50 mm) and flexural strength (40 × 40 × 160 mm) of the geopolymers were measured with an EHC-1300 mechanical tester from Xingao Technology, China. In the measurements of strength, at least three specimens were tested, and the average value was used. Fourier-transform infrared (FTIR) spectroscopy (Nexus, Thermo Nicolet, USA) was used to identify the geopolymer gel in the binders. The transmittance spectra were gathered over a wave number range of 40 to 4000 cm^{-1} with a resolution of 2 cm^{-1}. Scanning electron microscope (SEM, JEOL JSM-5610LV) equipped with energy dispersive X-ray (EDX) analyzer was used to observe the microstructure of the geopolymers. The multipoint Brunauer, Emmett, and Teller (BET) surface area, pore volume and pore size of the geopolymers were measured using a fully automated analyzer from Quantachrome Instruments, USA of model Nova Touch 1F. ^{29}Si nuclear magnetic resonance (NMR) spectra of the geopolymers were obtained by a NMR spectroscopy (Bruker AVANCE III) operating at 79.49 MHz. In this measurement, only geopolymer gel was collected from the specimens to avoid interfere from quartz sand. The powder specimens were packed into 7 mm in diameter ZrO_2 rotors. Spectra were acquired at spinning speeds of 12 kHz with peak positions referenced to an external standard of tetramethylsilane (TMS) and recorded with 1 s delay time.

Table 1
XRF analysis of the geothermal clay.

Component	SiO_2	Al_2O_3	SO_3	K_2O	Fe_2O_3	P_2O_5	TiO_2	ZrO_2	CaO	CuO	Na_2O
Mass (%)	67.2	15.5	7.25	7.15	1.18	1.16	0.31	0.19	0.04	< 0.01	< 0.01

Table 2
Preparation regimen of geothermal clay-based geopolymers.

Samples	Mixtures		Steel fibers (volume %)	Na_2SiO_3 (mol)	NaOH (mol)	H_2O (mol)	Na/Al
	Geothermal clay (mass%)	Silica sand (mass %)					
SGC-0	100	0	0	0.50	0.25	8	1.8
SGC-1	90	10	0	0.45	0.225	7.2	1.8
SGC-2	80	20	0	0.40	0.20	6.4	1.8
SGC-3	70	30	0	0.35	0.175	5.6	1.8
SGC-4	60	40	0	0.30	0.15	4.8	1.8
SGC-5	50	50	0	0.25	0.125	4.0	1.8
SGC-5.5	45	55	0	0.225	0.113	3.6	1.8
SGC-6	40	60	0	0.20	0.10	3.2	1.8
SFGC-1	60	40	1%	0.30	0.15	4.8	1.8
SFGC-2	60	40	2%	0.30	0.15	4.8	1.8
SFGC-3	60	40	3%	0.30	0.15	4.8	1.8

Results and discussion

Role of silica sand in the geothermal metakaolin-based geopolymers

Fig. 2 gives the compressive strength of the geopolymers synthesized with various silica sand replacements. Without silica sand, the compressive strength was 37.89 MPa. It suggests that geothermal clay possesses higher activity than normal clay (e.g., kaolinite) in alkaline activation reactions, because limited calcination (200 °C for 6 h) induces satisfactory compressive strength for the binder. With replacement of 10% silica sand, compressive strength of the geopolymer decreased slightly to 35.66 MPa. And then, the compressive strength kept a plateau as increasing silica sand to 50%. These results indicate that geothermal clay-based geopolymers was formed through the incorporation of silica sand into geopolymer gel. However, the compressive strength decreased sharply to 26.67 and 19.6 MPa as increasing silica sand replacements to 55% and 60%, respectively. At silica sand replacements higher than 50%, the formed geopolymer gel was not enough to maintain high compressive strength of the binders.

Fig. 3 shows the XRD patterns of the geopolymers synthesized with various silica sand replacements. Without silica sand, the concrete presents featureless amorphous diffraction pattern with one hump centered at approximately 27-29° 2θ, which represents the geopolymer gel, as well as some peaks of cristobalite and alunite, which are from the geothermal clay. With replacement of moderate silica sand (20% and 50%), the peak of quartz becomes distinct and that of albite appears, suggesting that silica sand is not dissolved in alkaline activation reactions. With high amounts of silica sand replacements (55% and 60%), the geopolymer gel hump becomes unclear, suggesting that the ratio of formed geopolymer gel decreased sharply. Furthermore, trona was formed at high silica sand replacements (50%, 55% and 60%), which suggests the excess of alkalis in these replacements. In summary, silica sand is undissolved during the alkaline activation reactions, so that a high amount of silica sand replacement results in low ratio of geopolymer gel, leading to the excess of alkalis and a sharp decrease of the compressive strength (Fig. 2).

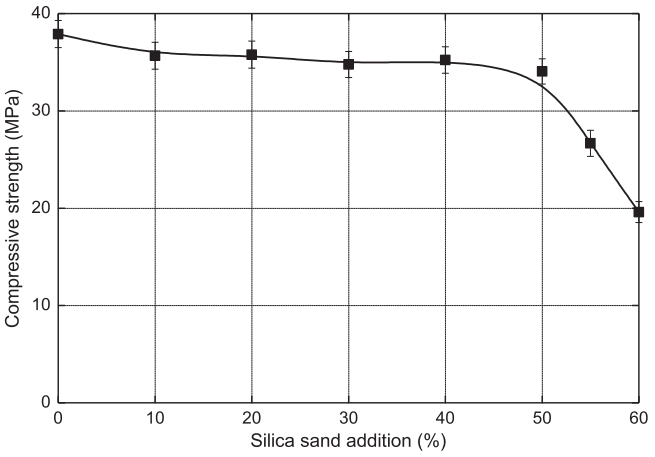

Fig. 2. Compressive strength of geothermal metakaolin-based geopolymers at various silica sand replacements.

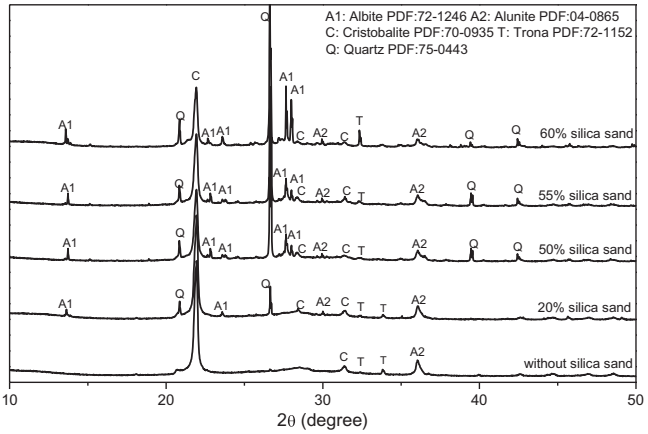

Fig. 3. XRD patterns of the geothermal metakaolin-based geopolymers synthesized with various silica sand replacements.

The change in compressive strength of the geopolymers synthesized with different silica sand replacements may be attributed to their porous structure. Table 3 presents the porous characteristics of the geopolymers with various silica sand replacements. The pore radius increased as increasing silica sand replacements, and macropores were formed at 55% and 60% of silica sand. As increasing silica sand from 0 to 50%, specific surface area and pore volume of the concrete increased slightly, suggesting that silica sand induced pores in the geopolymers, so the compressive strength decreased on a small scale. As increasing silica sand continually to 55% and 60%, the specific surface area and pore volume decreased dramatically because of the formation of macropores, which also caused the sharp decrease in compressive strength (Fig. 2).

Fig. 4 shows morphologically the porous structure of the geopolymers synthesized with various silica sand replacements in SEM images. Holes were formed in all images after shedding the cristobalite and silica sand particles in preparing the specimens. And in comparison, geopolymer of homogeneous binder structure was formed without silica sand replacement. With increasing silica sand replacement to 20% and 50%, pores and cracks are observed and increased. With silica sand replacement of 55%, the cracks become larger and much obvious. It corresponds well with the physical characteristics of the geopolymers.

Some reports stated that compressive strength of alkali-activated geopolymer concrete was enhanced by nano- and micro- silica sand [12,14]. But in this study, compressive strength of the geopolymer concrete decreased slightly with replacement of silica sand (< 50%). As reported previously [11], silica sand of different size ranges induced

Table 3
Physical characteristics of geothermal metakaolin-based geopolymers synthesized with various silica sand replacements.

Samples	SGC-0	SGC-2	SGC-5	SGC-5.5	SGC-6
Silica sand (mass%)	0	20	50	55	60
Specific surface area ($m^2 g^{-1}$)	10.10	11.23	13.81	6.37	3.21
Pore volume ($cm^3 g^{-1}$)	0.0798	0.0937	0.1358	0.0279	0.0222
Pore radius (nm)	14.60	40.82	45.12	62.09	71.81

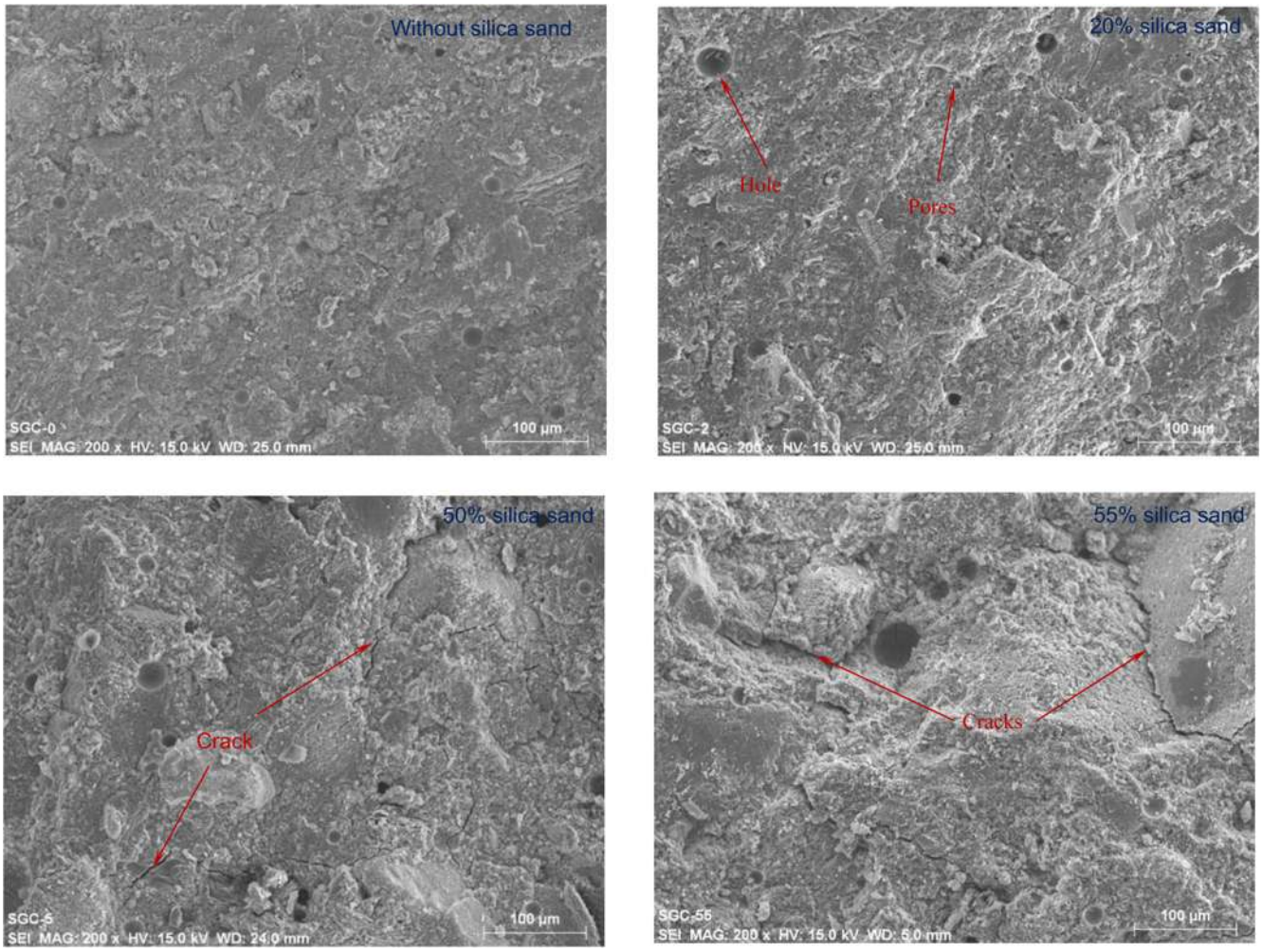

Fig. 4. SEM images of geothermal metakaolin-based geopolymers synthesized with various silica sand replacements.

different effects on the mechanical properties of metakaolin-based geopolymer. The dissolution of sand surface and the formation of polysiloxo (-Si-O-) combination associated it into geopolymer gel and reinforced the metakaolin-based geopolymer. This reinforcement was optimal at particles size range of 32–75 μm, while particles of big size (180–240 μm) are difficult to be combined into geopolymer gel because the formation of combination was in nanometers and insufficient to combine big particles. Therefore, the silica sand of size range in 0.3–0.6 mm induced a slight decrease in compressive strength of the concrete as increasing its ratio from 0 to 50%. However, the dissolution of silica sand and formation of combination can also be evidenced through NMR measurements. Fig. 5 gives the ^{29}Si NMR spectra of the geopolymer gel and their deconvolution, which adopted Gaussian peak deconvolution to separate and quantify Q^n(mAl) species ($0 \le m \le n \le 4$) [15]. In geopolymer gel, all the silicon and aluminum site were in tetrahedral coordination, so $n = 4$ [16]. And the resonance of a Q^4(mAl) center with the replacement of each aluminum by silicon is an approximate −5 ppm chemical shift, with Q^4(4Al), Q^4(3Al), Q^4(2Al), Q^4(1Al), Q^4(0Al) resonating at approximately −84, −89, −93, −99 and −108 ppm, respectively [17]. Without silica sand, the *Q^4(4Al)*, sum of *Q^4(3Al)*, *Q^4(2Al)* and *Q^4(1Al)*, and *Q^4(0Al)* in geopolymer gel were 9%, 71.4% and 19.6%, respectively. With increasing silica sand to 60%, the *Q^4(0Al)* kept almost the same at around 20%. While the *Q^4(4Al)* were converted into *Q^4(3Al)*, *Q^4(2Al)* and *Q^4(1Al)*, of which the *Q^4(4Al)* decreased to 8.4%, 5.7%, 5.4% and 3.9% at 20%, 50%, 55% and 60% of silica sand, respectively. It suggests that more tetrahedral silicon was formed as increasing silica sand, which is attributed to the dissolution of silica sand and combination formation on its surface.

Role of steel fiber in geothermal metakaolin-based geopolymers

Table 4 gives the mechanical properties of the geopolymers synthesized with various steel fiber additions. Compressive strength of the geopolymers remained around 35 MPa with additions of 1%, 2% and 3% steel fiber in volume fractions, indicating that steel fiber has negligible effect on compressive strength of the geopolymers. While the flexural strength increased steadily from 3.1 MPa to 3.19, 3.36 and 3.6 MPa as increasing steel fiber from 0 to 1%, 2% and 3% in volume fractions, respectively. However, because of the short curing time (7 days) of the geopolymers, this increase was small compared with the reported study elsewhere [13].

Fig. 6 gives the FTIR spectra of geothermal metakaolin-based geopolymers synthesized with various steel fiber additions. The absorption peaks at 3450 cm^{-1}, 1650 cm^{-1} and 1454 cm^{-1} are OH^- stretching vibrations, H-OH bonds of free water and asymmetric stretching of O-C-O bonds in CO_3^{2-} groups, corresponding to the adsorbed water and carbonation during curing process [18]. The peaks at 795 cm^{-1}, 696 cm^{-1}, 621 cm^{-1} and 476 cm^{-1} represents O-Si-O bonds in quartz, Si-O and Al-O bonds in unreacted kaolinite, and zeolite framework in the geopolymer [19,20]. And the band around 1000 cm^{-1} represents the Si-O-T bonds (T is tetrahedral Si or Al) in geopolymer gel, showing tiny difference at different steel fiber additions. It suggests that steel fiber affect negligibly the geopolymer gel formation in the geopolymers, so does the

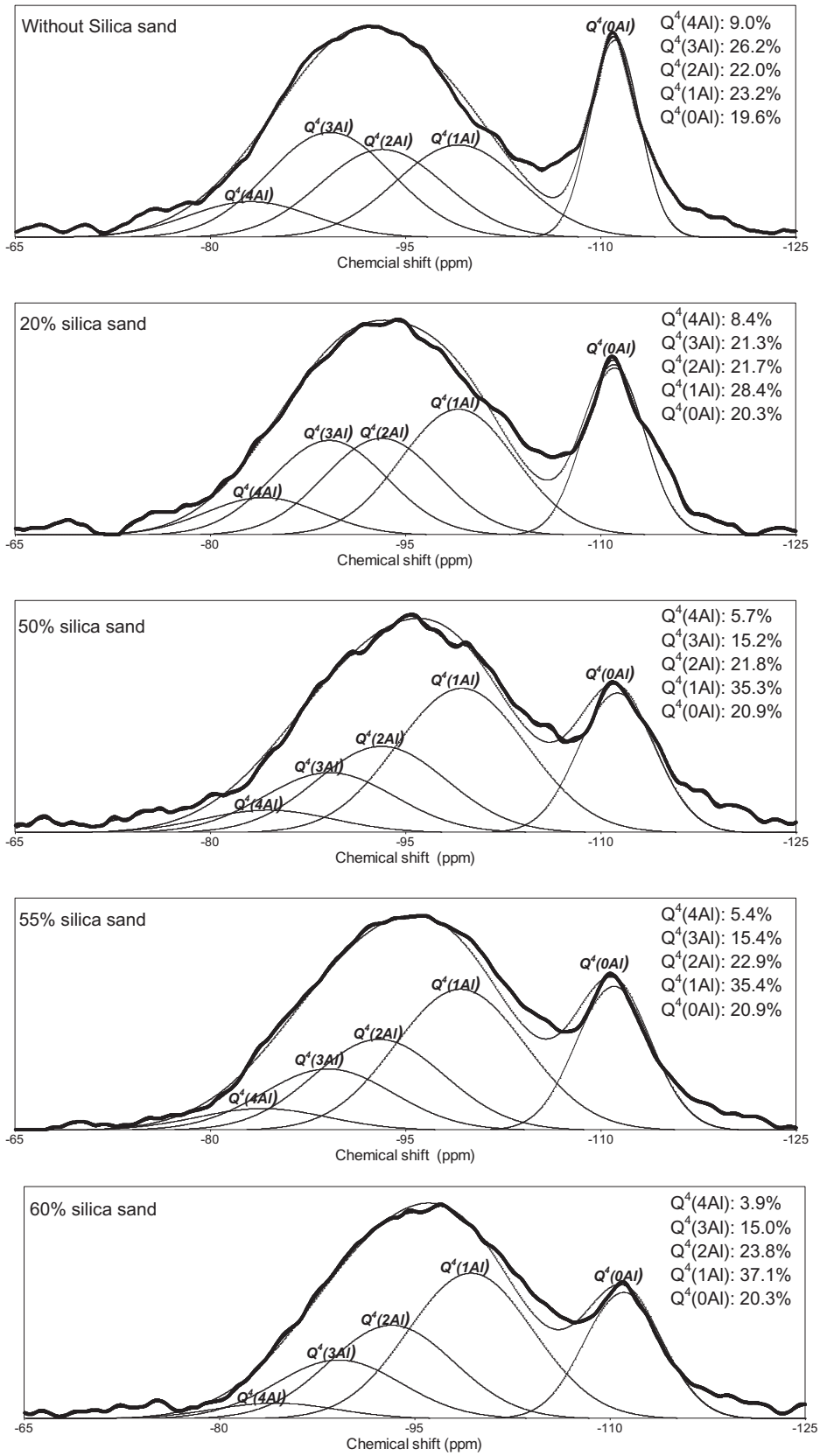

Fig. 5. ^{29}Si NMR spectra and their deconvolution of geopolymer gel in the geopolymers synthesized with various silica sand replacements.

compressive strength (Table 4).

Fig. 7 shows morphologically the incorporation of silica sand, geopolymer gel and steel fiber in the geopolymer in SEM image, in which the component materials were determined by element analysis through EDX. The geopolymer gel functions as binder material for silica sand and steel fiber. And cracks along with steel fiber are larger than those

Table 4
Mechanical properties of the geopolymer concrete with various steel fiber additions.

Steel fiber (vol%) Mechanical properties	0	1	2	3
Compressive strength (MPa)	35.33	34.65	35.22	34.01
Flexural strength (MPa)	3.1	3.19	3.36	3.6

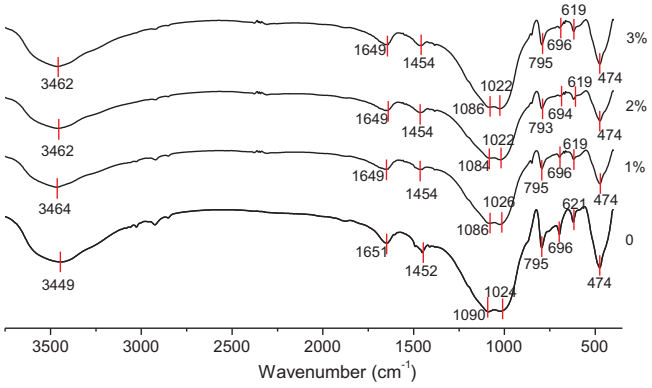

Fig. 6. FTIR spectra of the geopolymer synthesized with 0, 1%, 2% and 3% steel fiber in volume fractions.

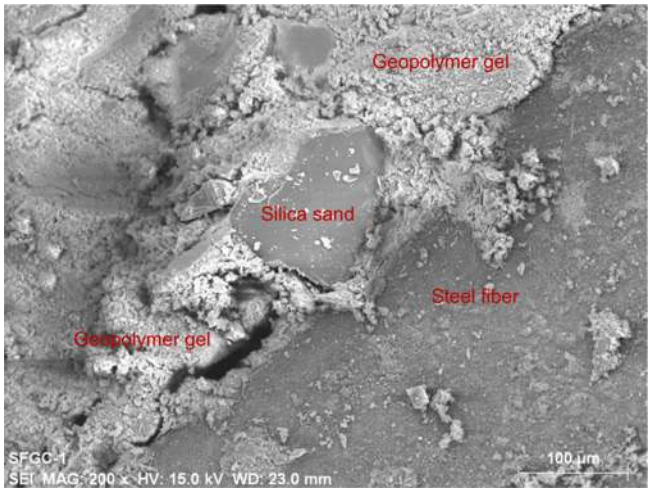

Fig. 7. SEM image of silica sand, geopolymer gel and steel fiber in the geopolymer.

with sand. It can be observed the formation of combination on silica sand surface.

Fig. 8 shows the load-deflection of geothermal metakaolin-based geopolymers synthesized at various steel fiber additions. The ultimate load and deflection increase as increasing steel fiber fractions and the post curves tend towards gently, which indicates the failure mode of the geopolymers was changed from brittle to ductile. It is in good agreement with the load-deflection curves in synthesizing steel fiber reinforced OPC concrete and fly ash-based geopolymers with micro steel fiber [21,22]. And the total area under the load-deflection curve increases with the addition of steel fiber. According to ASTM C1018-85 (USA), this area represents the flexural fracture toughness of the concrete. Therefore, the toughness of geothermal clay-based geopolymer concrete was reinforced by steel fiber, which might be attributed to the formation of bridge in the crack and more tortuous crack propagation path.

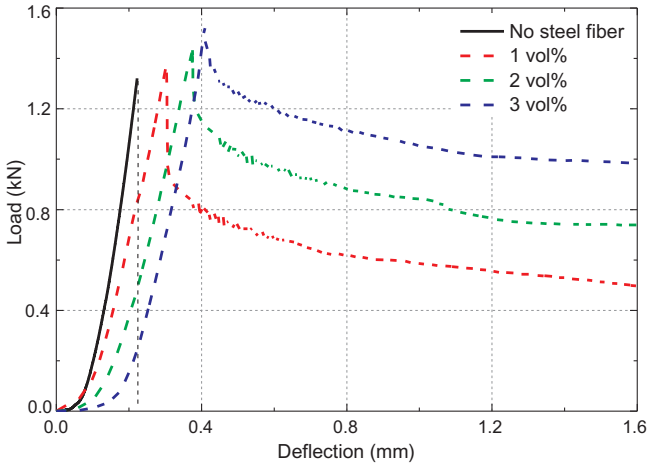

Fig. 8. Load-deflection of the geopolymers at various steel fiber additions.

Conclusion

1) The compressive strength of the geothermal metakaolin-based geopolymers decreases sharply as increasing the silica sand replacement more than 50%. This replacement of silica sand induces porous structure in the geopolymer binders, and macropores are formed in geopolymers with high silica sand contents. The formation of combination on silica sand particle surface prompts their incorporation. As increasing silica sand from 0 to 50%, more tetrahedral silicon coordination of $Q^4(3Al)$, $Q^4(2Al)$ and $Q^4(1Al)$ is formed.
2) Steel fiber gives negligible effect on compressive strength of the geopolymers, but it enhances their flexural strength and flexural fracture toughness. The geopolymer gel functions as binder material for silica sand and steel fiber.

Acknowledgement

This study was financially supported for by the Consejo Nacional de Ciencia y Tecnología (CONACyT) of Mexico under the Grant No. 270186, the Natural Science Foundation of Hubei Province of China under the Grant No. 2016CFA013 and the Wuhan Science and Technology Bureau of China under the Project No. 2016070204020156, for which the authors are grateful. X. Li would like to thank the CONACyT for offering her the scholarship No. 831134 during her PhD studies.

References

[1] Davidovits J. Geopolymers and geopolymeric materials. J Therm Anal 1989;35:429–41.
[2] Duxson P, Fernández-Jiménez A, Provis JL, Lukey GC, Palomo A, Van Deventer JSJ. Geopolymer technology: the current state of the art. J Mater Sci 2007;42:2917–33.
[3] Rao F, Liu Q. Geopolymerization and its potential application in mine tailings consolidation: a review. Miner Process Extr Metall Rev 2015;36:399–409.
[4] Wongsa A, Boonserm K, Waisurasingha C, Sata V, Chindaprasirt P. Use of municipal solid waste incinerator (MSWI) bottom ash in high calcium fly ash geopolymer matrix. J Clean Prod 2017;148:49–59.
[5] Islam A, Alengaram UJ, Jumaat MZ, Bashar II. The development of compressive strength of ground granulated blast furnace slag-palm oil fuel ash-fly ash based geopolymer mortar. Mater Des 2014;56:833–41.
[6] Mas A, Guisseau D, Mas PP, Beaufort D, Genter A, Sanjuan B, et al. Clay minerals related to the hydrothermal activity of the Bouillante geothermal field (Guadeloupe). J Volcanol Geotherm Res 2006;158:380–400.
[7] Wan Q, Rao F, Song S, León-Patiño CA. Geothermal clay-based geopolymer binders: Synthesis and microstructural characterization. Appl Clay Sci 2017;146:223–9.
[8] Iñiguez-Sánchez CA, Gómez-Zamorano LY, Alonso MC. Impact of nano-geothermal silica waste and chloride content on pore solution, microstructure, and hydration products in Portland cement pastes. J Mater Sci 2012;47:3639–47.
[9] Gomez-Zamorano LY, Vega-Cordero E, Struble L. Composite geopolymers of metakaolin and geothermal nanosilica waste. Constr Build Mater 2016;115:269–76.
[10] Moosberg-Bustnes H, Lagerblad B, Forssberg E. The function of fillers in concrete.

Mater Struct 2004:37–74.
[11] Wan Q, Rao F, Song S, Cholico-González DF, Ortiz NL. Combination formation in the reinforcement of metakaolin geopolymers with quartz sand. Cem Concr Compos 2017;80:115–22.
[12] Kuenzel C, Grover LM, Vandeperre L, Boccaccini AR, Cheeseman CR. Production of nepheline/quartz ceramics from geopolymer mortars. J Eur Ceram Soc 2013;33:251–8.
[13] Bernal S, De Gutierrez R, Delvasto S, Rodriguez E. Performance of an alkali-activated slag concrete reinforced with steel fibers. Constr Build Mater 2010;24:208–14.
[14] Shaikh F, Haque S. Effect of nano silica and fine silica sand on compressive strength of sodium and potassium activators synthesised fly ash geopolymer at elevated temperatures. Fire Mater 2017:324–35.
[15] Lee SK, Stebbins JF. The degree of aluminum avoidance in aluminosilicate glasses. Am Mineral 1999;84:937–45.
[16] Rahier H, Van Mele B, Biesemans M, Wastiels J, Wu X. Low-temperature synthesized aluminosilicate glasses. J Mater Sci 1996;31:71–9.
[17] Engelhardt G, Michel D. High-resolution solid-state NMR of silicates and zeolites. United States; 1987. p. 187–8.
[18] Wan Q, Rao F, Song S, García RE, Estrella RM, Patiño CL, et al. Geopolymerization reaction, microstructure and simulation of metakaolin-based geopolymers at extended Si/Al ratios. Cem Concr Compos 2017;79:45–52.
[19] Hajimohammadi A, Provis JL, Van Deventer JSJ. One-part geopolymer mixes from geothermal silica and sodium aluminate. Ind Eng Chem Res 2008;47:9396–405.
[20] Mostafa NY, El-Hemaly SAS, Al-Wakeel EI, El-Korashy SA, Brown PW. Characterization and evaluation of the pozzolanic activity of Egyptian industrial by-products: I: Silica fume and dealuminated kaolin. Cem Concr Res 2001;31:467–74.
[21] Barr BIG, Liu K, Dowers RC. A toughness index to measure the energy absorption of fibre reinforced concrete. Int J Cem Compos Light Concr 1982;4:221–7.
[22] Ranjbar N, Mehrali M, Mehrali M, Alengaram UJ, Jumaat MZ. High tensile strength fly ash based geopolymer composite using copper coated micro steel fiber. Constr Build Mater 2016;112:629–38.

Available online at www.sciencedirect.com

jmr&t
Journal of Materials Research and Technology
www.jmrt.com.br

Original Article

Deterioration in the microstructure of metakaolin-based geopolymers in marine environment

Xing Li[a,b], Feng Rao[a,b,*], Shaoxian Song[c], Qinyong Ma[d]

[a] School of Zijin Mining, Fuzhou University, Fuzhou, Fujian 350108, China
[b] CONACYT Instituto de Investigación en Metalurgia y Materiales, Universidad Michoacana de San Nicolás de Hidalgo, Morelia, Michoacán 58030, Mexico
[c] School of Resources and Environmental Engineering, Wuhan University of Technology, Wuhan, Hubei 430070, China
[d] School of Civil Engineering and Architecture, Anhui University of Science and Technology, Huainan, Anhui 232001, China

ARTICLE INFO

Article history:
Received 24 January 2019
Accepted 28 March 2019
Available online 25 May 2019

Keywords:
Metakaolin geopolymer
Microstructure
Marine environment
NMR spectra

ABSTRACT

In this research, metakaolin-based geopolymers were synthesized to study their deterioration in marine environment. The geopolymers were exposed in air, seawater, dry-wet and heat-cool cycles of seawater for 30, 60 and 90 days. The mechanical property of the geopolymers was characterized through compressive strength measurements, and their microstructures were measured by X-ray diffraction (XRD), scanning electron microscope (SEM) and nuclear magnetic resonance (NMR) apparatus. It was found that seawater environment inhibited the geopolymerization reactions, so that a low amount of tetrahedral silicon of $Q^4(4Al)$, $Q^4(3Al)$ and $Q^4(2Al)$ were formed.

1. Introduction

Concrete of coastal and offshore structures that exposes in seawater with dry-wet and heat-cool cycles has to endure complicated chemical attach from corrosive ions such as Cl^-, SO^{2-}_4 and Mg^{2+} [1,2]. For ordinary Portland cement (OPC) concrete, corrosive ions can react with the hydration products, namely calcium silicate hydrate (CSH) and calcium hydroxide $Ca(OH)_2$, forming Friedel's salt, ettringite, brucite, magnesium silicate hydrate, etc. [3]. The precipitation and crystallization of these salts in pores of the OPC concrete, which are accelerated by the dry-wet and heat-cool cycles, lead to the formation of cracks and corrosion [4,5]. Therefore, special concrete with high resistance to marine environment is studied extensively [6–8]. In recent years, some researchers explored geopolymers to serve as high anticorrosion concrete for marine structures [9–12]. Geopolymers are alkaline- or alkali-silicate-activated aluminosilicate binders with three dimensional (3D) amorphous microstructures [13]. The compact tetrahedral silica and aluminum structure of geopolymers may give this concrete protection from intrusion of corrosive ions in marine environment [14]. For example, it was reported that chloride diffusion coefficient in fly ash-based geopolymers was half

* Corresponding author.
E-mail: fengrao@umich.mx (F. Rao).
https://doi.org/10.1016/j.jmrt.2019.03.010

Table 1 – Chemical analysis of the geothermal clay.

Components	SiO_2	Al_2O_3	SO_3	K_2O	Fe_2O_3	P_2O_5	TiO_2	ZrO_2	CaO	CuO	Na_2O
Mass (%)	67.2	15.5	7.25	7.15	1.18	1.16	0.31	0.19	0.04	<0.01	<0.01

of that in OPC concrete [15]. Skvara et al. immersed a fly ash-based geopolymer into 44 g/L Na_2SO_4 or 5 g/L $MgSO_4$ solutions for 720 days, and found that the mass and dimension of the geopolymers kept constant [16]. Zhang et al. prepared metakaolin-based geopolymers to serve as protection coatings for OPC concrete in marine environment. The geopolymer concrete showed low permeability (permeability coefficient around 10^{-6} μm^2) and high anticorrosion property against seawater, which were attributed to their low porosity (22.3%) and small open pores (<20 nm) [17,18]. A fly ash-based geopolymer concrete was prepared, cured in air for 28 days and then exposed in tidal zone of marine environment for 3 years, of which the compressive strength increased slightly, low chloride intrusion and steel corrosion were observed [19]. These studies provide clues for the anticorrosion of geopolymers from intrusive ions in marine environment. However, explanations of the anticorrosion properties were based on ambiguous and indirect evidences. For example, low permeability was used to verify their ability from chloride intrusion [19]. There is lack of study on the evolution of tetrahedral silica and aluminum structures in geopolymer under marine environment with dry-wet and heat-cool cycles.

The present work used geothermal clay which is rich in kaolinite to synthesize a metakaolin-based geopolymer. It studied the evolution in microstructure of the geopolymer when they were cured in artificial seawater under dry-wet and heat-cool cycles of 30, 60 and 90 days. The geothermal clay is an industrial waste produced in geothermal energy exploitation, which was reported in the synthesis of metakaolin-based geopolymers elsewhere [20].

2. Experimental

2.1. Materials

Geothermal clay rock was collected from the Los Azufres geothermal field, Mexico at the depth of 250 m where the temperature exceeds 150 °C. The rock was crushed and ground into powder with the d_{50} and d_{85} values of 13.0 and 27.4 μm, respectively, measured from a Beckman Coulter (USA) particle size analyzer. Table 1 gives the chemical analysis of the geothermal clay measured by an X-ray fluorescence (XRF, PA Nalytical Axios, Holland). SiO_2 and Al_2O_3 are the main components, and the Si/Al ratio is around 3.7:1. X-ray diffraction (XRD, Bruker D8, Germany) pattern of the geothermal clay (Fig. 1) shows main components of kaolinite and cristobalite. The geothermal clay was calcined at 800 °C for 6 h to prepare metakaolin. Sodium silicate (Na_2SiO_3) and sodium hydroxide (NaOH) with reagent grade ACS were purchased from Sigma-Aldrich and used as alkali activator in the syntheses. Distilled water was used for the synthesis, while artificial seawater was prepared for the exposure of geopolymers. The seawater in 10-fold concentration was prepared with 292.5 g/L NaCl, 7.45 g/L KCl, 36 g/L $MgSO_4$, and this seawater was renewed every 7 days during the curing process.

2.2. Methods

In syntheses of the geopolymers, 0.25 molar NaOH, 0.5 molar Na_2SiO_3 and 12 molar water (H_2O) were first mixed to prepare the alkaline solution, then 222 g calcined geothermal clay was added into the alkaline solution and agitated for 5 min. The Si/Al, Na/Al and solid to liquid ratios in the syntheses were 3.7:1, 1.8:1 and 1.4:1, respectively. Next, the mixture was cast into cubic steel molds (50 mm × 50 mm × 50 mm), which were vibrated on a vibration table for 3 min to liberate the air bubbles. After that, the samples were sealed and cured at 60 °C for 6 h and room temperature for 7 days to obtain the initial geopolymer.

The obtained metakaolin-based geopolymers were further exposed under four types of conditions. They were (1) in air, where the geopolymer samples were exposed in air at room temperature; (2) in seawater, where the geopolymer samples were exposed under seawater; (3) in dry-wet seawater cycle, where the geopolymer samples were exposed under the cycle of 12 h in air (25 ± 2 °C) and 12 h in artificial seawater (25 ± 2 °C); (4) in heat-cool seawater cycle, where the geopolymer samples were exposed under the cycle of 12 h in freezer (−15 ± 2 °C) and 12 h in seawater (25 ± 2 °C). For each condition, the geopolymer was exposed for 30, 60 and 90 days, and then the mechanical property and microstructure were characterized.

Compressive strength of the geopolymers was measured with an EHC-1300 mechanical tester from Xingao Technology, China. In each measurement, three specimens were tested and the average value was given. Scanning electron microscope (SEM) of JEOL JSM-5610LV, Japan was used to characterize the microstructure of the geopolymers. X-ray diffraction (XRD) patterns of the geopolymers were obtained by a Brucker D8, Germany diffraction meter, using monochromatic Cu-$K\alpha_1$ radiation ($\lambda = 1.5406$ Å). ^{29}Si nuclear magnetic

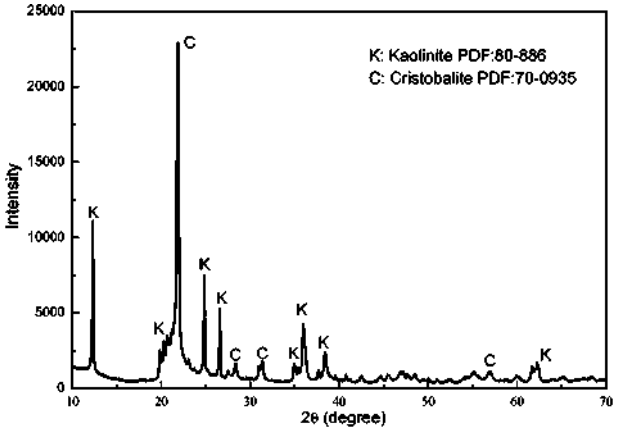

Fig. 1 – XRD pattern of the geothermal clay.

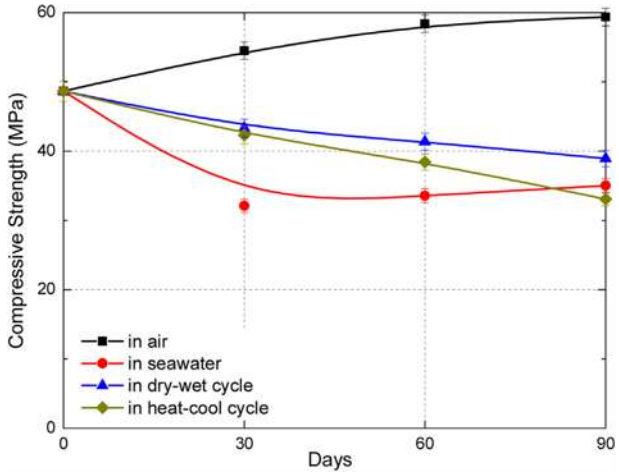

Fig. 2 – Compressive strengths of the metakaolin-based geopolymers exposed differently.

resonance (NMR) spectra of the geopolymers were obtained by using the NMR spectroscopy (Bruker AVANCE III) at 79.49 MHz. Powdered binder specimens were packed into 7 mm ZrO_2 rotors. Spectra were acquired at spinning speeds of 5 kHz with peak positions referenced to an external standard of tetramethylsilane (TMS) and recorded with 5 s delay time. The excitation pulse for ^{29}Si was 6 μs with a recycle time of 5 s.

3. Results and discussion

Fig. 2 gives the compressive strength of the geopolymers exposed in various conditions. The initial geopolymers cured at 7 days had a compressive strength of 48.7 MPa. For the exposure in air, the compressive strength increased steadily to 54.5, 58.4 and 59.4 MPa at 30, 60 and 90 days, respectively. Such a high compressive strength suggests that metakaolin obtained through the calcination of geothermal clay has a high activity in the geopolymerization reactions [20,21]. For the exposure in seawater, the compressive strength decreased significantly to 32.1 MPa at 30 days, which may be attributed to the dilution effect of seawater in geopolymerization reactions [17,22–24]. Then it increased slightly to 33.6 and 35.0 MPa at 60 and 90 days, respectively, indicating the slow rate of geopolymerization reactions in seawater. For the exposure in dry-wet cycle, compressive strength of the geopolymers decreased steadily to 43.3, 41.4 and 38.9 MPa at 30, 60 and 90 days, respectively. For the exposure in heat-cool cycle, the compressive strength decreased more than that in dry-wet cycle, which was eventually of 33.1 MPa at 90 days. The compressive strengths of dry-wet and heat-cool cycles suggest the deterioration in mechanical properties of the metakaolin-based geopolymers in simulated marine conditions, which is in agreement with the report of OPC concrete [25].

Fig. 3 shows the SEM images of the geopolymers exposed in air, seawater, dry-wet and heat-cool cycles for 90 days. All the geopolymers show homogeneous binder structures, suggesting the seawater environment only influence the formation of metakaolin-based geopolymers moderately. However, halite precipitation is observed on the geopolymer exposed in

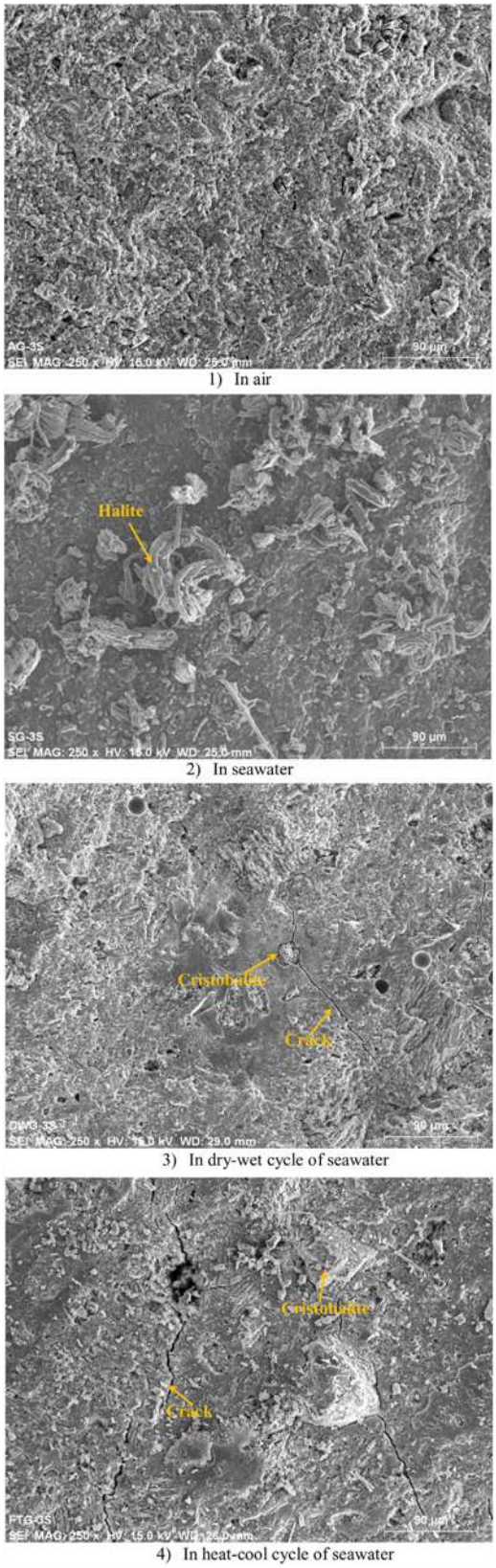

Fig. 3 – SEM images of the geopolymers exposed differently for 90 days.

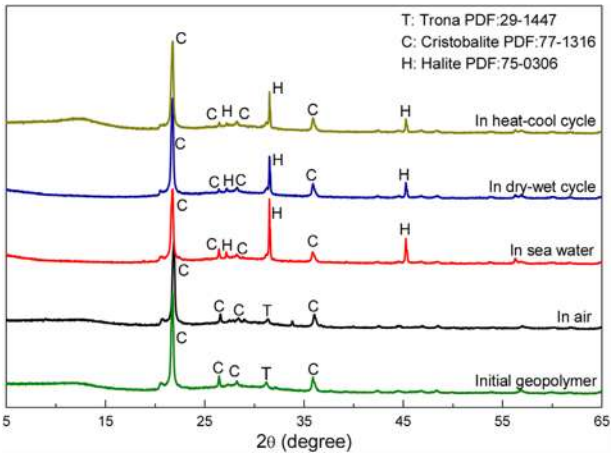

Fig. 4 – XRD patterns of the geopolymers cured differently for 90 days.

seawater. The geopolymer exposed in dry-wet cycle shows small cracks along the cristobalite particle, and the geopolymer exposed in heat-cool cycle shows larger cracks in binder. The precipitation of halite and the formation of cracks may be the reasons for the lower compressive strengths of the geopolymers (Fig. 2).

Fig. 4 presents the XRD patterns of the geopolymers exposed in air, seawater, dry-wet and heat-cool cycles of seawater for 90 days, in which the XRD pattern of the initial geopolymer is given as a comparison. The hump of geopolymer gel centered at approximately 27–29° 2θ is featureless for these geopolymers, which may be attributed to the noise of high cristobalite content in the geothermal clay. The cristobalite and the trona are observed in the initial geopolymer. The cristobalite in the raw geothermal clay maintain after 90-days exposure in the four types of conditions, indicating its inert property in geopolymerization reactions. The formation of trona is attributed to the high alkali concentration and carbonation in the syntheses. It therefore disappears after exposure under seawater, dry-wet and heat-cool cycles of seawater, because of the dilution of the alkali by the seawater. However, halite is observed in the exposure conditions with seawater, which is in good agreement with SEM images (Fig. 3). It indicates that substantial salts are formed when the geopolymers were exposed in seawater.

The ^{29}Si nuclear magnetic resonance (NMR) spectra had found great success in studying the microstructures of geopolymers, particularly their short-range ordering and molecular structure [26]. The lack of spectral resolution for silicon has been overcome by adopting Gaussian peak deconvolution to separate and quantify Q^n(mAl) species ($0 \le m \le n \le 4$, m, n = integer) [27]. In the geopolymer gel, it has been reported that all silicon and aluminum sites are in tetrahedral coordination, thus $n = 4$ [28–30]. And the resonance of a Q^4(mAl) center with the replacement of each aluminum by silicon is an approximate −5 ppm difference in δ, with Q^4(4Al), Q^4(3Al), Q^4(2Al), Q^4(1Al) and Q^4(0Al) resonating at approximately −84, −89, −93, −99 and −108 ppm, respectively [27]. Fig. 5 gives the ^{29}Si NMR spectra and the deconvolution of the geopolymers exposed differently for 30, 60 and 90 days,

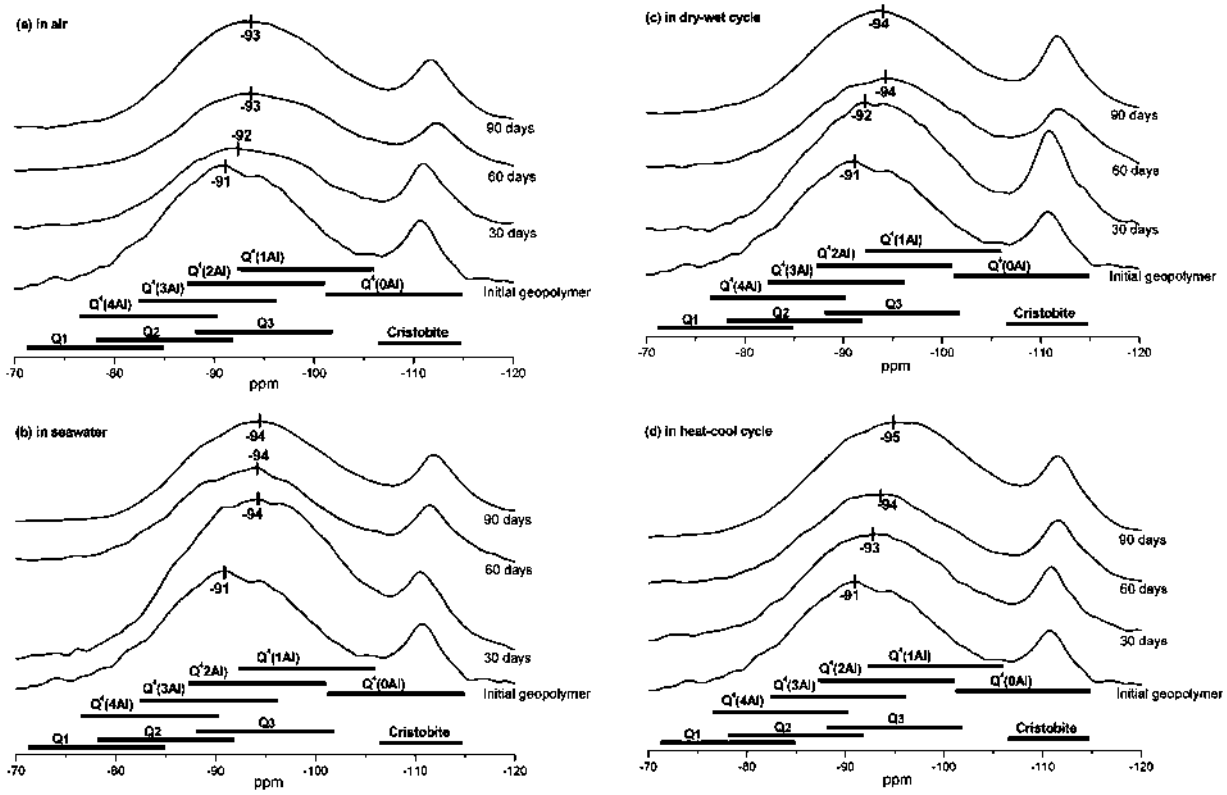

Fig. 5 – ^{29}Si NMR spectra and the deconvolution of geopolymers exposed differently for 30, 60 and 90 days.

Table 2 – ^{29}Si MAS NMR spectral deconvolution of the geopolymer samples (Fig. 5).

Samples		Q1	Q2	Q3	Q^4(4Al)	Q^4(3Al)	Q^4(2Al)	Q^4(1Al)	Q^4(0Al)
Curing condition	Curing time (days)								
Initial geopolymer	7	4.0%	10.1%	10.0%	0.8%	23.3%	18.2%	15.8%	9.4%
In air	30	1.2%	3.8%	5.8%	2.2%	23.0%	17.6%	23.5%	10.4%
	60	0.9%	1.3%	4.6%	3.3%	19.4%	20.2%	27.5%	13.0%
	90	0.4%	0.7%	2.7%	4.7%	20.6%	21.6%	27.0%	12.6%
In seawater	30	2.3%	2.5%	7.3%	3.3%	21.3%	18.1%	26.2%	13.2%
	60	2.0%	3.7%	3.4%	4.1%	21.5%	18.2%	26.1%	12.9%
	90	0.1%	0.8%	3.7%	2.6%	19.2%	22.8%	27.2%	13.0%
In dry-wet cycle	30	1.4%	7.1%	6.5%	2.9%	16.0%	22.5%	21.4%	9.6%
	60	1.1%	2.5%	7.9%	3.6%	17.8%	20.7%	23.4%	12.7%
	90	0.9%	1.1%	3.6%	4.1%	17.0%	25.7%	24.0%	11.1%
In heat-cool cycle	30	1.8%	6.8%	6.9%	1.9%	19.4%	20.7%	21.0%	11.5%
	60	1.9%	5.0%	6.5%	2.6%	18.2%	21.7%	21.0%	12.1%
	90	0.6%	0.9%	4.0%	4.0%	17.2%	21.1%	28.4%	14.4%

in which the spectrum of the initial geopolymer is given as a comparison. The spectra not only show a broad peak of geopolymer gel, but also show sub-peaks that represent the formation of silicate derivatives. These silicate derivatives show structures of single tetrahedral structure from the monosilicates (Q0) to the end groups (Q1), to the chain middle groups (Q2), to the layers and the branching sites (Q3), and finally to the three-dimensional networks (Q4). Here the resonances of Q1, Q2 and Q3 resonate at approximately −79, −85 and −95 ppm, respectively, and the resonance of Q4 is the same as the Q^4(0Al) of the geopolymer gel [31]. In addition, the peak with resonance at −112 ppm is attributed to the remained cristobalite in the geopolymers [32]. After deconvolution, all units of the species are shown by bars in the bottom of Fig. 5. The bars are centered at the deconvoluted peaks of the species, and their lengths represent the widths of the peaks.

Fig. 5 shows the main peak of the geopolymer gel is centered at δ of −91 ppm for the initial geopolymer, while that for the geopolymers exposed for a period of days is centered at a δ less than −91 ppm. Because the Q^4(4Al), Q^4(3Al), Q^4(2Al), Q^4(1Al), Q^4(0Al) resonate at approximately −84, −89, −93, −99 and −108 ppm, respectively, the lower values in δ suggest the formation of less sites of tetrahedral aluminum linking with the tetrahedral silicon. With considering the high Si/Al ratio of 3.7 in the raw materials, this result suggests that geopolymerization reactions are started with aluminum precursors and last for a long time [30]. However, the geopolymers exposed in seawater have the peaks that are centered at the δ of much lower ppm, than that exposed in air. For example, the geopolymer exposed in heat-cool cycle of seawater for 90 days has the peak centered at the δ of −95 ppm, while that exposed in air is −93 ppm. It indicates that the marine conditions inhibit the geopolymerization reactions.

Based on the deconvolutions of the spectra in Fig. 5, the percentages of each species in the geopolymers are shown in Table 2. In the initial geopolymer, the sum of silicate derivatives (Q1, Q1 and Q3) is 24.1%. As exposing the geopolymers for 30, 60 and 90 days, silicate derivatives are transformed into geopolymer gel. For example, as exposing in air for 90 days, silicate derivatives decrease to 3.8%, while the geopolymer gel increases from 67.5% to 86.5%. It suggests that the geopolymerization reactions proceed for a long time. In addition, the sum of Q^4(4Al), Q^4(3Al) and Q^4(2Al) is 47% for exposing in air of 90 days, while they are 44.6%, 44.8% and 42.3% for exposing in seawater, dry-wet and heat-cool cycles in seawater. It suggests again that the marine conditions inhibit the geopolymerization reactions.

4. Conclusion

1. Compressive strength of metakaolin-based geopolymers increases as exposing in air until to 90 days, while it decreases as exposing in seawater, dry-wet and heat-cool cycles of seawater. Cracks and salts such as halite are formed in the exposure conditions with seawater, leading to the decrease in compressive strength.
2. In the exposure for 90 days, species of silicate derivatives (Q1, Q1 and Q3) transform into geopolymer gel in proceeding the geopolymerization reactions. However, seawater environments inhibit the geopolymerization reactions, resulting in the formation of less amount of geopolymer gel in Q^4(4Al), Q^4(3Al) and Q^4(2Al).

Conflicts of interest

The authors declare no conflicts of interest.

Acknowledgements

This study was financially supported by the Consejo Nacional de Ciencia y Tecnología (CONACyT) of Mexico under the Grant No. 270186, the Natural Science Foundation of Hubei Province of China under the Grant No. 2016CFA013 and the Wuhan Science and Technology Bureau of China under the Project No. 2016070204020156, for which the authors are grateful. X. Li would like to thank the CONACyT for offering her the scholarship No. 831134 during her PhD studies.

Appendix A. Supplementary data

Supplementary data associated with this article can be found, in the online version, at doi:10.1016/j.jmrt.2019.03.010.

REFERENCES

[1] Mehta PK. Concrete in the marine environment. CRC Press; 2005.
[2] De Weerdt K, Justnes H, Geiker MR. Changes in the phase assemblage of concrete exposed to sea water. Cem Concr Compos 2014;47:53–63.
[3] Li G, Zhang A, Song Z, Shi C, Wang Y, Zhang J. Study on the resistance to seawater corrosion of the cementitious systems containing ordinary Portland cement or/and calcium aluminate cement. Constr Build Mater 2017;157:852–9.
[4] Zhang J, Gao Y, Han Y. Interior humidity of concrete under dry-wet cycles. J Mater Civ Eng 2011;24(3):289–98.
[5] Arbi K, Nedeljkovic M, Zuo Y, Ye G. A review on the durability of alkali-activated fly ash/slag systems: advances, issues, and perspectives. Ind Eng Chem Res 2016;55(19): 5439–53.
[6] Erdogdu S, Bremner TW, Kondratova IL. Accelerated testing of plain and epoxy-coated reinforcement in simulated seawater and chloride solutions. Cem Concr Res 2001;31(6):861–7.
[7] Papadakis VG. Effect of supplementary cementing materials on concrete resistance against carbonation and chloride ingress. Cem Concr Res 2000;30(2):291–9.
[8] Kwan WH, Cheah CB, Ramli M, Chang KY. Alkali-resistant glass fiber reinforced high strength concrete in simulated aggressive environment. Mater Constr 2018;68(329):147.
[9] Jaya NA, Abdullah MMAB, Li LY, Sandu AV, Hussin K, Ming LY. Durability of metakaolin geopolymers with various sodium silicate/sodium hydroxide ratios against seawater exposure. AIP Conf Proc AIP Publ 2017 1887;1:020063.
[10] Bayuaji R, Darmawan MS, Wibowo B, Husin NA, Subekti S. Utilization of high calcium content fly ash: flexural strength of geopolymer concrete beams in sea water environment. Open Civ Eng J 2016;10:782–93.
[11] Seon-Ju K, Kyung-Sub C, Tae-Hoon K, Chan-Ki K, Chae-yong L. Characteristics of seawater-resistance for Geo-polymer type of grout agen. In: 2011 PAN-AM CGS geotechnical conference. The Canadian Geotechnical Society and the International Society for Soil Mechanics and Geotechnical Engineering; 2011.
[12] Astutiningsih S, Nurjaya DM, Ashadi HW, Swastika N. Durability of geopolymer concretes upon seawater exposure. Adv Sci Technol 2010;69:92–6.
[13] Palomo A, Alonso S, Fernandez-Jiménez A, Sobrados I, Sanz J. Alkaline activation of fly ashes: NMR study of the reaction products. J Am Ceram Soc 2004;87(6):1141–5.
[14] Albitar M, Ali MSM, Visintin P, Drechsler M. Durability evaluation of geopolymer and conventional concretes. Constr Build Mater 2017;136:374–85.
[15] Tennakoon C, Shayan A, Sanjayan JG, Xu A. Chloride ingress and steel corrosion in geopolymer concrete based on long term tests. Mater Des 2017;116:287–99.
[16] Skvara F, Jilek T, Kopecky L. Geopolymer materials based on fly ash. Ceramics-Silikaty 2005;49(3):195–204.
[17] Zhang Z, Yao X, Zhu H. Potential application of geopolymers as protection coatings for marine concrete I. Basic properties. Appl Clay Sci 2010;49(1–2):1–6.
[18] Zhang Z, Yao X, Zhu H. Potential application of geopolymers as protection coatings for marine concrete II. Microstructure and anticorrosion mechanism. Appl Clay Sci 2010;49(1–2):7–12.
[19] Chindaprasirt P, Chalee W. Effect of sodium hydroxide concentration on chloride penetration and steel corrosion of fly ash-based geopolymer concrete under marine site. Constr Build Mater 2014;63:303–10.
[20] Wan Q, Rao F, Song S, León-Patiño CA. Geothermal clay-based geopolymer binders: synthesis and microstructural characterization. Appl Clay Sci 2017;146:223–9.
[21] Pandey S, Jana KK, Aswal VK, Rana D, Maiti P. Effect of nanaoparticle on the mechanical and gas barrier properties of thermoplastic polyurethane. Appl Clay Sci 2017;146:468–74.
[22] Bascarevic Z, Komljenovic M, Miladinovic Z, Nikolic V, Marjanovic N, Petrovic R. Impact of sodium sulfate solution on mechanical properties and structure of fly ash based geopolymers. Mater Struct 2015;48(3):683–97.
[23] Bakharev T. Resistance of geopolymer materials to acid attack. Cem Concr Res 2005;35(4):658–70.
[24] Rashad AM, Ouda AS, Sadek DM. Behavior of alkali-activated metakaolin pastes blended with quartz powder exposed to seawater attack. J Mater Civ Eng 2018;30(8):4018159.
[25] Liu Z, Diao B, Zheng X. Effects of seawater corrosion and freeze–thaw cycles on mechanical properties of fatigue damaged reinforced concrete beams. Adv Mater Sci Eng 2015:536487.
[26] Klinowski J. Nuclear magnetic resonance studies of zeolites. Prog Nucl Magn Reson Spectrosc 1984;16:237–309.
[27] Engelhardt G, Michel D. High-resolution solid-state NMR of silicates and zeolites; 1987.
[28] Barbosa VFF, MacKenzie KJD, Thaumaturgo C. Synthesis and characterisation of materials based on inorganic polymers of alumina and silica: sodium polysialate polymers. Int J Inorg Mater 2000;2(4):309–17.
[29] Rahier H, Van Mele B, Biesemans M, Wastiels J, Wu X. Low-temperature synthesized aluminosilicate glasses. J Mater Sci 1996;31(1):71–9.
[30] Duxson P, Provis JL, Lukey GC, Separovic F, van Deventer JSJ. ^{29}Si NMR study of structural ordering in aluminosilicate geopolymer gels. Langmuir 2005;21(7):3028–36.
[31] Singh PS, Bastow T, Trigg M. Structural studies of geopolymers by ^{29}Si and ^{27}Al MAS-NMR. J Mater Sci 2005;40(15):3951–61.
[32] Fernandez-Jimenez A, Palomo A, Sobrados I, Sanz J. The role played by the reactive alumina content in the alkaline activation of fly ashes. Micropor Mesopor Mater 2006;91(1–3):111–9.

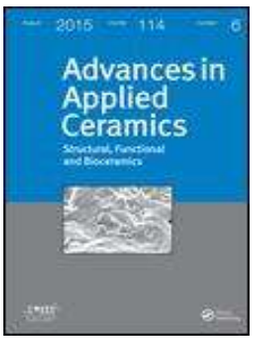

Advances in Applied Ceramics

Structural, Functional and Bioceramics

ISSN: 1743-6753 (Print) 1743-6761 (Online) Journal homepage: https://iom3.tandfonline.com/loi/yaac20

Effect of cristobalite on the mechanical behaviour of metakaolin-based geopolymer in artificial seawater

Xing Li, Feng Rao, Shaoxian Song & Qinyong Ma

To cite this article: Xing Li, Feng Rao, Shaoxian Song & Qinyong Ma (2019): Effect of cristobalite on the mechanical behaviour of metakaolin-based geopolymer in artificial seawater, Advances in Applied Ceramics, DOI: 10.1080/17436753.2019.1687208

To link to this article: https://doi.org/10.1080/17436753.2019.1687208

Published online: 06 Nov 2019.

ADVANCES IN APPLIED CERAMICS
https://doi.org/10.1080/17436753.2019.1687208

The Institute of Materials, Minerals and Mining

Taylor & Francis
Taylor & Francis Group

Effect of cristobalite on the mechanical behaviour of metakaolin-based geopolymer in artificial seawater

Xing Li[a,b], Feng Rao [a,b], Shaoxian Song [c] and Qinyong Ma[d]

[a]School of Zijin Mining, Fuzhou University, Fuzhou, People's Republic of China; [b]CONACYT Instituto de Investigación en Metalurgia y Materiales, Universidad Michoacana de San Nicolás de Hidalgo, Morelia, Mexico; [c]School of Resources and Environmental Engineering, Wuhan University of Technology, Wuhan, People's Republic of China; [d]School of Civil Engineering and Architecture, Anhui University of Science and Technology, Huainan, People's Republic of China

ABSTRACT

Few studies have focused on the effect of mineral composition on the mechanical behaviour and evolution of a geopolymer binder in artificial seawater environment. In this study, a geothermal clay-based geopolymer rich in micron-size cristobalite and metakaolin was compared with a metakaolin-based geopolymer in artificial seawater. The effects of the cristobalite on the mechanical behaviour and microstructure of geopolymers were characterised through compressive strength measurements, x-ray diffraction (XRD), scanning electron microscope (SEM) and nuclear magnetic resonance (NMR). The micro-size cristobalite enhanced the compressive strength of the geothermal clay-based geopolymer. Without cristobalite, zeolite formed in metakaolin-based geopolymer and led to compressive strength decrease obviously first then increase slightly. The formation of the geothermal clay-based geopolymer gel was delayed in seawater. The cristobalite in the geothermal clay-based geopolymer hindered the formation of Q^4(4Al), Q^4(3Al) and Q^4(2Al).

ARTICLE HISTORY
Received 27 July 2019
Revised 19 October 2019
Accepted 25 October 2019

KEYWORDS
Cristobalite; zeolite; geopolymer; properties; artificial seawater

Introduction

The deterioration of ordinary Portland cement (OPC) concrete over time due to the corrosive ions in seawater has been widely observed [1–4]. Corrosive ions, such as Cl^-, $SO2-4$, Mg^{2+}, etc., permeate into the open pores of OPC concrete and attack the calcium hydroxide ($Ca(OH)_2$) and calcium silicate hydrate (C–S–H). The reacted productions cause strength loss and expansion, which deteriorate the concrete. In addition, the dry–wet cycles in tidal areas intensify the deterioration [5]. Compared to OPC concrete, geopolymers give good performance outcomes in seawater [6,7]. This is because the main product in geopolymer is a N–A–S–H gel with a three-dimensional structure, which is different from the C–S–H structure, and $Ca(OH)_2$ is not usually presented in the gel [8].

Generally, the anticorrosion characteristics of geopolymers are better than those of OPC concrete [9]. However, the attack mechanism of seawater on a geopolymer is not yet fully understood, primarily due to the wide range of compositions of geopolymers. Different compositions of geopolymers lead to diverse microstructures, mechanical properties and chemical properties, which are related to corrosion resistance [10]. For example, Astutiningsih et al. [11] synthesised a metakaolin-based geopolymer concrete and a fly ash-based geopolymer concrete, and then exposed them to the seawater for 90 days. The compressive strength of the metakaolin-based geopolymer remained almost constant and the compressive strength of the fly ash-based geopolymer showed a decrease before 56 days and then remained stable. Likewise, Rashad et al. [12] synthesised alkali-activated metakaolin using 40% quartz powder to replace metakaolin by weight. The samples with 40% quartz powder exposed to seawater for 12 months showed a 40% strength loss while the metakaolin-only samples showed a 50% strength loss. These researchers suggest that a geopolymer will gain different anticorrosion characteristics with changing compositions. Therefore, it is important to know how these compositions affect the anticorrosion characteristics of a geopolymer.

Current studies on geopolymers in seawater are mainly focused on their mechanical properties and durability [13–16]. However, few studies have focused on how the mineral compositions of the raw materials affect the mechanical properties or how a geopolymer gel evolves in seawater environment. Geothermal clay, which was studied in our previous research, is rich in kaolin and micron-size cristobalite. The alkali-activated-geothermal clay geopolymer presented higher mechanical properties [17,18]. Therefore, in

CONTACT Feng Rao fengrao@umich.mx School of Zijin Mining, Fuzhou University, Fuzhou, Fujian 350108, People's Republic of China, CONACYT Instituto de Investigación en Metalurgia y Materiales, Universidad Michoacana de San Nicolás de Hidalgo, Morelia, Michoacán 58030, México; Shaoxian Song shaoxian@uaslp.mx School of Resources and Environmental Engineering, Wuhan University of Technology, Wuhan, Hubei 430070, People's Republic of China

this study, through a comparison of a metakaolin geopolymer and a geothermal clay geopolymer, which were exposed to 10-fold concentrated artificial seawater, the deterioration of the mechanical properties and microstructures were observed and the effect of cristobalite was studied.

Experimental

Materials

The kaolin was obtained from Hubei Province, China. The geothermal clay was collected from the Los Azufres geothermal field, Mexico at a depth of 250 m where the temperature exceeds 150°C. The kaolin and geothermal clay were performed calcination at 800°C for 6 h to obtain metakaolin and calcinated geothermal clay [19]. The d_{50} and d_{85} particle sizes of the metakaolin powder were 13.2 and 26.9 μm, respectively, and the d_{50} and d_{85} particle sizes of geothermal clay powder were 13.0 and 27.4 μm, respectively, as measured using a Beckman Coulter (USA) particle size analyser. Figure 1 presented the XRD patterns of the kaolin and geothermal clay before and after calcination. It was observed that the peak of kaolin disappeared after calcination. Muscovite and quartz were abundant in metakaolin, while cristobalite was rich in the geothermal clay. Table 1 presented the mineral compositions of metakaolin and geothermal clay. The Si/Al ratio of metakaolin was 1:1, while Si/Al ratio of geothermal clay was 3.6:1. American Chemical Society (ACS) reagent grade sodium silicate (Na_2SiO_3) powder and sodium hydroxide (NaOH) pellets were purchased from Sigma-Aldrich, and they were used as the alkali activator in the syntheses. Artificial seawater with a 10-fold concentration was prepared with 292.5 g L^{-1} NaCl, 7.45 g L^{-1} KCl, 36 g L^{-1} $MgSO_4$, and this seawater was renewed every 7 days during the curing process.

Synthesis of geopolymers and seawater curing

To obtain the optimal compressive strengths, metakaolin-based geopolymers and geothermal clay-based geopolymers were synthesised with different mix ratios, which were used in the previous studies [18,19]. Table 2 presents the preparations of metakaolin-based geopolymer and geothermal clay-based geopolymer. The different S/L ratios were the optimal S/L ratio in the syntheses of metakaolin-based and geothermal clay-based geopolymers, which were in the range of S/L ratios in geopolymer formation [20]. The alkaline solution was prepared and then mixed with the precursor (metakaolin or geothermal clay) for 5 min. Next, these mixtures were cast into cubic steel moulds (50 mm × 50 mm × 50 mm). The moulds were vibrated on a vibration table for 1 min to liberate air bubbles. After this step, the samples were sealed and cured at 60°C for 6 h and then at room temperature for 7 days to obtain the initial strength. Then some of the

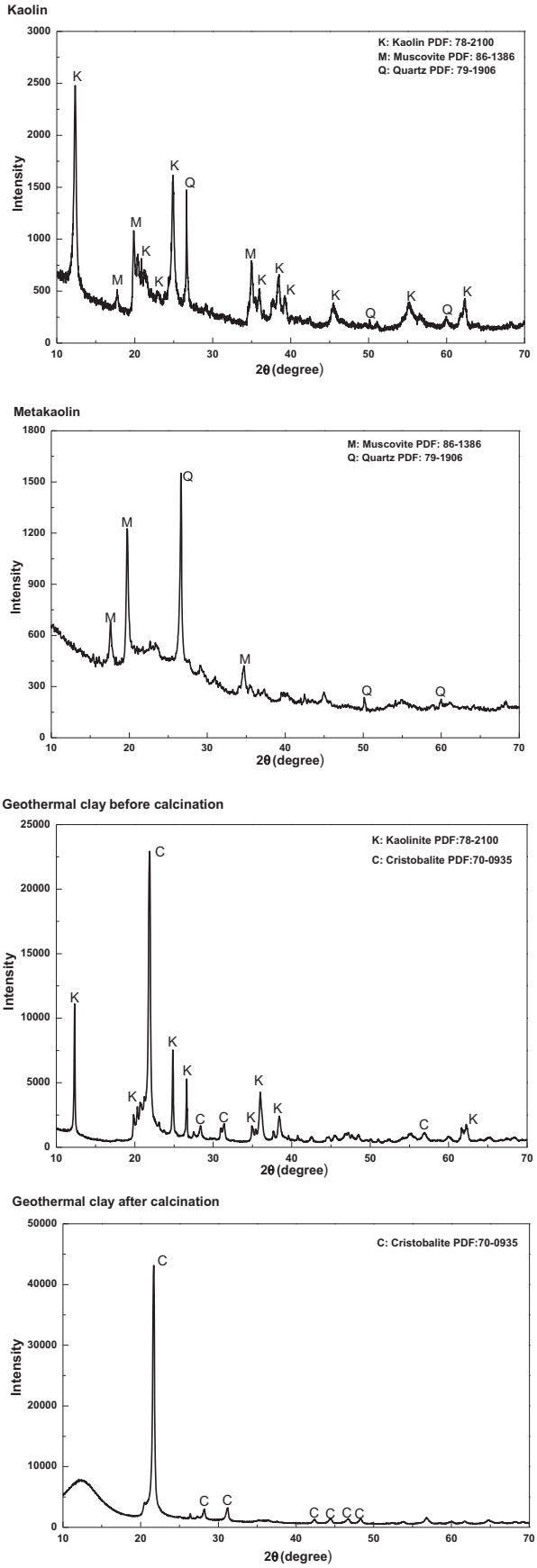

Figure 1. XRD patterns of raw materials.

Table 1. Mineral compositions of metakaolin and geothermal clay.

	Raw material	
Mineral composition	Metakaolin (mass %)	Geothermal clay (mass %)
SiO_2	59.48	67.2
Al_2O_3	35.13	15.5
K_2O	2.56	7.15
Fe_2O_3	0.97	1.18
MgO	0.43	–
TiO_2	0.21	0.31
SO_3	0.15	7.25
Na_2O	0.08	<0.01
P_2O_5	0.05	1.16
PbO	0.02	–
Rb_2O	0.02	–
As_2O_3	0.01	–
ZrO_2	<0.01	0.19
SrO	<0.01	–
CaO	<0.01	0.04
CuO	–	<0.01

specimens were analysed as the initial metakaolin-based geopolymer (M-In) samples and the initial geothermal clay-based geopolymer (G-In) samples; others were exposed to one of three conditions: (1) curing in air: the metakaolin-based geopolymer (MA) samples and geothermal clay-based geopolymer (GA) samples were kept in air at room temperature; (2) curing in seawater: the metakaolin-based geopolymer (MS) samples and geothermal clay-based geopolymer (GS) samples were cured in artificial seawater (25 ± 2° C); (3) curing with dry–wet cycles of seawater: the metakaolin-based geopolymer (MDW) samples and geothermal clay-based geopolymer (GDW) samples were cured with cycles of 12 h in air (25 ± 2°C) and 12 h in artificial seawater (25 ± 2°C). For each curing condition, the compressive strengths and the microstructures of the geopolymers were measured at 30, 60 and 90 days, respectively.

Characterisation

The compressive strength values of the geopolymer samples were measured with Zwick/Roell, Zwick Z100 mechanical tester from Zwick/Roell Zwick GmbH & Co. KG, Germany. In each group of measurements, the average value was obtained from at least three samples. A scanning electron microscope (SEM, JEOL JSM-5610LV, Japan) was used to characterise the morphology of the geopolymers. The XRD patterns

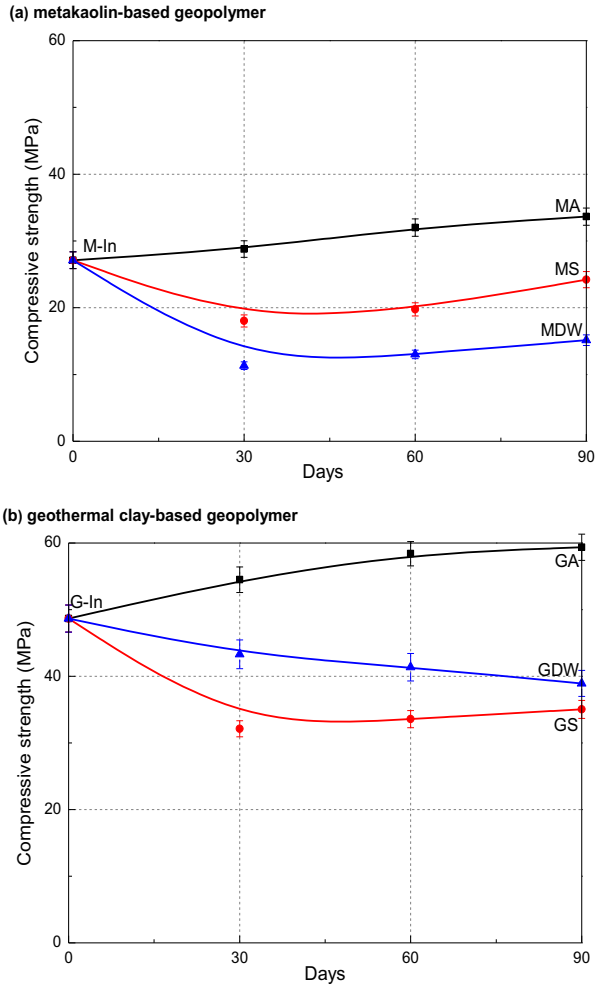

Figure 2. Compressive strengths of (a) metakaolin-based geopolymers and (b) geothermal clay-based geopolymers cured in different conditions.

of the geopolymers were obtained using a Brucker D8 (Germany) X-ray diffractometer. The parameters of the XRD measurements were monochromatic Cu-Kα1 radiation, $\lambda = 1.5406$ Å, 0.2° 2θ steps, 0.6 s step^{-1} over a 10–65° 2θ degree range. The ^{29}Si nuclear magnetic resonance (NMR) spectra of the alkaline activated binder gel in the concrete specimens were obtained by operating at 79.49 MHz. The powder specimens were packed into 7 mm diameter ZrO_2 rotors. The spectra were acquired at spinning speeds of 12 kHz with the peak positions were referenced to an external standard of tetramethylsilane (TMS) and recorded with a 1 s delay time. The samples for the SEM, XRD and NMR

Table 2. Preparation regimen of geopolymer and curing conditions.

		Alkaline activators (g)						
Sample ID	Precursor	NaOH	Na_2SiO_3	H_2O	Si/Al	Na/Al	Solid/liquid	Curing condition
M-In	Metakaolin (222 g)	0	122	162	2.1:1	1.3:1	2.1:1	–
MA								In air
MS								In seawater
MDW								In dry–wet cycles
G-In	Geothermal clay (222 g)	10	61	216	4.4:1	1.8:1	1.4:1	–
GA								In air
GS								In seawater
GDW								In dry–wet cycles

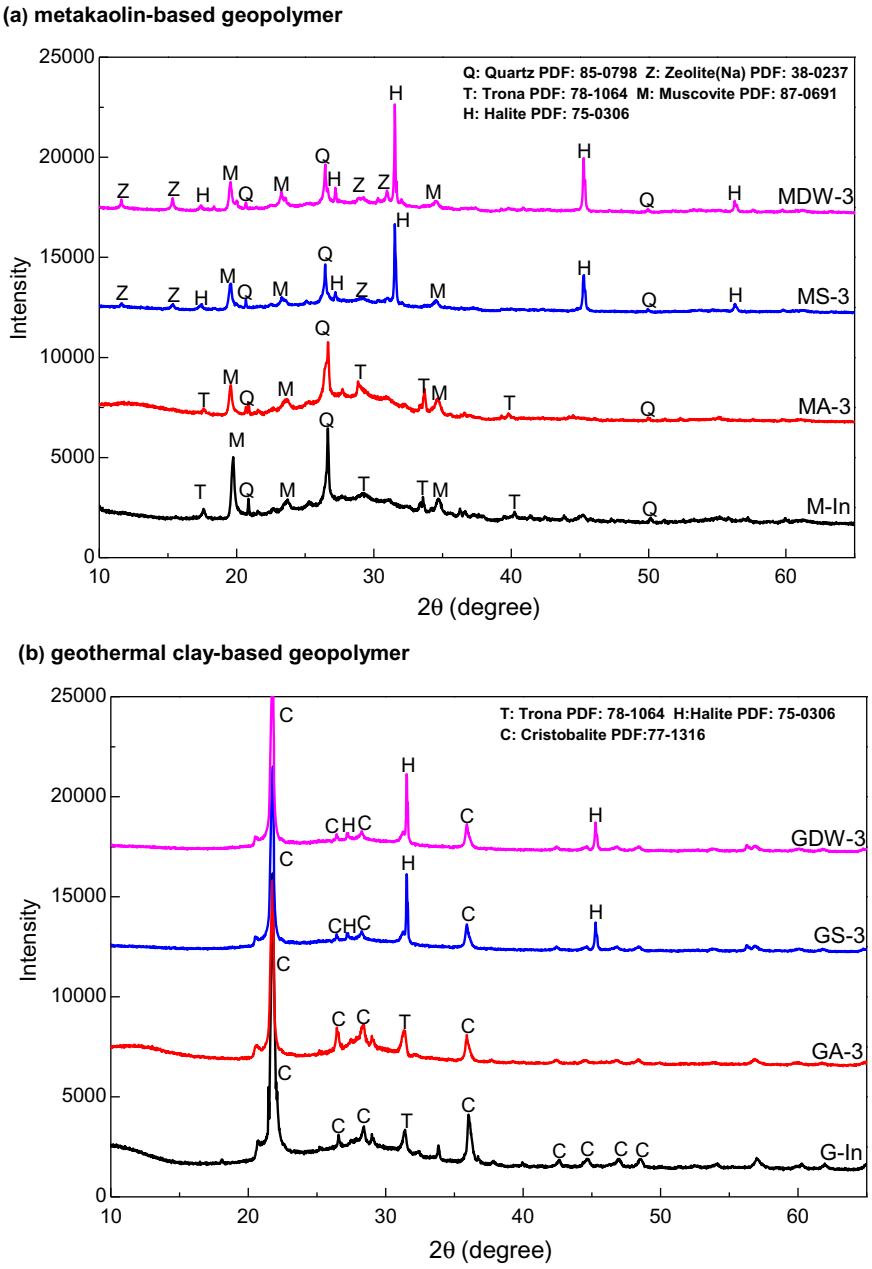

Figure 3. XRD patterns of (a) metakaolin-based geopolymers and (b) geothermal clay-based geopolymers exposed to different curing conditions for 90 days.

measurements were collected at the depth of 2–5 mm inside the geopolymer specimens.

Results and discussion

Figure 2 shows the changes in the compressive strength values of geopolymer samples exposed to different conditions. The starting compressive strength of M-In is 27.11 MPa and that of G-In is 48.66 MPa. The compressive strength values of both MA and GA increase with time. After 90 days, the compressive strength value of MA is 33.65 MPa and that of GA is 59.37 MPa. The compressive strength of MS decreases to 18.03 MPa at 30 days and then increases to 24.21 MPa at 90 days. These values are higher than those of MDW, which decreases to 11.33 MPa, then increases slightly to 15.13 MPa at 30 and 90 days, respectively. The compressive strength value of GS decreases to 32.12 MPa at 30 days, then increases to 35.04 MPa at 90 days. However, these values are lower than those of GDW, which decreases gradually to 38.93 MPa at 90 days.

It can be noted that (1) the compressive strength values of samples exposed to seawater environment decrease. This may be associated with the dilution effect of seawater in geopolymerisation reactions [12,13]. (2) The compressive strength values of the geothermal clay-based geopolymers are much higher than those of the metakaolin-based geopolymer. This is because the micron-size cristobalite enhances the

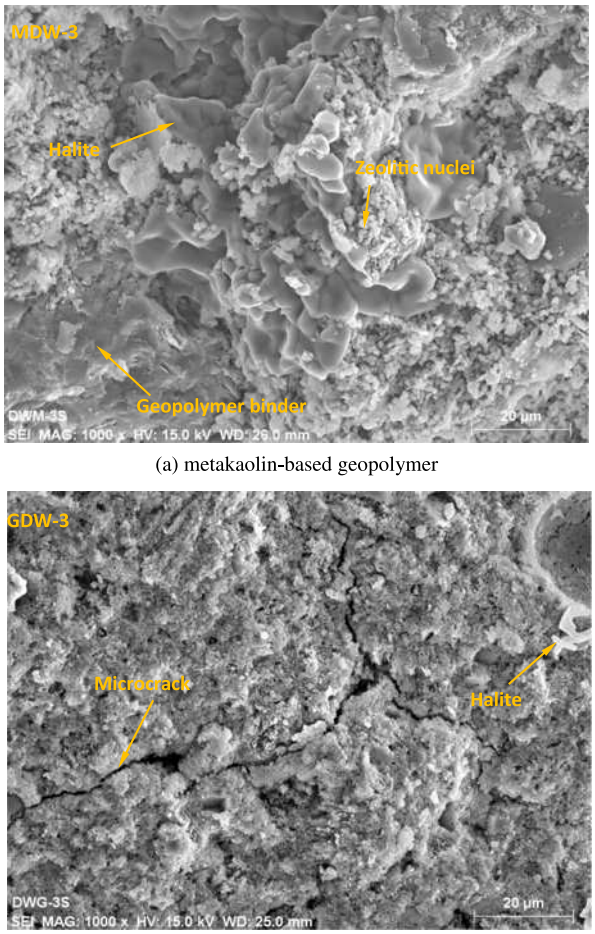

Figure 4. SEM patterns of geopolymer cured in dry–wet cycles of seawater for 90 days.

compressive strengths of the geopolymers. It is consistent with the reports of Wan et al. [21] and Shaikh and Haque [22].

Figure 3 shows the XRD analyses of the initial geopolymer mortars M-In and G-In, metakaolin-based geopolymer cured in air for 90 days (MA-3), in seawater for 90 days (MS-3) and in dry–wet cycle for 90 days (MDW-3), and geothermal clay-based geopolymer cured in air for 90 days (GA-3), in seawater for 90 days (GS-3) and cured in dry–wet cycle for 90 days (GDW-3). All the samples contain the phases originating from the starting raw materials: the muscovite and quartz in the metakaolin and the cristobalite in the geothermal clay. Meanwhile, the formation of new phases due to the reactions with magnesium and sulphate ions is not indicated. The amorphous XRD patterns with one hump centred at approximately 27–29° 2θ are rarely observed in the MS-3, MDW-3, GS-3 and GDW-3 specimens, which indicate the seawater inhabited the formation of geopolymer gel. The trona appearing in M-In, MA-3, G-In and GA-3 is related to excessive alkali, and then it disappears in the MS-3, MDW-3, GS-3 and GDW-3 samples, it is related to the dilution of the alkali by the seawater. Zeolites are formed in MS-3 and MDW-3 samples but not in GS-3 and GDW-3 samples, which may be attributed to the metakaolin-based geopolymer with low Si/Al ratio (2.1:1) in the seawater environment shows low reactivity [23,24]. In addition, the dry–wet cycles of seawater seem to promote more zeolite formation in the metakaolin-based geopolymer. These zeolites hold substantial halite permeation in the samples. Therefore, the peak intensities of halite that appear in the MDW-3 specimens are higher. Meanwhile, many of these zeolites reduce the compressive strength of metakaolin-based geopolymer cured in dry–wet cycle greatly than those cured in seawater, which is agreement with the reports that increasing the amount of zeolite in the geopolymer reduces strength [8,25].

Figure 4 shows the SEM images of geopolymers synthesised with metakaolin and geothermal clay cured in dry–wet cycles of seawater for 90 days. For sample MDW-3, the geopolymer binder, halite and a number of zeolitic nuclei are observed. Most of these nuclei are not dispersed in the geopolymer binder. The cracks due to dry–wet cycles of seawater are not observed, because the zeolites could hold a lot of halite. For sample GDW-3, halite is not obvious. The cracks are presented in the geopolymer, and these cracks cause the compressive strength of geothermal clay-based geopolymer to decrease gradually in the dry–wet cycles of seawater.

Systematic ^{29}Si MAS-NMR spectra are used to understand the evolution of geopolymer gel in this study. The ^{29}Si NMR spectra and their deconvolution of the metakaolin-based geopolymer and the geothermal clay-based geopolymer exposed to different conditions for 90 days are shown in Figures 5 and 6. All the samples are deconvoluted by fitting the Gaussian peak of the $Q^n(m\text{Al})$ ($0 \le m \le n \le 4$?m, n = integer). It is reported that all the silicon sites are in tetrahedral coordination, thus $n = 4$ and $Q^4(4\text{Al})$, $Q^4(3\text{Al})$, $Q^4(2\text{Al})$, $Q^4(1\text{Al})$, $Q^4(0\text{Al})$ resonating at approximately −84, −89, −93, −99 and −108 ppm, respectively [26]. Meanwhile, the sub-peaks represent the formation of silicate derivatives. These silicate derivatives show structures of single tetrahedral structure of the monosilicates (Q0) to the end groups (Q1), to the chain middle groups (Q2), to the layers and the branching sites (Q3), and finally to the three-dimensional networks (Q4). Here the Q1, Q2 and Q3 resonate at approximately −79, −85 and −95 ppm, respectively, and the Q4 is the same as the $Q^4(0\text{Al})$ of the geopolymer gel [26]. In addition, the MDW-3 shows two shoulders at approximately −88 and −95 ppm, which is associated with zeolite and Q3 [27,28]. The peak with resonance at −112 ppm in the geothermal clay-based geopolymer is attributed to the cristobalite [29].

From Figures 5 and 6, the sum of $Q^4(4\text{Al})$, $Q^4(3\text{Al})$ and $Q^4(2\text{Al})$ of M-In is 57.2%, and the sums of samples MA-3, MS-3 and MDW-3 are 61.3, 58.7 and 57.7%, respectively. Meanwhile, the sum of $Q^4(4\text{Al})$, $Q^4(3\text{Al})$

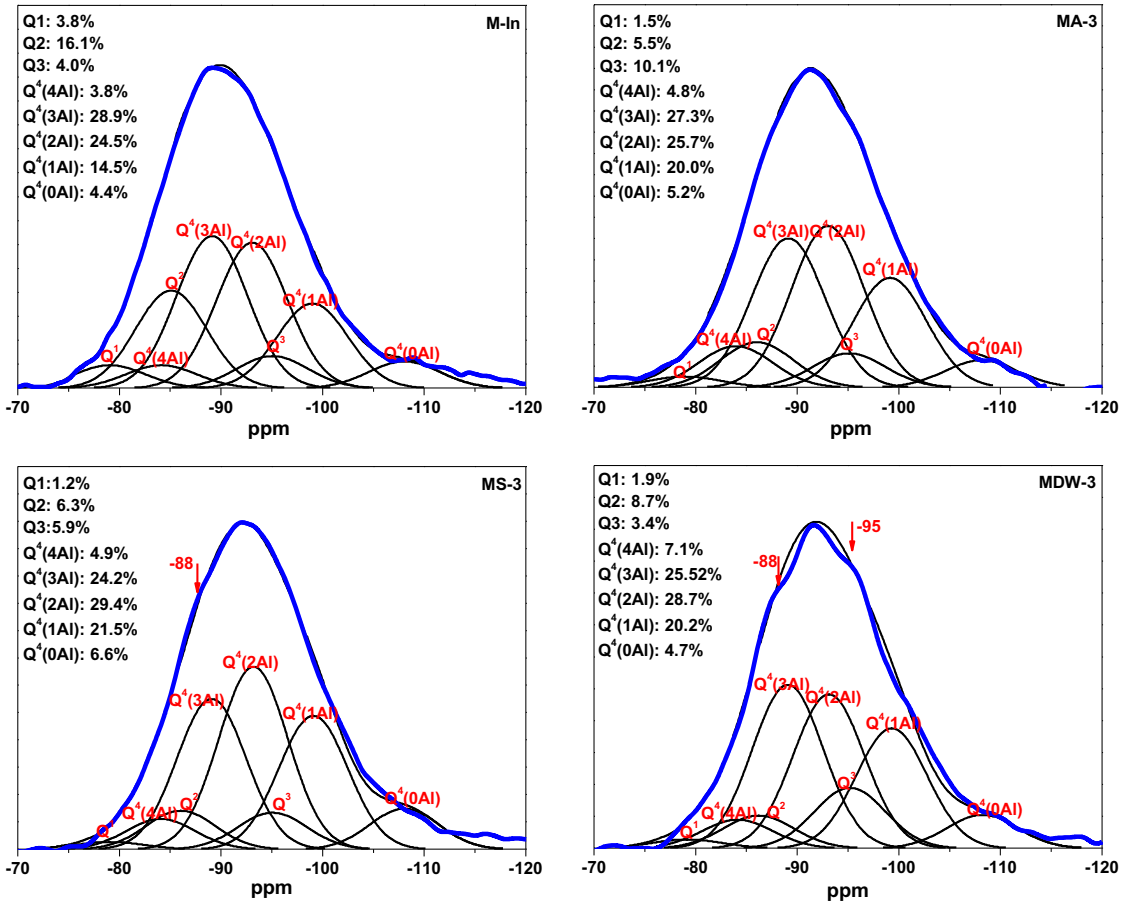

Figure 5. The ^{29}Si NMR spectra and their deconvolution of the metakaolin-based geopolymer gel cured in different curing conditions for 90 days.

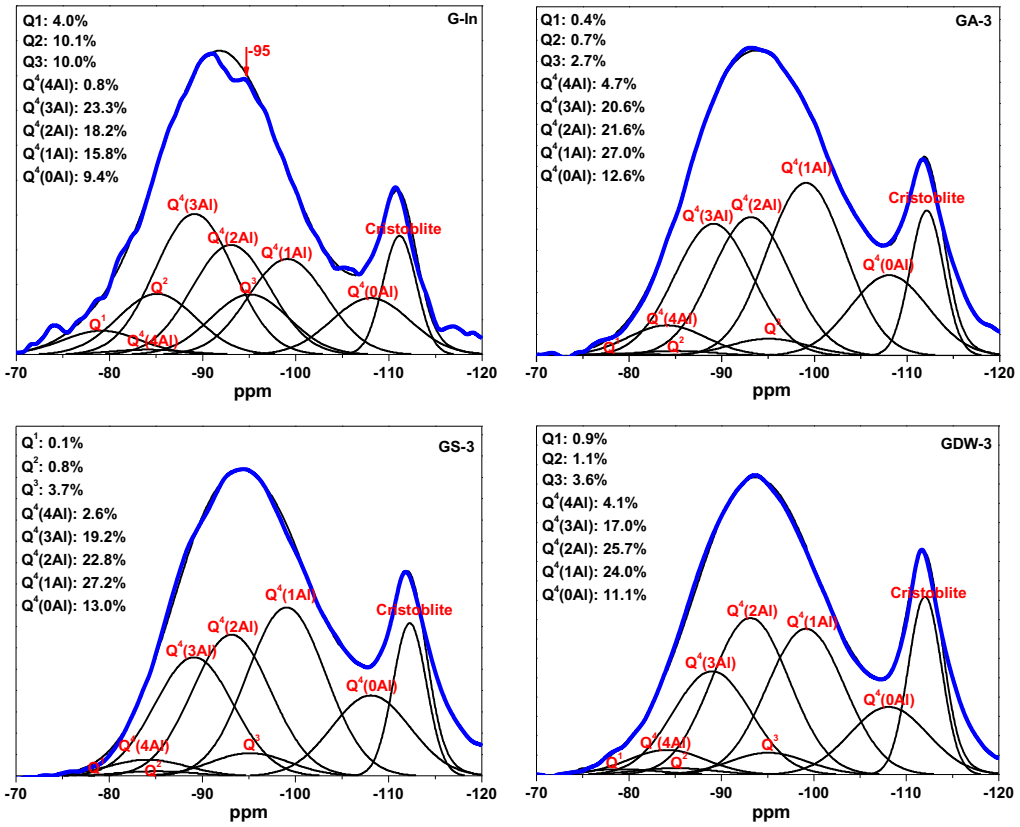

Figure 6. The ^{29}Si NMR spectra and their deconvolution of geothermal clay-based geopolymer gel cured in different curing conditions for 90 days.

and Q^4(2Al) of G-In samples is 42.3%, and the sums of samples GA-3, GS-3 and GDW-3 are 47.0, 44.6 and 46.8%, respectively. After curing for 90 days, all the sums of Q^4(4Al), Q^4(3Al) and Q^4(2Al) increase, indicating that the formation of the geopolymer gel proceeds for a long time. The sum of Q^4(4Al), Q^4(3Al) and Q^4(2Al) in MA-3 is more than those of MS-3, MDW-3 and GA-3 is more than those of GS-3 and GDW-3, respectively, which suggests that the seawater environment delays the formation of the geopolymer gel. The sums of Q^4(4Al), Q^4(3Al) and Q^4(2Al) of the metakaolin-based geopolymers are more than 57.2% while those of the geothermal clay-based geopolymer are less than 47.0%, which is related to the large amounts of cristobalite present in geothermal clay hindering the formation of geopolymer gel.

Conclusions

Metakaolin-based geopolymers and geothermal clay-based geopolymers have different properties in artificial seawater because the cristobalite plays an important role. It is noted that the mineral compositions of the geopolymer binder have a very important effect in controlling the geopolymers' properties. Through studying their compressive strengths and microstructures, it is found that:

(1) Cristobalite enhances the compressive strength of geothermal clay-based geopolymer. They also improve the Si/Al ratio to prevent the formation of zeolite. Without zeolites, the compressive strengths of samples cured in dry–wet cycles decrease gradually. While many zeolites in metakaolin-based geopolymer cured in dry–wet cycles first obviously decrease compressive strength then increase slightly.
(2) The geothermal clay-based geopolymer shows a separate peak associated with cristobalite. The cristobalite reduces the formation of Q^4(4Al), Q^4(3Al) and Q^4(2Al).

Disclosure statement

No potential conflict of interest was reported by the authors.

Funding

This study was financially supported by the Consejo Nacional de Ciencia y Tecnologia (CONACyT) of Mexico under the grant number 270186, the Natural Science Foundation of Hubei Province of China under the grant number 2016CFA013 and the Wuhan Science and Technology Bureau of China under the project no. 2016070204020156, for which the authors are grateful. X. Li would like to thank the CONACyT for offering her the scholarship number 831134 during her PhD studies.

ORCID

Shaoxian Song http://orcid.org/0000-0003-3570-6401
Qinyong Ma http://orcid.org/0000-0001-7278-7875

References

[1] De Weerdt K, Justnes H, Geiker MR. Changes in the phase assemblage of concrete exposed to sea water. Cem Concr Compos. 2014;47:53–63.
[2] Li G, Zhang A, Song Z, et al. Study on the resistance to seawater corrosion of the cementitious systems containing ordinary Portland cement or/and calcium aluminate cement. Constr Build Mater. 2017;157:852–859.
[3] Mehta PK. Concrete in the marine environment. New York: CRC Press; 2005.
[4] Page CL. Mechanism of corrosion protection in reinforced concrete marine structures. Nature. 1975;258:514–515.
[5] Edouard J-B. Experimental evaluation of the durability of fly ash-based geopolymer concrete in the marine environment. Baca Raton: Florida Atlantic University; 2011.
[6] Zhang Z, Yao X, Wang H. Potential application of geopolymers as protection coatings for marine concrete III. Field experiment. Appl Clay Sci. 2012;67-68:57–60.
[7] Chindaprasirt P, Chalee W. Effect of sodium hydroxide concentration on chloride penetration and steel corrosion of fly ash-based geopolymer concrete under marine site. Constr Build Mater. 2014;63:303–310.
[8] Provis JL, Van Deventer JSJ. Geopolymers: structures, processing, properties and industrial applications. New York: Elsevier; 2009.
[9] Davidovits J. Properties of geopolymer cements. First International Conference on Alkaline Cements and Concretes; Kiev, Ukraine; 1994. p. 131–149.
[10] Duxson P, Fernández-Jiménez A, Provis JL, et al. Geopolymer technology: the current state of the art. J Mater Sci. 2007;42:2917–2933.
[11] Astutiningsih S, Nurjaya DM, Ashadi HW, et al. Durability of geopolymer concretes upon seawater exposure. Adv Sci Technol Trans Tech Publ. 2010;69:92–96.
[12] Rashad AM, Ouda AS, Sadek DM. Behavior of alkali-activated metakaolin pastes blended with quartz powder exposed to seawater attack. J Mater Civ Eng. 2018;30:04018159.
[13] Zhang Z, Yao X, Zhu H. Potential application of geopolymers as protection coatings for marine concrete I. Basic properties. Appl Clay Sci. 2010;49:1–6.
[14] Seon-Ju K, Kyung-Sub C, Tae-Hoon K, et al. Characteristics of seawater-resistance for geo-polymer type of grout agent. 2011 Pan-Am CGS Geotechnical Conference, Canada; 2011.
[15] Bayuaji R, Darmawan MS, Wibowo B, et al. Utilization of high calcium content fly ash: flexural strength of geopolymer concrete beams in sea water environment. Open Civ Eng J. 2016;10:782–793.
[16] Jaya NA, Abdullah MMAB, Li L-Y, et al. Durability of metakaolin geopolymers with various sodium silicate/sodium hydroxide ratios against seawater exposure. AIP Conference Proceedings; AIP Publishing; 2017. p. 20063.
[17] Wan Q, Rao F, Song S, et al. Geopolymerization reaction, microstructure and simulation of metakaolin-

based geopolymers at extended Si/Al ratios. Cem Concr Compos. 2017;79:45–52.
[18] Li X, Rao F, Song S, et al. Effects of aggregates on the mechanical properties and microstructure of geothermal metakaolin-based geopolymers. Results Phys. 2018;11:267–273.
[19] Wan Q, Rao F, Song S. Reexamining calcination of kaolinite for the synthesis of metakaolin geopolymers-roles of dehydroxylation and recrystallization. J Non-Cryst Solids. 2017;460:74–80.
[20] Wan Q, Rao F, Song S, et al. Geothermal clay-based geopolymer binders: Synthesis and microstructural characterization. Appl Clay Sci. 2017;146:223–229.
[21] Wan Q, Rao F, Song S, et al. Combination formation in the reinforcement of metakaolin geopolymers with quartz sand. Cem Concr Compos. 2017;80:115–122.
[22] Shaikh F, Haque S. Effect of nano silica and fine silica sand on compressive strength of sodium and potassium activators synthesised fly ash geopolymer at elevated temperatures. Fire Mater. 2018;42(3):324–335.
[23] Yan H, Xue-min C, Liu L, et al. The hydrothermal transformation of solid geopolymers into zeolites. Microporous Mesoporous Mater. 2012;161:187–192.
[24] Yu Y, Li X, Zou X, et al. Effect of seawater salinity on the synthesis of zeolite from coal fly ash. Front Environ Sci Eng. 2014;8:54–61.
[25] De Silva P, Sagoe-Crenstil K. Medium-term phase stability of Na_2O–Al_2O_3–SiO_2–H_2O geopolymer systems. Cem Concr Res. 2008;38:870–876.
[26] Engelhardt G, Michel D. High-resolution solid-state NMR of silicates and zeolites. New York, United States; 1987.
[27] Singh PS, Bastow T, Trigg M. Structural studies of geopolymers by ^{29}Si and ^{27}Al MAS-NMR. J Mater Sci. 2005;40:3951–3961.
[28] Ramdas S, Klinowski J. A simple correlation between isotropic 29Si-NMR chemical shifts and T–O–T angles in zeolite frameworks. Nature. 1984;308:521–523.
[29] Fernández-Jiménez A, Palomo A, Sobrados I, et al. The role played by the reactive alumina content in the alkaline activation of fly ashes. Microporous Mesoporous Mater. 2006;91:111–119.

Available online at www.sciencedirect.com

jmr&t Journal of Materials Research and Technology

https://www.journals.elsevier.com/journal-of-materials-research-and-technology

Original Article

Microstructural evolution in sulfate solutions of alkali-activated binders synthesized at various calcium contents

Xing Li[a,b], *Owen Xu Li*[c], *Feng Rao*[a,b,*], *Shaoxian Song*[d], *Noemi Ortiz-Lara*[b], *Ena A. Aguilar-Reyes*[b]

[a] *School of Zijin Mining, Fuzhou University, Fuzhou, Fujian 350108, China*
[b] *CONACYT Instituto de Investigación en Metalurgia y Materiales, Universidad Michoacana de San Nicolás de Hidalgo, Morelia, Michoacán 58030, Mexico*
[c] *The American School Foundation, Mexico City, 01120, Mexico*
[d] *School of Resources and Environmental Engineering, Wuhan University of Technology, Wuhan, Hubei 430070, China*

ARTICLE INFO

Article history:
Received 19 January 2020
Accepted 11 July 2020

Keywords:
Alkali-activated binder
Sulfate solution
Compressive strength
N-A-S-H gel
NMR spectra

ABSTRACT

Alkali-activated binders based on metakaolin, fly ash and slag without curing were exposed directly in air, Na_2SO_4 and $MgSO_4$ solutions for studying the evolution in mechanical strength and microstructure. A series of binders were synthesized and characterized on 7, 21, 45, 60, 75 and 90 days, respectively. Compressive strength measurement, scanning electron microscope (SEM) mapping, X-ray diffraction (XRD) and unclear magnetic resonance (NMR) were applied in the study. It is found that the exposure in sulfate solutions leaded to the deterioration of the binders by the dissolution of alkalis. In Na_2SO_4 solution, a higher percentage of zeolite was formed in the binders. While in $MgSO_4$, a precipitate layer (e.g., brucite and gypsum), forming on the binder surface plays an important role in protecting the formation of gel, promoting the compressive strength improvement of alkali-activated slag, and compensating the decrease in compressive strength of alkali-activated metakaolin. These results provide clues for the direct preparation of alkali-activated concrete in aggressive sulfate environment.

1. Introduction

Alkali-activated binders are cementitious materials formed by alkali activated calcium and aluminosilicate materials or industrial by-products [1–3]. Compared to the ordinary Portland cement (OPC) concrete, these binders possess compact ceramic-like gel in their microstructure, which can be classified into systems of low, medium and high calcium contents. The system of low CaO is represented as the $(Na,K)_2O–Al_2O_3–SiO_2–H_2O$ (N–A–S–H) gel [4–6]. In the high CaO system, one structure is the calcium silicate hydrate (C–S–H) gel, the other structure is of a disordered tobermorite that contains significant aluminum substituents, namely the $(Na,K)_2O–CaO–Al_2O_3–SiO_2–H_2O$ ((N,C)–A–S–H) gel [7–10]. Other structures like AFm ($3CaO–Al_2O_3–CaSO_4–12H_2O$) type phases

* *Corresponding author at*: School of Zijin Mining, Fuzhou University, Fuzhou, Fujian 350108, China.
E-mail: fengrao@umich.mx (F. Rao).

https://doi.org/10.1016/j.jmrt.2020.07.041

Table 1 – Chemical analysis of the raw materials.

Materials (%)	SiO_2	Al_2O_3	CaO	Fe_2O_3	K_2O	MgO	TiO_2	SO_3	P_2O_5	CuO	PbO
Metakaolin	52.5	42.1	0	1.0	2.6	0.4	0.2	0.2	0	0	0
Fly ash	49.9	28.3	8.51	5.5	1.4	0.6	2.2	2.0	1.2	0	0
Slag	18.5	5.5	27.6	25.6	0.6	1.0	0.4	5.1	1.7	3.1	0.9

Table 2 – Preparation regimen of the alkali-activated binders and exposure conditions.

ID	Raw materials (g)	Alkali activator (g)		Si/Al	Ca/Si	Liquid/solid	Exposure conditions
		Na_2SiO_3	H_2O				
M–A M–Na M–Mg	Metakaolin (222)	122	162	1:1	0	0.48	Air Na_2SO_4 solution $MgSO_4$ solution
FA–A FA–Na FA–Mg	Fly ash (222)	122	198	1.4:1	0.2:1	0.58	Air Na_2SO_4 solution $MgSO_4$ solution
S–A S–Na S–Mg	Slag (222)	36.6	54	2.8:1	1.6:1	0.21	Air Na_2SO_4 solution $MgSO_4$ solution

[11,12], as well as the Si-containing AFm phase strätlingite ($2CaO–SiO_2–Al_2O_3–8H_2O$) in silicate-activated binders [13,14], hydrotalcite [15,16], and zeolites such as gismondine and garronite [17,18], which are mainly formed in medium CaO contents, depend on the exact chemistry of the precursor materials and the activator [19]. Many studies reported that alkali-activated binders showed high durability against sulfate attack, which was attributed to the different microstructure in N–A–S–H and (N,C)–A–S–H gels [20]. For example, when undergoing 32 heating-cooling cycles in 5% magnesium sulfate ($MgSO_4$) solution, compressive strength of an alkali-activated fly ash binder lost 12.7%, while that of an OPC concrete lost 17.8% [21]. In another comparison, after 21 days of immersion in sulfate solution, an alkali-activated fly ash mortar showed no change in appearance while the OPC mortar exhibited superficial fractures caused by the gypsum and ettringite formation [22].

However, the reported alkali-activated concretes were synthesized and cured sufficiently before immersion in sulfate solutions, while some applications require exposure of the binders in sulfate solutions during the synthesizing process, e.g., the marine concrete and underground pipes [23,24]. Limited studies were contributed to the evolution in microstructure of alkali-activated binders without curing when exposing in sulfate solutions [25,26]. For example, Salami et al. [27] reported that the compressive strength of an alkali-activated palm oil fuel ash based-binder decreased from 24.2 to 16.2 MPa in sulfate solutions, and the dissolution of alkalis was attributed as the main reason. For another alkali-activated fly ash-based binder without curing, the geopolymer gel was destroyed and the Si was leached out when exposing in Na_2SO_4 solution [28].

Therefore, the present work attempted to study the evolution in microstructure and mechanical property of alkali-activated binders without curing in sulfate solutions. Furthermore, the evolution of different gels (e.g., N–A–S–H and (N,C)–A–S–H) was investigated. The binders of high, medium and low CaO were prepared to obtain different gel in the microstructure of the binders. The sulfate solutions of Na_2SO_4 and $MgSO_4$ were applied. We hypothesize that the binders of different gel would be deteriorated in varying degrees in sulfate solutions. It is found that the Na^+ and Mg^{2+} ions promoted the degradation of the binders.

2. Experimental

2.1. Materials

Metakaolin was obtained by the calcination of kaolin (Hubei province, China) at 800 °C for 6 h. It was measured the particle size at 50% (D_{50}) and 85% (D_{85}) of cumulative undersize of 13.2 and 26.9 μm respectively, from a Beckman Coulter (USA) particle size analyzer. Fly ash was collected from the Tianjiaan power plant, China, of which the D_{50} and D_{85} were 30.2 and 65.4 μm, respectively. Slag was a by-product of *pyrometallurgical zinc refining* collected from the Zincamex metallurgy plant, Mexico, of which the D_{50} and D_{85} after grinding were 42.1 and 78.3 μm respectively. Table 1 gives the chemical analysis of the metakaolin, fly ash and slag measured by X-ray fluorescence (XRF, PANalytical Axios). The SiO_2 and Al_2O_3 were main components in the metakaolin and fly ash, while the SiO_2, CaO and Fe_2O_3 were dominant in the slag. The content of CaO was low, medium and high in the metakaolin, fly ash and slag, respectively. And the metakaolin and fly ash contained more K_2O, while the slag was higher in SO_3, P_2O_5, CuO and PbO. In addition, sodium silicate (Na_2SiO_3) with reagent grade ACS was purchased from Sigma-Aldrich as alkali-activator for the syntheses. Solutions of 50 g/L Na_2SO_4 or $MgSO_4$ were prepared with distilled water.

2.2. Methods

Table 2 gives the preparation regime of alkali-activated binders with metakaolin, fly ash and slag. Different dosages of alkali activator (Na_2SiO_3) were used to obtain the maximum compressive strength for the three binders. The Ca/Si mole ratios were 0, 0.2:1 and 1.6:1 for the metakaolin, fly ash and slag-

Table 3 – pH values of the sulfate solutions after exposure of the alkali-activated binders.

Binders	Metakaolin-binders		Fly ash-binders		Slag-binders	
	Na_2SO_4	$MgSO_4$	Na_2SO_4	$MgSO_4$	Na_2SO_4	$MgSO_4$
0	8.37	8.31	8.37	8.31	8.37	8.31
7 days	13.41	9.46	13.45	9.40	13.45	9.40
90 days	13.84	10.53	13.73	11.02	13.78	10.50

based binders. In the syntheses, alkali activator of Na_2SiO_3 was first prepared and then mixed with the raw materials, namely metakaolin, fly ash or slag, for 5 min. Next, these mixtures were cast into cubic steel molds ($50 \times 50 \times 50$ mm). The molds were vibrated on a vibration table for 3 min to liberate air bubbles. After that, the samples were sealed and cured at 60 °C for 6 h and then slowly cooled about 18 h to room temperature (RT). Subsequently, the binders were de-molded and exposed to three types of conditions: 1) in air at RT; 2) in 50 g/L Na_2SO_4 solution and 3) in 50 g/L $MgSO_4$ solution. For each exposure condition, the compressive strengths and the microstructures of the samples were characterized at 7, 21, 45, 60, 75 and 90 days, respectively.

2.3. *Characterization*

Compressive strength of the alkali-activated binders was measured through a Zwick/Roell Z100 mechanical tester from Zwick GmbH & Co. KG, Germany. In each measurement, three specimens were tested and the average value was used. The microstructural morphology of the binders was characterized by a scanning electron microscope (SEM, JEOL JSM-5610LV, Japan), on which the equipped energy-dispersive X-ray was used to obtain the elemental mapping of the specimens. The X-ray diffraction (XRD) patterns of the binders were obtained using a Brucker D8 (Germany) X-ray diffractometer. The parameters of the XRD measurements were: monochromatic Cu-Kα1 radiation, $\lambda = 1.5406$ Å, 0.2° 2θ steps, 0.6 s step^{-1} over a 10–65° 2θ degree range. The ^{29}Si nuclear magnetic resonance (NMR) spectra of the alkali-activated binders were obtained by operating at 79.49 MHz. The powdered specimens were packed into 7 mm diameter ZrO_2 rotors. Spectra were acquired at spinning speeds of 5 kHz with peak positions referenced to an external standard of tetramethylsilane (TMS) and recorded with 5 s delay time. The excitation pulse for ^{29}Si was 6 μs with a recycle time of 5 s.

3. Results and discussion

Fig. 1 shows the compressive strength of the alkali-activated binders exposed in air, Na_2SO_4 and $MgSO_4$ solutions for 90 days. For the exposure in air, compressive strength of the metakaolin-based binder increased slightly from 46 to 51.1 MPa on 7–90 days. In comparison, the fly ash and slag-based binders showed a lower compressive strength, which increased slightly from around 19–23 MPa in curing for 90 days. It suggests the formation of geopolymer gel in the metakaolin-based binder, leading to superior mechanical property [29].

For the exposure in Na_2SO_4 solution, compressive strength of the metakaolin-based binder decreased gradually from 40.8 to 15.7 MPa on 7 to 90 days. Compressive strength of the fly ash-based binder decreased from 17.1 to 11.1 MPa on 7 to 21 days, and then it kept a constant. The reduction of compressive strength suggests that the Na_2SO_4 solution dissolves alkalis in the binders, so that the alkaline activation process was

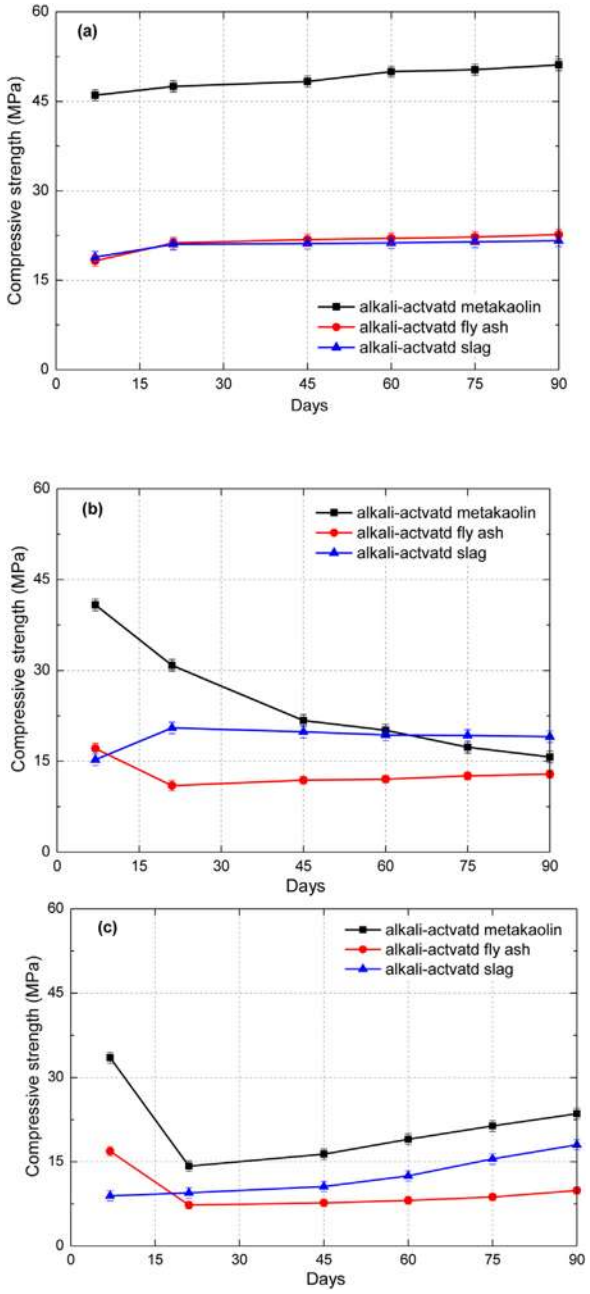

Fig. 1 – Compressive strengths of alkali-activated binders exposed in (a) air, (b) Na_2SO_4 and (c) $MgSO_4$ solutions.

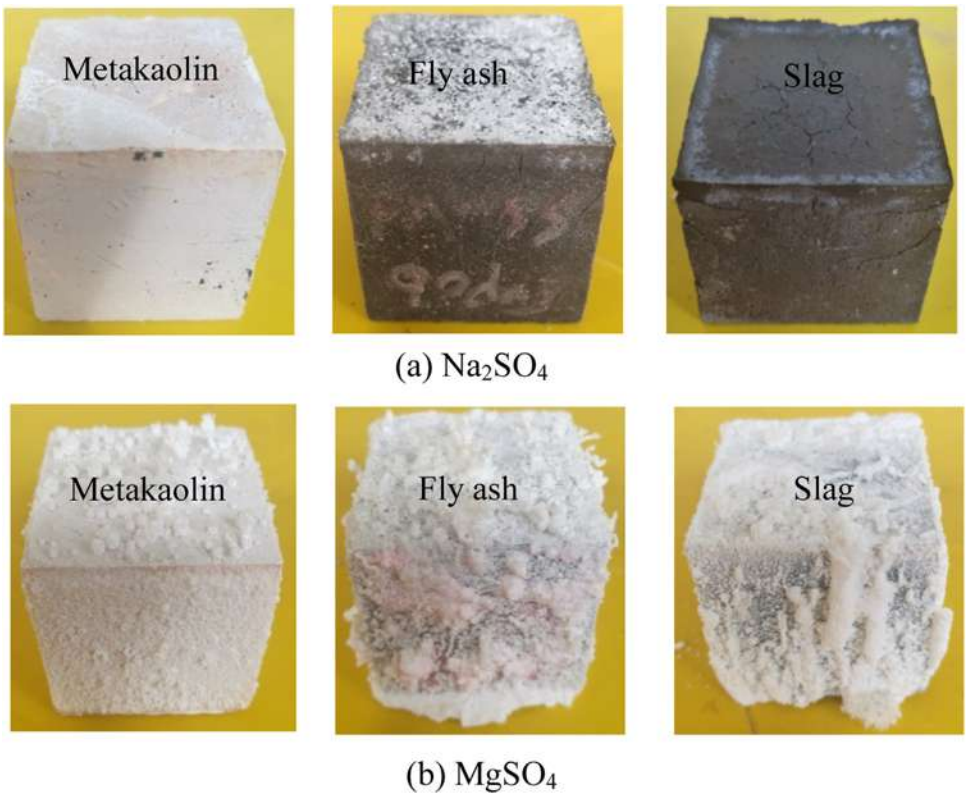

Fig. 2 – Photos of the alkali-activated binders exposed in (a) Na_2SO_4 and (b) $MgSO_4$ solutions for 90 days.

Table 4 – Summary of N-A-S-H, (N,C)-A-S-H and C-S-H gels in the alkali-activated binders after deconvolution.

Binders		N-A-S-H gel		(N,C)-A-S-H and C-S-H gels
		Q^4(mAl)	sum of Q^4(4Al), Q^4(3Al) and Q^4(2Al)	(Q^1+Q^2+Q^3)
Metakaolin	Air	100%	83.3%	0
	Na_2SO_4	100%	49.7%	0
	$MgSO_4$	100%	72.6%	0
Fly ash	Air	91.8%	56.2%	8.2%
	Na_2SO_4	89.3%	49.1%	10.7%
	$MgSO_4$	91.3%	45.9%	8.7%
Slag	Air	72.6%	56.7%	27.4%
	Na_2SO_4	68.3%	29.2%	31.7%
	$MgSO_4$	69.7%	52.4%	30.3%

weakened by deterioration of the N-A-S-H gel [26,27,30]. However, compressive strength of the slag-based binders increased from 15.3 to 20.5 MPa on 7 to 21 days, and then remained constant. In the slag-based binders, high contents of (N,C)–A–S–H and C–S–H gels were formed, because of high CaO in the raw slag [31]. Therefore, the increase in compressive strength suggests that alkali dissolution affects less on the formation of (N,C)–A–S–H and C–S–H gels [6,32,33]. Furthermore, Yip et al. [34] reported that C-S-H gel worked as a micro-aggregate in the binder, resulting in homogeneous and dense structure.

For the exposure in $MgSO_4$ solution, compressive strength of metakaolin and fly ash-based binders decreased sharply from 33.5 and 16.9 MPa to 14.2 and 7.3 MPa on 7 to 21 days, respectively, and then they increased moderately to 23.6 and 9.87 MPa on 90 days, respectively. Compressive strength of the slag-based binder increased steadily from 8.9 to 18 MPa on 7 to 90 days. Compared to the exposure in Na_2SO_4 solution, pre-

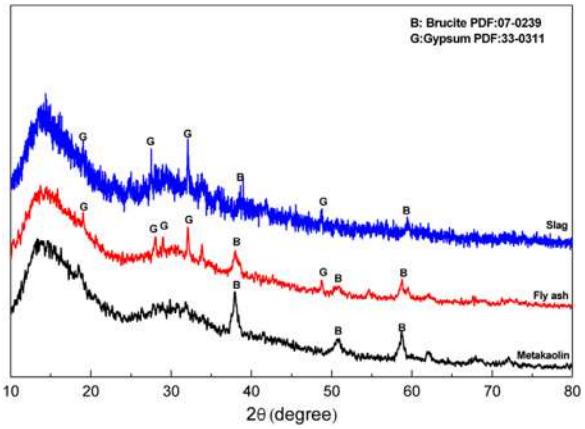

Fig. 3 – XRD of precipitates on the surfaces of samples.

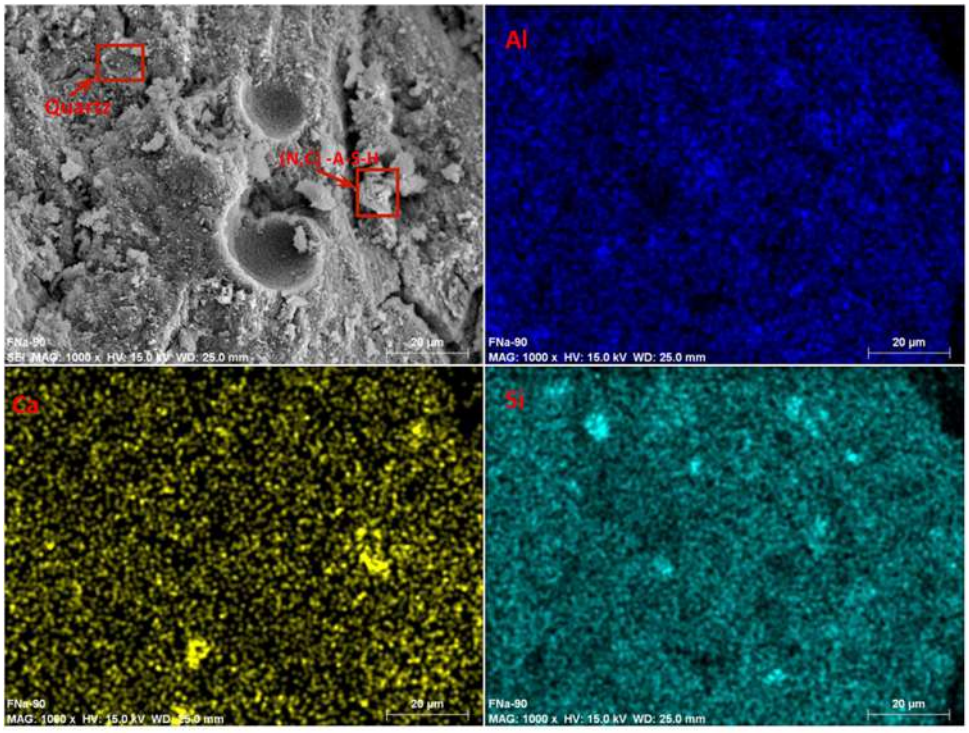

(a) Fly ash-based binder exposed in Na_2SO_4 solution for 90 days

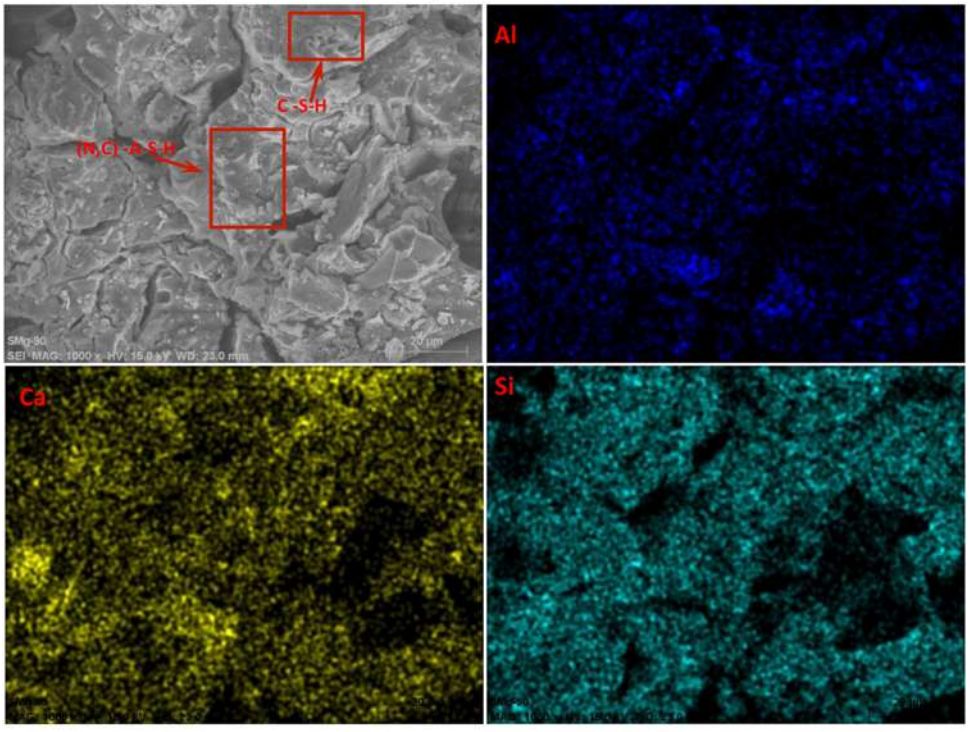

(b) Slag-based binder exposed in $MgSO_4$ solution for 90 days

Fig. 4 – SEM images and corresponding elemental mapping of the binders.
(a) Fly ash-based binder exposed in Na_2SO_4 solution for 90 days.
(b) Slag-based binder exposed in $MgSO_4$ solution for 90 days.

cipitates of $Mg(OH)_2$ and $CaSO_4$ might be formed on surface of the binders, which protected them from the dissolution of alkalis, resulting in higher increases in compressive strength on 90 days [35,36].

Fig. 2 shows photos of the alkali-activated binders exposed in Na_2SO_4 and $MgSO_4$ solutions for 90 days. In Na_2SO_4 solution, there is no macroscopic change on the binders' surface, indicating Na_2SO_4 attack is undetected in either the deterioration of the binder or the formation of precipitates. While in $MgSO_4$ solution, through XRD analysis (Fig.3), it was found that the white precipitates of brucite ($Mg(OH)_2$) and gypsum ($CaSO_4$) were formed on the surface of alkali-activated fly ash and alkali-activated slag. It is indicated that the Mg^{2+} ions not only precipitate with alkalis, but also promote the precipitation of $CaSO_4$. Table 3 gives the pH values of the sulfate solutions in 90 days. Initial pH of both the Na_2SO_4 and $MgSO_4$ solutions were around 8.3. In Na_2SO_4 solution, it increased to pH 13.4 in 7 days and further to around pH 13.8 in 90 days for the exposure of the three binders. While in $MgSO_4$ solution, it increased to around pH 9.5 in 7 days and further to around pH 11 in 90 days. The increase of the pH suggests the dissolution of alkali from the binders [28,36], and the lower increase of pH in $MgSO_4$ solution is attributed to the fact that the precipitated brucite acted as an insoluble and protective layer for the binders [37].

Fig. 4 shows the SEM images and corresponding elemental mapping of the fly ash and slag -based binders exposed in Na_2SO_4 and $MgSO_4$ solutions, respectively. Compared with the surface photos of the binders (Fig. 2), their microstructural morphology shows homogeneous gel structure. It indicates that the sulfate attack merely affects the gel formation in the alkali-activated binders. In elemental mapping of both the fly ash and slag-based binders, the Ca, Al and Si elements are evenly distributed throughout. It suggests that the N–A–S–H, (N,C)–A–S–H and C–S–H gels were formed evenly in the binders.

Fig. 5 presents the XRD patterns of the metakaolin, fly ash and slag-based binders exposed differently for 90 days. For the metakaolin-based binders, impurities of quartz and muscovite were observed because they are inert minerals in alkaline activation process. The binder exposed in air shows featherless amorphous XRD pattern with one hump centered at approximately $2\theta = 27-29^{\circ}$, which suggests the formation of geopolymer N–A–S–H gel [38]. However, the binder exposed in Na_2SO_4 solution presents the characteristic peaks of zeolite, which is attributed to the dissolution of alkalis [39]. The zeolite crystals weaken the formation of N–A–S–H gel, leading to the decrease in mechanical property of the binders [29,40], which is in agreement of the compressive strength results (Fig. 1). While the binders exposed in $MgSO_4$ solution show amorphous XRD pattern without zeolite peaks, which might be due to precipitated brucite delaying the dissolution of alkalis. For the fly ash-based binders, quartz is originated from the raw materials. Zeolite forms in the three exposure conditions, which is attributed to higher content of unreacted material and higher Si/Al ratio of gel [41]. In addition, the C–S–H gel is observed when exposing in Na_2SO_4 and $MgSO_4$ solutions, which indicates that the diluted alkali from the binder leads to the formation of C–S–H gel [42]. For the slag-based binders, zoisite, calcite, quartz and maghemite are from the raw materials. The C–S–H gel is observed in the three exposing conditions. Gypsum and ettringite form in the alkali-activated slag cured in Na_2SO_4 and $MgSO_4$ solution. And no obvious peaks of brucite and hydrotalcite are observed. It is suggested that a small amount of Mg ions diffuse into of the samples [43,44].

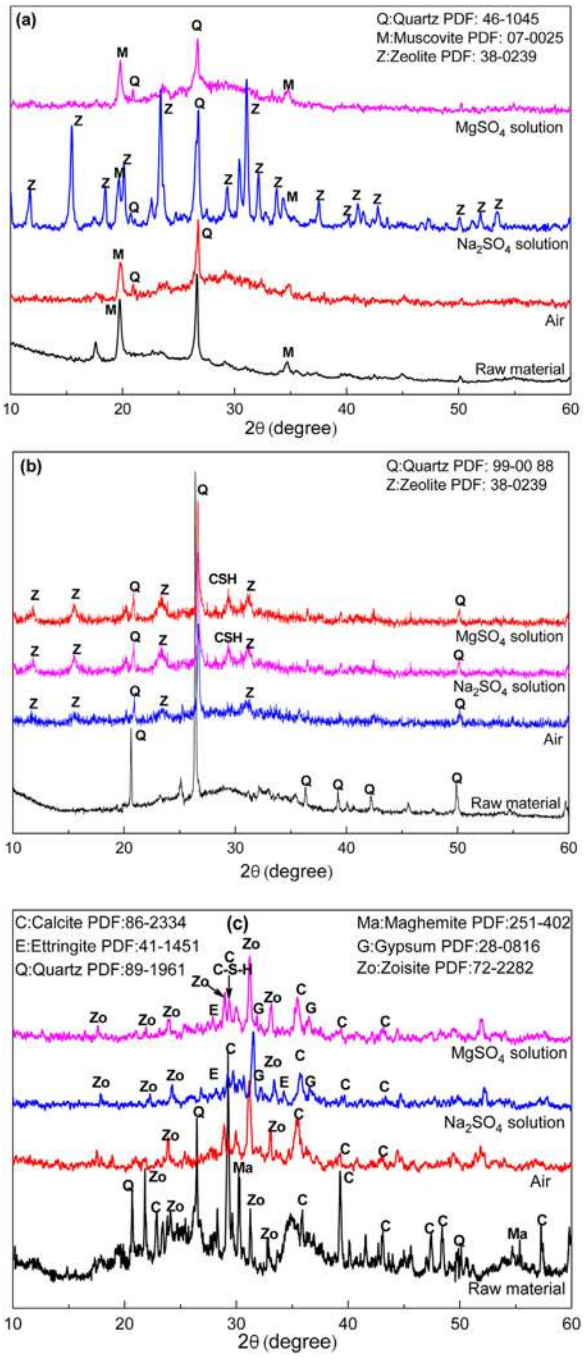

Fig. 5 – XRD patterns of the (a) metakaolin, (b) fly ash and (c) slag-based binders exposed differently for 90 days.

In studying the microstructure of alkali-activated binders, short-range ordering and molecular structure have been investigated with great success using NMR spectroscopy [45]. The lack of spectral resolution for Si in the binders has been

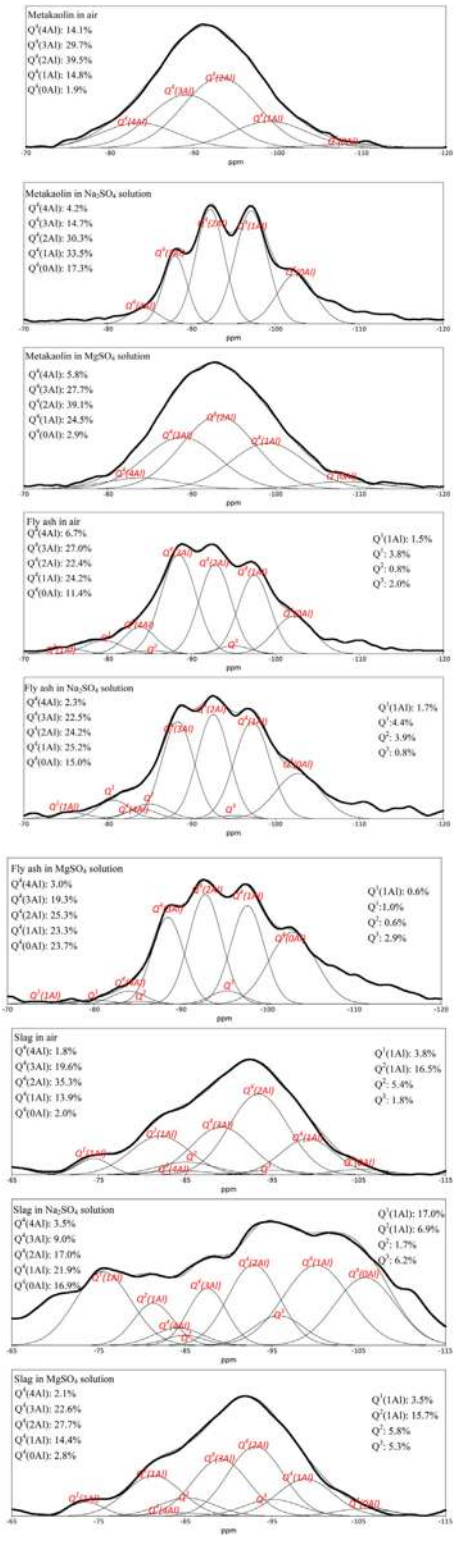

Fig. 6 – The ^{29}Si NMR spectra and their deconvolution of the alkali-activated binders cured differently.

overcome by adopting Gaussian peak deconvolution to separate and quantify $Q^n(mAl)$ species ($0 \le m \le n \le 4$, m, n = integer) [46]. In geopolymer N-A-S-H gel, it is reported that all the Si sites are in tetrahedral coordination, thus n = 4 and the $Q^4(4Al)$, $Q^4(3Al)$, $Q^4(2Al)$, $Q^4(1Al)$, $Q^4(0Al)$ resonate at approximately −84, −89, −93, −99 and −108 ppm, respectively [47]. In the (N,C)–A–S–H and C–S–H gels, the silicate derivatives show structures of the end groups (Q^1), the chain middle groups (Q^2), the layers and the branching sites (Q^3) [48]. Here the Q^1, Q^2 and Q^3 resonate at approximately −70, −79, −85 and −95 ppm, respectively, the peak at −74 and −84 represent $Q^1(1Al)$, $Q^2(1Al)$ when Al is involved, respectively. Fig. 6 presents the ^{29}Si NMR spectra and their deconvolution of the alkali-activated binders exposed in different conditions. For the metakaolin-based binders, the spectra of the binders exposed in air and $MgSO_4$ solution show a broad peak, while that exposed in Na_2SO_4 solution shows several peaks in the spectrum. It corresponds well with the XRD results (Fig. 5) that only the binder exposed in Na_2SO_4 solution showed high contents of zeolite. For the fly ash-based binders, the spectra show several peaks in air, Na_2SO_4 and $MgSO_4$ solutions, corresponding well to the observation of zeolite in XRD patterns (Fig. 5). For the slag-based binders, one broad peak spectra is observed when exposing in air and in $MgSO_4$ solution, and several peaks in the spectrum when exposing in Na_2SO_4 solution.

Table 4 gives the summary of N–A–S–H, (N,C)–A–S–H and C–S–H gels in the alkali-activated binders after deconvolution. For the metakaolin-based binders, only N–A–S–H gel is formed. For the fly ash -based binders, about 91.8%, 89.3% and 91.3% N–A–S–H gel formed in the binders exposed in air, Na_2SO_4 and $MgSO_4$ solutions, respectively. For the slag-based binders, about 72.6%, 68.3% and 67.3% N–A–S–H gel are formed in the binders exposed in air, Na_2SO_4 solution, and $MgSO_4$ solution, respectively. It is suggested that N–A–S–H gel is the main gel in the alkali-activated binder. The sum of $Q^4(4Al)$, $Q^4(3Al)$ and $Q^4(2Al)$ in the N-A-S-H gel representing a better cross-linked aluminosilicate structure is also presented. It can be observed that the sums of alkali-activated binder cured in sulfate solution are lower than them cured in air. It is suggested that sulfate solutions inhibit the geopolymerization through dissolving the alkalinity of the samples.

4. Conclusion

1 Alkali-activated binders of different calcium contents, which are based on metakaolin, fly ash and slag, are synthesized and exposed in air, Na_2SO_4 and $MgSO_4$ solutions. When exposing in sulfate solutions, deterioration of the binders takes place, being mainly attributed to the dissolution of alkalis.

2 The Na_2SO_4 solution leads to zeolite formation in the binders, which decreases their compressive strength. While in $MgSO_4$ solution, a layer of precipitated minerals (e.g., brucite) formed on the surface of the binders, which inhibits the deterioration of the binders.

3 The dissolution of alkali in sulfate solutions leads to the formation of more C–S–H gel in the alkali-activated fly ash and slag based-binders, which compensates the decrease in compressive strength of the binders.

Declaration of interests

The authors declare that they have no known competing financial interests or personal relationships that could have appeared to influence the work reported in this paper.

Acknowledgement

This study was financially supported by the Consejo Nacional de Ciencia y Tecnología (CONACyT) of Mexico under the Grant No. 270186, the National Natural Science Foundation of China under the project No. 51974093 and the Natural Science Foundation of Hubei Province of China under the Grant No. 2016CFA013, for which the authors are grateful. X. Li would like to thank the CONACyT for offering her the scholarship No. 831134 during her PhD studies.

REFERENCES

[1] Provis JL, Van Deventer JSJ. Alkali activated materials: state-of-the-art report, RILEM TC 224-AAM. Springer Science & Business Media; 2013.
[2] Rao F, Liu Q. Geopolymerization and its potential application in mine tailings consolidation: a review. Miner Process Extr Metall Rev 2015;36(6):399–409.
[3] Luukkonen T, Abdollahnejad Z, Yliniemi J, Kinnunen P, Illikainen M. One-part alkali-activated materials: a review. Cem Concr Res 2018;103:21–34.
[4] Khan MZN, Hao Y, Hao H. Synthesis of high strength ambient cured geopolymer composite by using low calcium fly ash. Constr Build Mater 2016;125:809–20.
[5] Noushini A, Aslani F, Castel A, Gilbert RI, Uy B, Foster S. Compressive stress-strain model for low-calcium fly ash-based geopolymer and heat-cured Portland cement concrete. Cem Concr Compos 2016;73:136–46.
[6] Mehta A, Siddique R. Strength permeability and micro-structural characteristics of low-calcium fly ash based geopolymers. Constr Build Mater 2017;141:325–34.
[7] Wang SD, Pu XC, Scrivener KL, Pratt PL. Alkali-activated slag cement and concrete: a review of properties and problems. Adv Cem Res 1995;7:93–102.
[8] Escalante-García JI, Fuentes AF, Gorokhovsky A, Fraire-Luna PE, et al. Hydration products and reactivity of blast-furnace slag activated by various alkalis. J Am Ceram Soc 2003;86(12):2148–53.
[9] Fernández-Jiménez A, Puertas F, Sobrados I, Sanz J. Structure of calcium silicate hydrates formed in alkaline-activated slag: influence of the type of alkaline activator. J Am Ceram Soc 2003;86(8):1389–94.
[10] Myers RJ, Bernal SA, San Nicolas R, Provis JL. Generalized structural description of calcium-sodium aluminosilicate hydrate gels: the cross-linked substituted tobermorite model. Langmuir 2013;29(27):5294–306.
[11] Bonk F, Schneider J, Cincotto MA, Panepucci H. Characterization by multinuclear high-resolution NMR of hydration products in activated blast-furnace slag pastes. J Am Ceram Soc 2003;86(10):1712–9.
[12] Schilling PJ, Butler LG, Roy A, Eaton HC. ^{29}Si and ^{27}Al MAS-NMR of NaOH-activated blast-furnace slag. J Am Ceram Soc 1994;77(9):2363–8.
[13] Lothenbach B, Gruskovnjak A. Hydration of alkali-activated slag: thermodynamic modelling. Adv Cem Res 2007;19(2):81–92.
[14] Chen W, Brouwers HJH. The hydration of slag, part 1: reaction models for alkali-activated slag. J Mater Sci 2007;42(2):428–43.
[15] Fernández-Jiménez A, Palomo A. Characterisation of fly ashes. Potential reactivity as alkaline cements. Fuel 2003;82(18):2259–65.
[16] Ben Haha M, Lothenbach B, Le Saout GL, Winnefeld F. Influence of slag chemistry on the hydration of alkali-activated blast-furnace slag-part I: effect of MgO. Cem Concr Res 2011;41(9):955–63.
[17] Bernal SA, de Gutierrez RM, Provis JL, Rose V. Effect of silicate modulus and metakaolin incorporation on the carbonation of alkali silicate-activated slags. Cem Concr Res 2010;40(6):898–907.
[18] Zhang YJ, Zhao YL, Li HH. Structure characterization of hydration products generated by alkaline activation of granulated blast furnace slag. J Mater Sci 2008;43(22):7141–7.
[19] Provis JL, Palomo A, Shi C. Advances in understanding alkali-activated materials. Cem Concr Res 2015;78:110–25.
[20] Komljenovic M, Bascarevic Z, Marjanovic N, Nikolic V. External sulfate attack on alkali-activated slag. Constr Build Mater 2013;49:31–9.
[21] Long T, Wang Q, Guan Z, Chen Y, Shi X. Deterioration and microstructural evolution of the fly ash geopolymer concrete against $MgSO_4$ solution. Adv Mater Sci Eng 2017;2017.
[22] Mobili A, Belli A, Giosue C, Bellezze T, Tittarelli F. Metakaolin and fly ash alkali-activated mortars compared with cementitious mortars at the same strength class. Cem Concr Res 2016;88:198–210.
[23] Zhang Z, Yao X, Wang H. Potential application of geopolymers as protection coatings for marine concrete III: field experiment. Appl Clay Sci 2012;67:57–60.
[24] Montes C, Allouche EN. Evaluation of the potential of geopolymer mortar in the rehabilitation of buried infrastructure. Struct Infrastruct Eng 2012;8(1):89–98.
[25] Zhang Y, Li T, Hou D, Zhang J, Jiang J. Insights on magnesium and sulfate ions' adsorption on the surface of sodium alumino-silicate hydrate (NASH) gel: a molecular dynamics study. Phys Chem Chem Phys 2018;20(27): 18297–310.
[26] Rajamane NP, Nataraja MC, Dattatreya JK, Lakshmanan N, Sabitha D. Sulphate resistance and eco-friendliness of geopolymer concretes. Indian Concr J 2012;86(1):13.
[27] Salami BA, Johari MAM, Ahmad ZA, Maslehuddin M. Durability performance of palm oil fuel ash-based engineered alkaline-activated cementitious composite (POFA-EACC) mortar in sulfate environment. Constr Build Mater 2017;131:229–44.
[28] Bascarevic Z, Komljenovic M, Miladinovic Z, Nikolic V, Marjanovic N, Petrovic R. Impact of sodium sulfate solution on mechanical properties and structure of fly ash based geopolymers. Mater Struct 2015;48(3):683–97.
[29] Provis JL, Van Deventer JSJ. Geopolymers: structures, processing, properties and industrial applications. Elsevier; 2009.
[30] Bakharev T. Durability of geopolymer materials in sodium and magnesium sulfate solutions. Cem Concr Res 2005;35(6):1233–46.
[31] Chindaprasirt P, De Silva P, Sagoe-Crentsil K, Hanjitsuwan S. Effect of SiO_2 and Al_2O_3 on the setting and hardening of high calcium fly ash-based geopolymer systems. J Mater Sci 2012;47(12):4876–83.
[32] Alonso S, Palomo A. Alkaline activation of metakaolin and calcium hydroxide mixtures: influence of temperature, activator concentration and solids ratio. Mater Lett 2001;47(1-2):55–62.
[33] Van Deventer JSJ, Provis JL, Duxson P, Lukey GC. Reaction mechanisms in the geopolymeric conversion of inorganic waste to useful products. J Hazard Mater 2007;13(3):9506–13.

[34] Yip CK, Lukey GC, Provis JL, van Deventer JSJ. Effect of calcium silicate sources on geopolymerisation. Cem Concr Res 2008;38(4):554–64.
[35] Yip CK, Lukey GC, van Deventer JSJ. The coexistence of geopolymeric gel and calcium silicate hydrate at the early stage of alkaline activation. Cem Concr Res 2005;35(9):1688–97.
[36] Kumar S, Kumar R, Mehrotra SP. Influence of granulated blast furnace slag on the reaction, structure and properties of fly ash based geopolymer. J Mater Sci 2010;45(3):607–15.
[37] De Weerdt K, Justnes H, Geiker MR. Changes in the phase assemblage of concrete exposed to sea water. Cem Concr Compos 2014;47:53–63.
[38] Duxson P, Provis JL, Lukey GC, Separovic F, van Deventer JSJ. ^{29}Si NMR study of structural ordering in aluminosilicate geopolymer gels. Langmuir 2005;21(7):3028–36.
[39] Naghizadeh A, Ekolu SO. Behaviour of fly ash geopolymer binders under exposure to alkaline media. Asian J Civ Eng 2019:1–14.
[40] De Silv P, Sagoe-Crenstil K. Medium-term phase stability of Na_2O-Al_2O_3-SiO_2-H_2O geopolymer systems. Cem Concr Res 2008;38(6):870–6.
[41] Fernández-Jiménez A, Palomo A. Composition and microstructure of alkali activated fly ash binder: effect of the activator. Cem Concr Res 2005;35(10):1984–92.
[42] Sukmak P, De Silva P, Horpibulsuk S, Chindaprasirt P. Sulfate resistance of clay-portland cement and clay high-calcium fly ash geopolymer. J Mater Civ Eng 2014;27(5):4014158.
[43] Lodeiro IG, Fernández-Jimenez A, Palomo A, Macphee DE. Effect on fresh CSH gels of the simultaneous addition of alkali and aluminium. Cem Concr Res 2010;40(1):27–32.
[44] Shi C, Qian J. High performance cementing materials from industrial slags-a review. Resour Conserv Recycl 2000;29(3):195–207.
[45] Youngman R. NMR spectroscopy in glass science: a review of the elements. Materials 2018;11(4):476.
[46] Lee SK, Stebbins JF. The degree of aluminum avoidance in aluminosilicate glasses. Am Mineral 1999;84(5-6):937–45.
[47] Engelhardt G, Michel D. High-resolution solid-state NMR of silicates and zeolites; 1987.
[48] Richardson IG. The nature of CSH in hardened cements. Cem Concr Res 1999;29(8):1131–47.